Acta Geologica Polonica, Vol. 55 (2005), No. 1, pp. 9-29

Event stratigraphy of the Badenian selenite evaporites (Middle Miocene) of the northern Carpathian Foredeep

MACIEJ BĄBEL

Institute of Geology, Warsaw University, Al. Żwirki i Wigury 93, PL-02-089 Warszawa, Poland.
E.mail: m.babel@uw.edu.pl

ABSTRACT:

BĄBEL, M. 2005. Event stratigraphy of the Badenian selenite evaporites (Middle Miocene) of the northern Carpathian Foredeep. *Acta Geologica Polonica*, **55** (1), 9-29. Warszawa.

The Middle Miocene (Badenian) evaporites of the northern Carpathian Foredeep were deposited in a salina-type basin. Calcium sulphate sediments were deposited mainly on the broad northern margins of the basin, on vast evaporite shoals (mainly as fine-grained microbialite gypsum) and in large shallow saline pans (as coarse-crystalline selenites). 125 sections of these primary deposits, exposed from Moldova, Ukraine, Poland to the Czech Republic, were subjected to stratigraphic analysis based principally on the methodology of event and high-resolution stratigraphy. Due to an extremely gentle relief and a predominantly aggradational type of deposition, typical of a salina basin, the environmental changes or events were recorded nearly instantaneously in the whole area. Some events, such as water-level or brine-level fluctuations (emersions and floods, which can be very rapid in a salina basin), fluctuations in the average pycnocline level, aeolian dust or ash falls, accretion of specific gypsum microbialites, produced sets of marker beds which are perfectly correlated over distances of tens to hundreds of kilometres. Some thin grass-like selenite beds, representing deposits of shallow flat-bottomed saline pans, were correlated precisely over such great distances and are interpreted as isochronous or near-isochronous. Each bed was presumably deposited during the average pycnocline level highstands in the saline pan. The thick-bedded selenite units do not show long-distance bed-by-bed correlation, presumably because they were deposited in deeper pans in which the pycnocline fluctuations were recorded by bedding planes (i.e. by intercalations of fine-grained gypsum or dissolution surfaces) only on the shallow slopes or swells. However some apparent growth zones in the gypsum crystals from such selenite units were correlated throughout the basin, proving that the selenite growth was isochronous.

Key words: Event stratigraphy, High-resolution stratigraphy, Evaporites, Gypsum, Marker bed, Isochronous correlation, Selenite crystals, Growth zoning, Badenian, Carpathian Foredeep.

INTRODUCTION

The Middle Miocene (Badenian) evaporite basin of the northern Carpathian Foredeep (Text-fig. 1) is one of the largest evaporite basins with preserved diagenetically unaltered gypsum deposits which include differentiated and spectacular primary selenite (coarse-crystalline gypsum) facies. The gypsum deposits are well exposed and undisturbed horizontal layers can be traced for tens of kilometres through a belt of outcrops along the whole northern periphery of the Foredeep from Moldova, Ukraine, through Poland, to the Czech Republic (Text-fig. 2). This makes this selenite-evaporite basin unique for sedimentologic and stratigraphic studies.

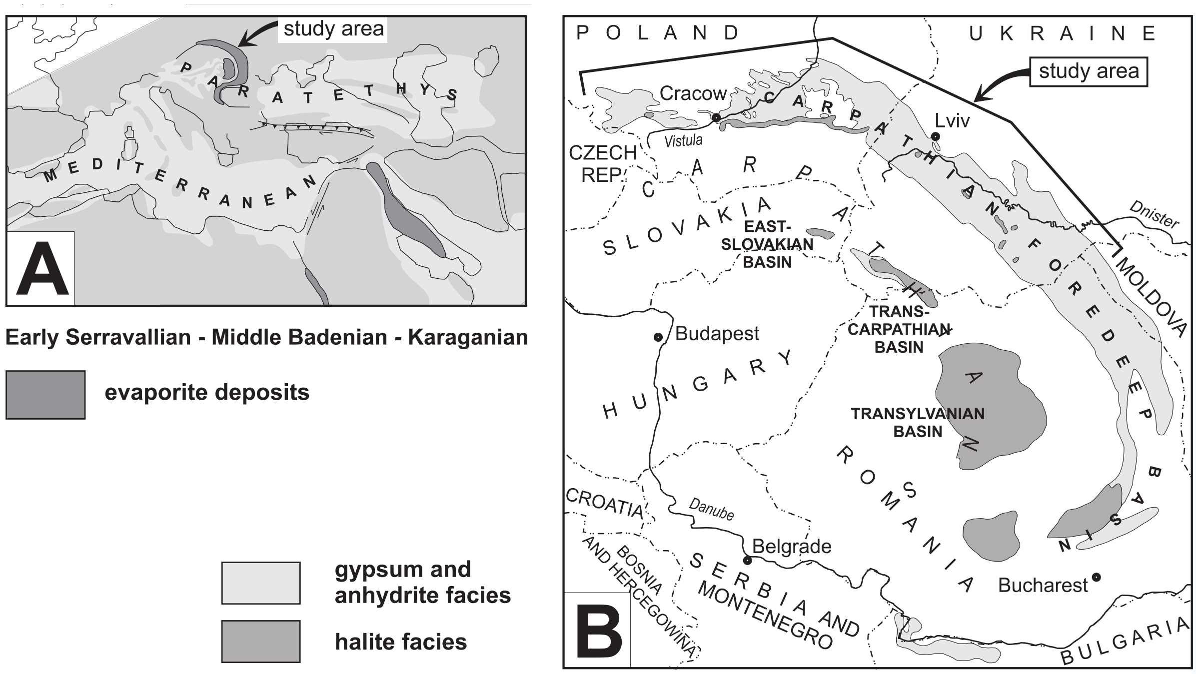

Fig. 1. Palaeogeography and distribution of Badenian evaporite basins. A) Palaeogeography of Paratethys and Mediterranean in the Middle Miocene and location of the Badenian evaporite basin studied (after RÖGL 1999). B) Present distribution of the Badenian evaporites in the Carpathian area (after KHRUSHCHOV & PETRICHENKO 1979, GARLICKI 1979, modified)

A correct reconstruction of the depositional history and palaeogeography of sedimentary basins is not possible without stratigraphic analysis. In bedded sequences of sedimentary rocks the best stratigraphic solution is to find as many as possible isochronous surfaces ('time lines') representing the floor of a basin evolving through time during sediment accumulation, erosion and/or non-deposition. The documentation of such isochronous surfaces in the Badenian evaporites of the northern Carpathian Foredeep and the establishment of a stratigraphic framework for gypsum basin analysis is the main aim of this paper.

The palaeogeography and geology of the Badenian evaporites studied were reviewed by BĄBEL (2004b). The evaporite basin, at least at its northern sulphate margin (Text-figs 1-2), was a salina-type basin (PERYT 2001), which showed water level fluctuations that did not coincide with the world sea level and apparently was supplied with marine water by seepage or occasional inflows through some morphologic barriers.

The analytic basis for this study consists of sedimentologic observations collected by the author during fieldwork on Badenian evaporites in Ukraine, Poland and the Czech Republic in 1992-2002. 125 gypsum sections were measured along the entire margin of the northern Carpathian Foredeep (see Appendix; available only in electronic version attached to the main paper, at the journal website: www.geo.uw.edu.pl/agp), of which 52 were selected as the most representative and shown on the summary scheme (Text-figs 2, 4). The other well documented gypsum and anhydrite sections, especially from outcrops in the Nida area (BĄBEL 1996, 1999b) and borehole cores from the northern part of the Polish Carpathian Foredeep (KUBICA 1992, KASPRZYK 1993), can be easily correlated and compared with the stratigraphic scheme presented.

The present paper supplements the previous stratigraphic studies in the Badenian evaporite basin (KUBICA 1992, PERYT & *al*. 1998, PERYT 2001), particularly those in the Nida area in Poland (WALA 1980; BĄBEL 1996, 1999b). Detailed observation and the large number of the gypsum sections studied enabled the identification and long-distance correlation of a more complete set of marker beds than previously recognised. Isochronous correlation was achieved by applying event and high-resolution stratigraphic methodology. Specific processes and depositional events characteristic of evaporite and selenite deposition were recognised and selected as the most useful for basinal isochronous correlation. Some new concepts for high-resolution correlation of selenite beds (see BĄBEL 2004a) were applied. The results obtained and ideas developed in this regional study can be useful for stratigraphic analyses of similar selenite dominated ancient evaporite basins.

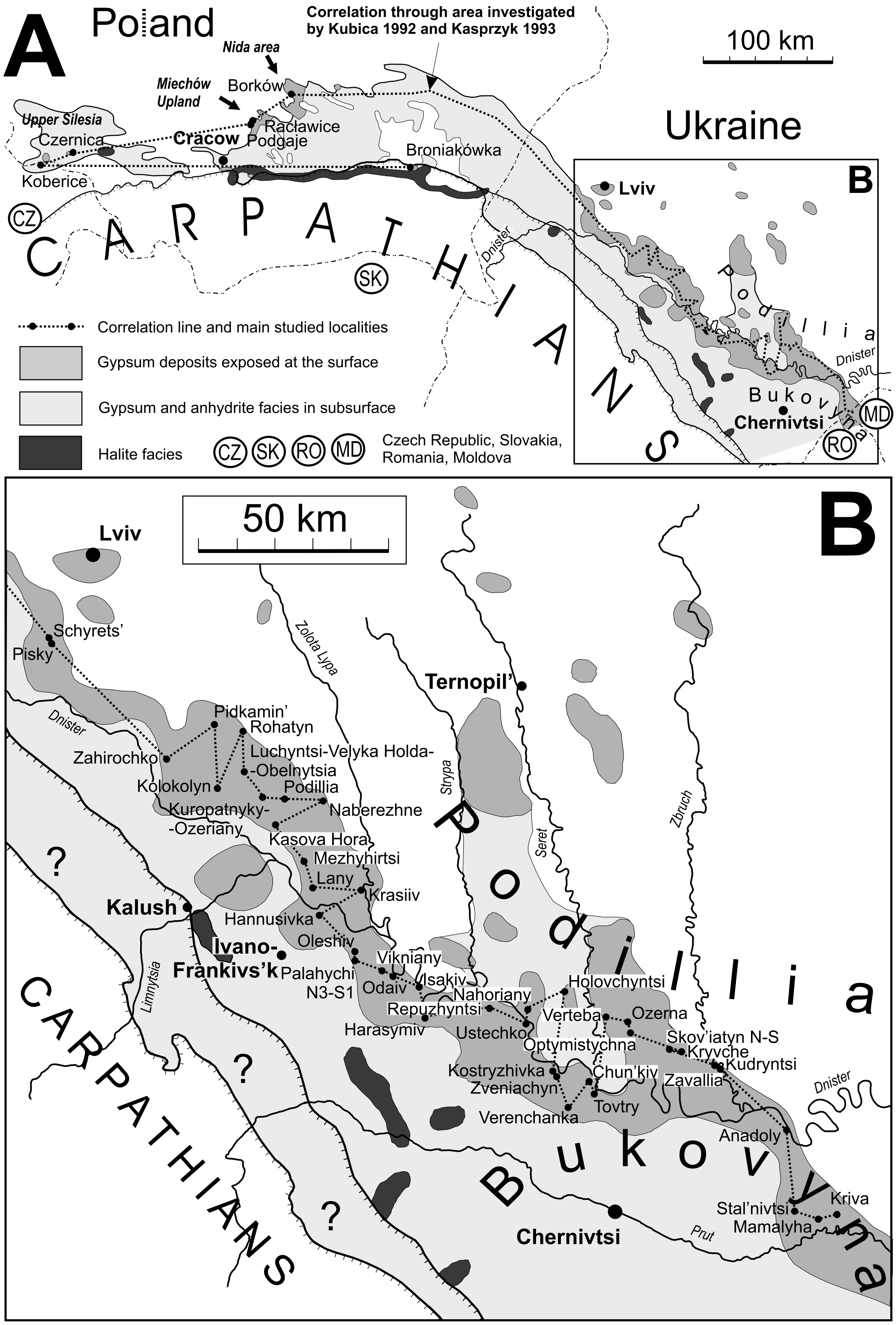

Fig. 2. Distribution of the gypsum sections studied in the Badenian (Middle Miocene) evaporite basin in the northern Carpathian Foredeep in Ukraine, Poland, Czech Republic and Moldova; after various sources cited in Bąbel 2004b and Appendix; A-B - Maps of the study area and correlation line for Text-figs 3-4

PREVIOUS STRATIGRAPHIC STUDIES

The Badenian gypsum deposits in the northern Carpathian Foredeep were roughly subdivided into two main stratigraphic units: the lower autochthonous and the upper allochthonous unit (Text-fig. 3; PERYT 1996, ROSELL & *al*. 1998, KASPRZYK 2003). The lower unit is up to ca. 25 m thick and contains widespread layers of coarse-crystalline bottom-grown gypsum crystals and therefore is also called the selenite unit. The upper unit, which locally attains 35 m in thickness, is composed of clastic or microcrystalline gypsum but also contains thin selenite beds. The lower unit is better exposed and the present study concerns mainly this lower part of the succession. Sections in Ukraine are commonly dominated by thick gypsum microbialite layers which, near the Zbruch River and the Ukraine–Moldova border, make up the entire 20 m thick section (PERYT 2001). The central areas of the basin, hidden in the subsurface near the Carpathian overthrusts, contain laminated anhydrite deposits, commonly with clay and halite intercalations (POŁTOWICZ 1993, PERYT 2000, KASPRZYK 2003). Thicker halite deposits are present in several subbasins identified from borehole cores (Text-figs 1B, 2). Stratigraphic correlation between these halite deposits in Poland and Ukraine, and between them and the marginal gypsum deposits analysed in this paper are still controversial (compare correlations by LADYZHENSKIY *in* LADYZHENSKIY & ANTIPOV 1961, p. 225; GARLICKI 1979, 1994; PETRICHENKO & *al*. 1997; KASPRZYK & ORTÍ 1998; PRYSJAZHNJUK 1998; BĄBEL 1999c; NOWAK & POŁTOWICZ 2000, p. 385; POBEREZHSKYY 2000; ANDREYEVA-GRIGOROVICH & *al*. 2003).

The present paper concerns the 'internal' stratigraphy of the Badenian gypsum deposits in the entire marginal zone of the northern Carpathian Foredeep. Their stratigraphy has been studied for the past forty-five years mainly by litho- and cyclostratigraphic methods, although some elements of event stratigraphic methodology were also attempted (WALA 1961, 1962, 1963, 1980; KUBICA 1992; KASPRZYK 1989a, 1993; PERYT & *al*. 1998; TURCHINOV 1999). NIEMCZYK (1988, 1995) and KASPRZYK (1994b, 1995b) combined cyclo-, sequence- and event stratigraphic correlation of sulphate and halite deposits in the Polish Carpathian Foredeep but the results of that approach remain controversial (GĄSIEWICZ & CZAPOWSKI 1995, KASPRZYK & ORTÍ 1998, BĄBEL 1999c). Scarce fauna (foraminifers and nannoplankton) allow only rough biostratigraphic correlation of the Badenian evaporites (see references in ANDREYEVA-GRIGOROVICH & *al*. 2003 and BĄBEL 2004b). A large quantity of geochemical data enables chemostratigraphic correlation (see KASPRZYK 1989b, fig. 4; 1994a, 2003; PERYT & *al*. 1997a, 2002; ROSELL & *al*. 1998).

Recently, a more precise and formal event stratigraphic approach, based on selected thin marker beds unequivocally interpreted as isochronous, was applied to the Badenian gypsum evaporites by PERYT (1996, 2001), BĄBEL (1996, 1999b), BĄBEL & *al*. (1998) and BĄBEL & BOGUCKIY (1999). KUBICA (1992) previously attempted isochronous correlation of some tuffite marker beds in gypsum cores and BĄBEL (1987) noted isochronous correlation of some growth zones in selenites.

METHODS OF STRATIGRAPHIC ANALYSIS

The event stratigraphic methodology used in this paper is supplemented by lithostratigraphy and elements of high-resolution stratigraphy and cyclostratigraphy. The high-resolution approach (cf. KAUFFMAN 1988) was used only for parts of the measured sections and was limited by the fact that the method of investigation was macroscopic. Correlation was made by a simple optic 'best fit correlation' (cf. STRASSER 1994, PITTET & STRASSER 1998).

The stratigraphic methodology applied required detailed recognition of sedimentary environments. These environments are well known from many previous studies (KWIATKOWSKI 1972; KASPRZYK 1993, 2003; PERYT 1996, 2000, 2001; PETRICHENKO & *al*. 1997; ROSELL & *al*. 1998; KASPRZYK & ORTÍ 1998; BĄBEL 1999a, 1999b, 2005 in print, with references). The event stratigraphic terminology was slightly modified and adapted to the nature of the evaporite deposits studied.

Sedimentary or depositional events are a crucial concept in event stratigraphy. They are commonly defined as very short (hours to days), usually rare intervals of rapid deposition within a system of relatively slow background sediment accumulation (EINSELE & *al*. 1996). Some authors suggested that events less than 100 ky in duration are satisfactorily short and useful in high-resolution stratigraphic analysis (KAUFFMAN 1988, KAUFFMAN & *al*. 1991). These definitions are applied mostly to clastic and carbonate deposits and are unsuited to high-resolution stratigraphic studies of evaporites. Evaporite deposition rate is very rapid in comparison with average sedimentation rates of clastic, carbonate or other sediments, hence evaporites are commonly treated as a single event bed. The Badenian evaporites of the Carpathian Foredeep were commonly considered as a single chemical sedimentation event which could have lasted only 20-40 ky (KUDRIN 1955, GARLICKI 1968, TRASHLIEV 1969, NIEMCZYK 1995, PETRICHENKO & *al*. 1997, cf. KREUTZ 1925). Events useful for high-resolution stratigraphy of evaporite deposits should be significantly shorter than this period.

The following terminology is used in this paper. The term *event* is used in a broad sense. It is defined as a basin-scale depositional process, or sequence of processes, which produced a well recognisable record in sediments. Non-deposition and erosion are included in these processes (cf. KAUFFMAN 1988, EINSELE 1998). This record is represented by a stratum or bundle of strata described as an *event bed*. Extremely thin event beds or discontinuity surfaces are distinguished as *event horizons* (EINSELE 1998). The process or processes defining the events should be of relatively short duration, but not necessarily shorter than that of the background sediment accumulation (cf. ERNST & *al*. 1983). Such a definition is chosen for practical reasons, taking into account the stratigraphic importance of some otherwise relatively short-term events in evaporite basins, like e.g. basin wide refreshments and/or dissolution; these events could be of very long duration when compared to the rapid background evaporite deposition. The event should be isochronus in the entire basin.

A *marker bed* is a selected event bed useful for long-distance correlation. A marker bed, by definition, should be thin, easily recognisable in outcrops, have a high correlation potential, and should represent a well recognised sedimentary event (or sequence of events) on a basinal scale (EINSELE & *al*. 1996). Event horizons useful for long-distance correlation are described as *marker horizons*. Helpful features for the recognition of marker beds are their constant position in the section (in relation to lithostratigraphic units) and their occurrence within bundles of strata that reflect a constant continuous sequence of basin-scale depositional processes or, in other words, a constant sequence of events (see SCHWARZACHER 2000). Marker beds or horizons of different origin occurring together in the same thin interval of the section and in a constant sequence are the most valuable for correlation (as in the case of the 'event-bundle' concept discussed by WIESE & KRÖGER 1998, pp. 269-270; cf. ERNST & *al*. 1983, figs 5-6; and the 'composite event' concept discussed by KAUFFMAN 1988, and KAUFFMAN & *al*. 1991).

The *isochronous surfaces* reflect 'time lines'. It is required that these surfaces, as far as possible, should be chronostratigraphic boundaries rather than marker beds, and have the best potential for high-resolution isochronous correlation. The isochronous surfaces are marked by very thin physical units, discontinuities or lithologic boundaries, representing a chosen basin-scale *isochronous event* most useful for high-resolution long-distance correlation. They are marked by a selected marker horizon, or at the top or base of some selected part of a given marker bed. In practice, isochronous surfaces are commonly placed on 'master bedding planes' (SCHWARZACHER 2000).

The following procedure was applied during the stratigraphic analysis. First, after detailed logging of the sections and careful sedimentologic and facies studies, sequences of sedimentary events were recognised and event beds and event horizons were distinguished and correlated. Secondly, the most useful event beds were selected as marker beds for long-distance correlation. Marker beds were designated on stratigraphic sections by small letters, often with additional numbers, corresponding to alphabetically designated lithostratigraphic units distinguished previously (Text-figs 3-4; WALA 1963, 1979, 1980; KUBICA 1992; Appendix, Fig. 3). Finally, based on these marker beds and the sequences of events responsible for their creation, isochronous surfaces were designated and isochronous events defined. The isochronous surfaces were designated by capital letters: A, C/D, Tb, Td, G/H, F1.

Two types of isochronous surfaces were distinguished: high-quality and low-quality isochronous surfaces (Text-figs 4-5). *High-quality isochronous surfaces* represent short-term events not connected with dissolution and/or erosion. They are represented by dust or ash falls and growth zoning of selenite crystals. *Low-quality isochronous surfaces* are connected to events such as non-deposition and/or erosion-dissolution. Non-deposition or erosion surfaces could represent relatively long periods of time with many unknown sedimentary events possibly hidden within. Nevertheless only one, the most significant and relatively short-term isochronous event recorded in a given surface was chosen as defining that surface. This event was also specifically selected to secure, as far as possible, the chronostratigraphic potential of the low-quality isochronous surfaces (similarly as unconformities representing sequence boundaries in sequence stratigraphy; e.g. NYSTUEN 1998, pp. 96-68). This chronostratigraphic potential is maintained only when such surfaces are real 'time barriers' and all of the strata below them are older than the strata above them within the whole basin (CATUNEANU 2002, p. 28).

The stratigraphic meaning of the non-deposition and/or dissolution-erosion surfaces of the evaporite basin corresponds to erosion surfaces formed during exceptionally rapid sea-level rise, and to condensed beds associated with maximum transgression (KAUFFMAN 1988, pp. 620, 622; KAUFFMAN & *al*. 1991, p. 805; cf. EINSELE 1998, p. 182). The water level fluctuations in salina-type basins, such as the Badenian basin studied, can be very rapid (even hours or only several years in duration) and large (BĄBEL 2004a, b; with references). Such short-term fluctuations can produce erosion or discontinuity surfaces and an associated sedimentary record useful for isochronous or near-isochronous correlation.

Events defining the low-quality isochronous surfaces are sometimes weakly documented and can be controversial. However, such a slightly arbitrary approach in defining isochronous events and surfaces presumably will help in future discussions of the stratigraphic value of these important surfaces and in correlation with other parts of the basin. Further analysis and comparison with more continuous sections may lead to reassessment and redefinition of the isochronous events defining time-lines around the marker beds.

LITHOSTRATIGRAPHY

Seven lithostratigraphic units lettered from A to G, originally called lithotypes or lithosomes, were distinguished in borehole cores in the Polish Carpathian Foredeep by Kubica (1985, 1992). These units continue to the east up to the environs of Horodenka in Ukraine (Text-figs 2-4). Further east there are three other units, described in more detail by Bąbel (2005 in press) and designated alphabetically as follows:

M – fine-grained gypsum deposits representing mainly gypsum microbialite facies and alabastrine facies

SH – selenite and selenite-gypsum microbialite deposits representing mainly facies with horizontal sabre crystals

SV – selenite deposits representing mainly sabre gypsum facies with crystals curved upward

In Upper Silesia and the Czech Republic (at Kobeřice), in the western area of the basin, and at Broniakówka, at the southern margin of the basin (Text-fig. 2A), the other units are distinguished. They are lettered similarly to the units by Kubica (1992) because they are exact lithologic equivalents of these units and occur in the same vertical sequence (Text-fig. 4). The lateral continuity of the gypsum layers between the studied western, southern, and northern areas of the basin is interrupted.

Units from A to G are recognised in most borehole cores in the northern area of the Polish Carpathian Foredeep (Kubica 1992; Kasprzyk, 1989a, 1993). They crop out in the Nida area and, except for unit F, in the Miechów Upland (Text-figs 2-4). The subsurface lateral continuity of units A-G in the northern area of the basin in Poland is well supported by geophysical methods (Kubica 1994). Such precise geophysical correlation is lacking in Ukraine, where only a few borehole cores were measured in detail (Kasprzyk 1995a). The lateral continuity of unit F, in particular, is poorly documented.

Units A-G change their appearance laterally, passing from west to east. In Ukraine, all the selenite deposits show massive structures unlike the porous ones typical of the Polish-Czech area of the basin. The sabre crystals within the SH and SV units, unlike those from units C-D, and F, which are grey in colour, are honey to brown due to included organic matter. The Ukrainian sections, and especially unit E, contain very little clay. Badenian gypsum deposits in Ukrainian outcrops are commonly entirely or partly altered into secondary alabaster. Most commonly the lowermost part of the section – unit A and the boundary area between units A and M - is composed of such secondary gypsum (Text-fig. 4). Some sections show, however, relict primary features that permit stratigraphic correlation (Appendix, Figs 8, 10, 12-14, 17).

GYPSUM CRYSTAL MORPHOLOGY AND FABRIC AS A STRATIGRAPHIC TOOL

Like those of many other evaporite basins (Richter-Bernburg 1973, Rouchy 1982, Dronkert 1985), the

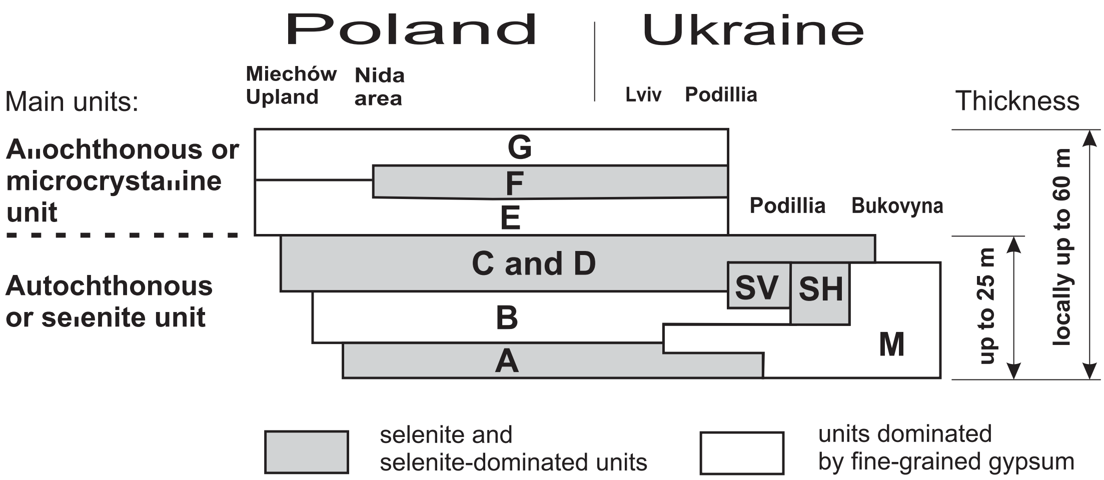

Fig. 3. Lithostratigraphy of the Badenian gypsum evaporites in the northern Carpathian Foredeep along the correlation line from Miechów Upland to Bukovyna (Text-fig. 2)

wkleja fig4 3/19/05 4:02 PM Page 1

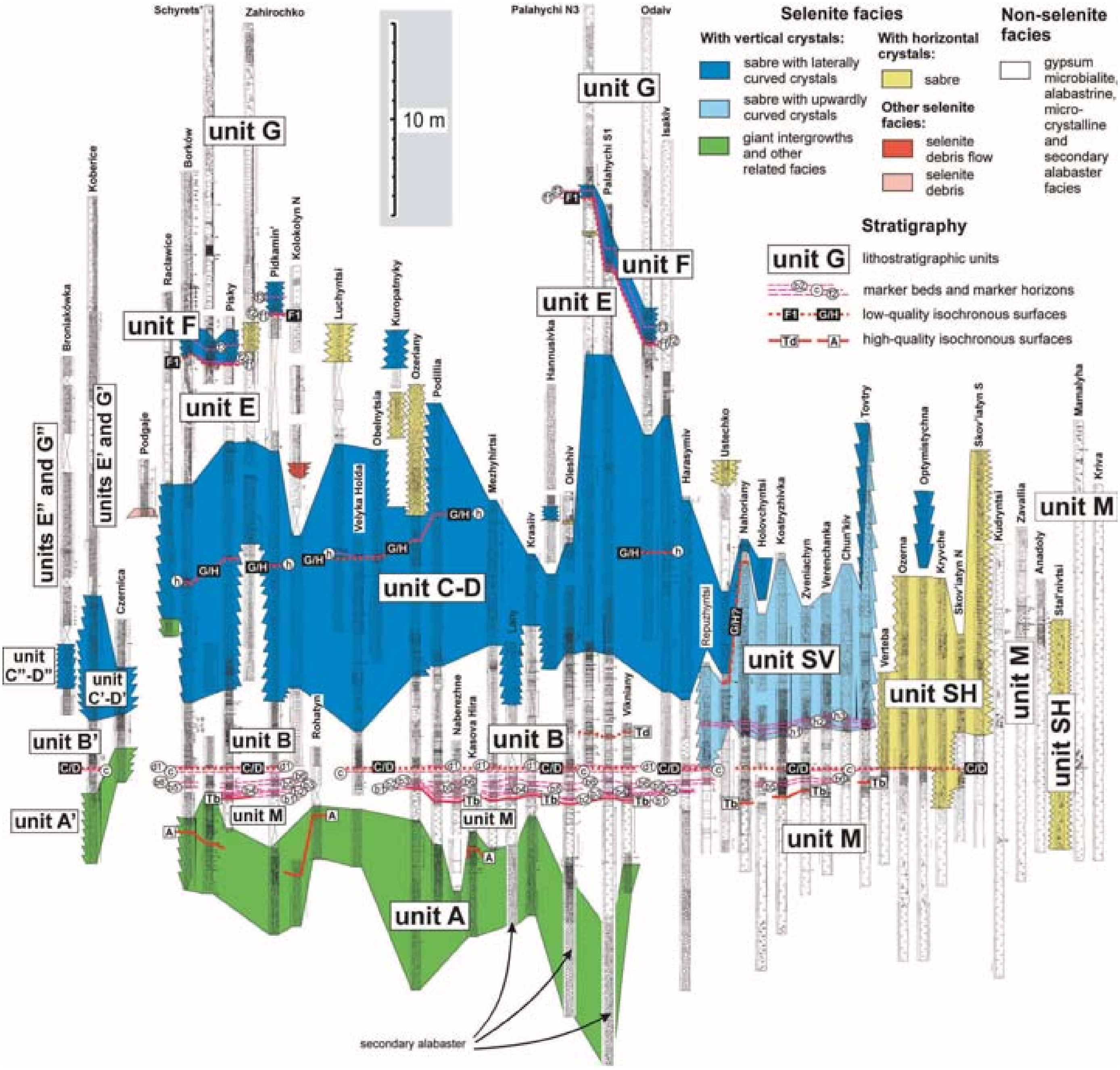

Fig. 4. Summary of facies and stratigraphic relations in representative sections of the Badenian gypsum deposits in the northern Carpathian Foredeep along the correlation line shown in Text-fig. 2 (details are shown in Appendix)

Badenian selenite beds form laterally continuous units which preserve the fabric and morphology of the gypsum crystals. The giant gypsum intergrowths show a peculiar morphology that has no known equivalent among modern and ancient evaporite gypsum crystals. This indicates the unique composition and properties of the brine in the evaporite basin (see BĄBEL 1991, RODRÍGUEZ-ARANDA & *al*. 1995). The presence of such peculiar non-recurring brines and conditions influencing the morphology of the crystallizing gypsum can be treated as an event of stratigraphic value, particularly in the case of the giant intergrowths (unit A, Text-fig. 4), which appear only once in the stratigraphic column.

Apart from the giant intergrowths, some other thin selenite beds also show a peculiar crystal morphology and fabric that is useful for stratigraphic purposes (for example beds h1 and f1, described later in this text; Pl. 5, Fig. 1; Pl. 6, Figs. 1-2; Appendix, Figs 9A-C, 12A-C, 13A-B). Similarly to the giant intergrowths, these thin selenite beds can be treated as event or marker beds reflecting the appearance in the evaporite basin of properties of brine and conditions determining the morphology and fabric of the growing gypsum crystals. Thin selenite beds showing a distinctive crystal habit and reflecting similar ‘events’ are known from other Neogene evaporites (e.g. SCHREIBER & *al*. 1977, RODRÍGUEZ-ARANDA & *al*. 1995).

The morphology of the gypsum crystals and the associated fabric features, size and arrangement of crystals, are very similar within lithostratigraphic units containing selenites, and usually differ between particular units (Text-fig. 4; Appendix, Figs 6-13, 15-18). This might suggest that these selenites were deposited from different brines. Moreover, there are vertical trends of changes in crystal morphology and fabric within these thick selenite units that are always the same in every outcrop. For example, it is a rule that within unit C-D sabre crystals become commoner and larger up-section (see hachure in selenite beds in Appendix, Figs 6B, 15A, 16A, 17A-D; and BĄBEL 1999b, fig. 2; 2004b, fig. 5). Constant sequences of changes in crystal morphology and fabric are also observed, from the base to the top, in selenite beds h1-h3 within unit SV, and f1-f3 within unit F (Text-fig. 4; Pl. 5, Fig. 1; Pl. 6, Figs 1-2; Appendix, Figs 9A-C, 12A-C, 13A-B). These characteristic crystallographic and fabric changes enable the recognition not only of the units mentioned, but also the stratigraphic position of even small samples of selenite rocks taken from them.

These general vertical trends of changes in crystal morphology can be interpreted as a reflection of the evolving properties and composition of the brine in the evaporite basin or in particular saline pans within the basin. In the case of unit C-D, one of the factors determining these changes in crystal morphology was presumably a gradual salinity rise (BĄBEL 1999b, pp. 435-436). The changing properties and parameters of the evolving brine, recorded by the sequence of changes in crystal morphology and crystal fabric, can be treated as events that are useful for rough long-distance correlation of the selenite deposits.

It was noticed from early studies that the morphology of gypsum crystals is tied to certain environmental conditions and to some extent can be used as an indicator of these specific conditions (e.g. LACROIX 1897, CODY & CODY 1991, MAGEE 1991). For example, the morphology of selenites from saltwork pans was found to be related to salinity (ORTÍ & *al*. 1984). Discussion of this problem, and recognition of the factors and brine properties which were responsible for the morphology of the Badenian gypsum crystals, requires further study (BĄBEL 1991, 2000) and is beyond the scope of this paper.

MARKER BEDS, EVENTS AND STRATIGRAPHY

Growth zoning in giant gypsum intergrowths

Description: Growth zoning of the giant gypsum intergrowths is very unclear (BĄBEL 1987). Three distinctive coloured zones are easily seen from macroscopic determination and correlation in the field: dark, white, and orange zones (Appendix, Figs 4-5)

Dark zones are discontinuous, ca. 0.5 cm thick, black to dark bands with diffuse boundaries that are best seen on the composition surfaces of the giant intergrowths (Pl. 1, Figs 1-2; BĄBEL 1987, pl. 3, fig. 1). They always occupy a constant position in the upper part of unit A (Appendix, Figs 4-5, 6A, 8A-C). The zones are usually parts of gypsum crystals enriched in flocculent inclusions of organic matter. The inclusions are dark to brown in transparent light under the optical microscope, and some of them are phytoclasts.

White zones, present in gypsum crystals, are seen as 1 mm thick, subhorizontal, continuous wavy to zigzag white laminae with sharp boundaries (Pl. 1, Fig. 2; BĄBEL 1987, pl. 9, figs 1-2). They cross-cut elongated gypsum subcrystals suggesting that formation of the zone was preceded by dissolution and flattening of the gypsum substrate. The zones represent a dense accumulation of trapped solid inclusions of some very small mineral particles. Radial aggregates of tabular to needle-like gypsum or anhydrite crystals are common among these zones as well.

Rarest of the zoning types are orange-coloured zones formed by tiny orange to brown spots scattered along a single growth zone (Appendix, Fig. 4). The spots appear to be iron oxide or hydroxide compounds.

Interpretation: The dark zones may represent longer periods of microbial and algal blooms in a perennial selenite pan after larger inflows of meteoric waters, such as observed in the Dead Sea (OREN 1999). The presence of phytoclasts suggests such inflows, namely transport by run-off waters from the land. The increased inflow of fresh water could induce some longer period of meromixis reflected by increased 'accumulation' of organic matter (see BĄBEL 2004a). Interpretation of the other zones requires additional studies.

Isochronous surfaces (A) *and isochronous events*: Up to nine numbered dark growth zones within the giant intergrowths form a bundle of zones designated as isochronous surface A (Text-fig. 4; BĄBEL 1996; 1999b, fig. 2; Appendix, Figs 6A, 8A-C). The bundle shows a proportional pattern of thickness changes and a constant position in relation to the other white and orange growth zones as well as to the major dissolution surfaces, thus enabling a best fit correlation in the Nida area and Ukraine (Pl. 1, Figs 1-2; Appendix, Figs 4-5; cf. MEYERS 1978, p. 382; ANDERSON 1984). The zones represent basin-scale rhythmic growth of giant selenites controlled by climate and hydrologic regimes of deep perennial saline pan.

Although dark growth zones are interpreted as isochronous, it does not mean that the giant intergrowths in Poland and Ukraine grew in the same pan. Growth zoning recorded in adjacent saline pans presumably can be very similar if driven by the same climatic changes, just like the pattern of varves in periglacial or meromictic lakes.

Remarks: Millimetre-scale crystal growth zoning is present in many selenite beds in modern and ancient deposits (e.g. WARREN 1982, 1999). FERSMAN (1919), working on the Saki lake in the Crimea, was probably the first to attempt to count and correlate growth zones in modern selenite crusts. He interpreted them as annual or seasonal and noted that coeval mm-thick zones show different thicknesses in various parts of the lake (similar to the isochronous growth zones recognised in particular parts of the Badenian basin; Appendix, Figs 4-5). Recently the selenites from saltwork pans were investigated by GEISLER-CUSSEY (1986), who found that growth zoning reflects both annual and seasonal (short-term) salinity fluctuations.

The regular mm-scale growth zones observed in some selenite beds presumably have a similar stratigraphic value to that of varves in Pleistocene-Holocene meromictic and periglacial lakes (e.g. ANDERSON & *al*. 1985, BJÖRCK & *al*. 1995), tree rings in dendrochronology (GRISSINO-MEYER 2005), or the 'chemical' varves in some ancient evaporite meromictic basins (RICHTER-BERNBURG 1985, KIRKLAND 2003). Selenites deposited in seasonally stratified (i.e. monomictic) deeper basins can reflect climatically driven seasonal events similar to those producing varves. Each zone can record a period of increased growth rate of gypsum crystals associated with dry season lowstand, destratification, mixing and homogenisation of the brine column (cf. WARREN 1999, pp. 14, 44; KIRKLAND 2003), and in an ideal case can represent one year (BĄBEL 2004a). Some mm-scale growth zones in the Badenian selenites were already interpreted as annual varves by KREUTZ (1925) and PETRICHENKO & *al*. (1997). The most regular, dense, presumably annual growth zones occur in the sabre gypsum crystals within unit C-D and require detailed analysis to reveal their basin-scale isochronous correlation.

Selenite sequences: selenite marker beds b1-b6

Description: The bundle or sequence of marker beds b1-b6 occurs within unit B (Text-figs 3-5). The sequence comprises up to 25 cm thick rows of selenite crystals and their aggregates, commonly of grass-like appearance, intercalated with microbialite, clastic, pedogenic and/or alabastrine gypsum or, rarely, clay. The constant position in the gypsum sequence (below marker bed c), the same proportional changes of thickness of particular selenite beds, and the distribution as well as the appearance of intercalated fine-grained gypsum, readily enables best fit correlation (Pl. 2, Figs 1-3; Pl. 3, Fig. 1; Pl. 4, Figs 1-2; Appendix, Figs 6-9; BĄBEL & *al*. 1998, fig. 1; BĄBEL & BOGUCKIY 1999). Some selenite beds contain characteristic intercalations of orange mud interpreted as dust or ash deposits, and one such intercalation is designated as an isochronous surface Tb (Pl. 3, Fig. 1). The other beds show laterally extensive dissolution surfaces. The tops of the selenite beds are commonly flatted or show pockets filled with clastic gypsum (PERYT 1996, figs 9-10). The selenite beds pass laterally into fine-grained gypsum deposits that commonly represent microbialite layers.

Interpretation: Orange mud Tb is interpreted as an isochronous deposit. It occurs, with only a few exceptions, within the same upper part of the selenite bed b1. This suggests that the whole of this bed is also isochronous. The other adjacent selenite beds showing proportionally changing thicknesses are probably also isochronous.

The regular alteration of selenites and fine-grained gypsum suggests cyclic sedimentation and requires an explanation for the driving forces of such a cyclicity. Some selenite beds show features of dissolution on their top surfaces, which are flattened and draped with clastic or pedogenic gypsum and clay, suggesting emersion (see Pl. 3, Fig. 2). These features permit the interpretation of such selenites and their covering layers of fine-grained gypsum as shallowing-upward units (cf. STRASSER & *al.* 1999, p. 205),

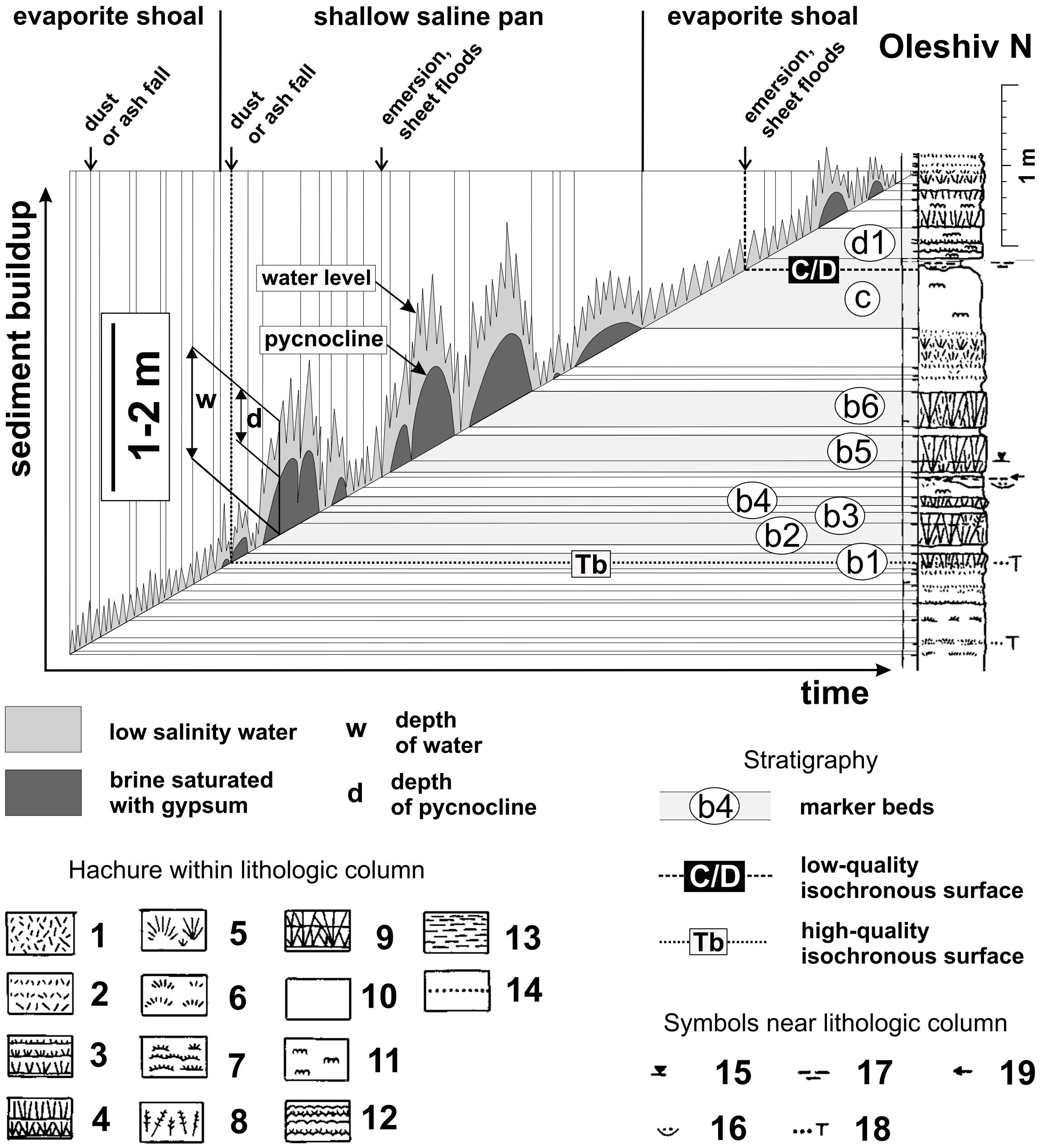

Fig. 5. Scheme showing main depositional events in the gypsum section at Oleshiv (Text-figs 2, 4). Selenite marker beds b1-b6 are interpreted as response to fluctuations in the average pycnocline level in a shallow flat-bottomed saline pan. 1-9 – Selenite components (hachure reflects arrangement, sizes and shapes of crystals): 1 – randomly scattered, straight rod-like crystals: short (left) and long (right); 2 – rows of rod-like crystals creating grass-like structures without a sharp base: short crystals (top), long crystals (bottom); 3 – rows of rod-like crystals showing grass-like structures and with a flat base: short crystals (top), long crystals (bottom); 4 – straight grass-like crystals showing palisade-parallel (top) and palisade-radial structure (bottom); 5 – radial or fan-like aggregates of straight crystals grown from common centres (right) and overgrowing fine-grained gypsum dome (left); 6 – rows of small grass-like crystals without a sharp base grown on fine-grained gypsum domes; 7 – rows of small grass-like crystals with a sharp base grown on fine-grained gypsum domes; 8 – aggregates of crystals resembling palm-tree leaves; 9 – flat horizontal synsedimentary dissolution surface within radial aggregates of the grass-like crystals showing syntaxial growth over this surface; 10 – fine-grained homogeneous gypsum (alabaster when massive and white), or other non-differentiated fine-grained or microcrystalline gypsum; 11 – fine-grained (alabaster-like) gypsum with traces of gypsified crenulated microbial mats; 12 – small grass-like crystals covering surfaces of gypsified crenulated microbial mats and intercalating gypsum microbialite deposits; 13 – clay and gypsum-clay deposit; 14 – orange dusty mud; 15 – synsedimentary dissolution surfaces; 16 – small channels filled with sugar-like clastic gypsum; 17 – clay intercalation; 18 – orange dusty mud interpreted as aeolian dust or pyroclastic ash deposit; 50 – horizontal discontinuity surfaces significant for correlation

and they also suggest that the deposition of the adjacent, over- and underlying selenite beds and intercalated fine-grained gypsum layers could have been similarly controlled by water level fluctuations. Periodic changes in water level and pycnocline level in a salina basin appear to be the simplest and presumably the best explanation for the cyclicity in question. The following detailed interpretation explores this idea, based on the concepts of gypsum deposition developed earlier (BĄBEL 2004a).

The Badenian evaporite basin was presumably a salina-type basin with typical frequent, large and rapid fluctuations of water level driven mainly by climate cycles (BĄBEL 2004b). The laterally continuous thin selenite beds intercalated with fine-grained gypsum represent deposits of a perennial shallow and flat-bottomed pan in such a basin (BĄBEL 2004a, figs 6-7). This saline pan showed monomictic to polymictic hydrologic regimes, with possible short periods of meromixis. The selenite beds were deposited mainly in the hypolimnion or monimolimnion zone below the average pycnocline level. This zone was characterised by a permanent cover of calcium sulphate-saturated brine over the depositional surface. Permanent immersion within such brines, i.e. within the hypolimnion or monimolimnion, is an essential feature enabling the syntaxial growth of thick selenite crusts. The simplest explanation for the ending of selenite crystallisation, and for the transition into the deposition or precipitation of fine-grained gypsum, is that a highly saline brine body was no longer covering the depositional surface. In the shallow perennial saline pan this change might be realised in three ways (BĄBEL 2004a): (1) complete brine dilution and transformation of the hydrologic regime of the pan into continuous polymixis which was unfavourable for selenite deposition; (2) deepening (lowering or drop in level) of the pycnocline so that the slope area of the pan came into contact with the upper epilimnetic or mixolimnetic water mass, which was permanently in a state favourable for the deposition of gypsum microbialite and fine-grained gypsum; (3) complete drop in the water level (and the pycnocline level) associated with drying out of the pan and the possible deposition of fine-grained pedogenic and clastic gypsum on an emerged selenite crust.

The fine-grained gypsum intercalating selenite crusts is interpreted as deposited on semi-emerged evaporite shoals (developed at the bottom of the pan during the water-level falls), and/or in the shallow epi- or mixolimnion zone above the average pycnocline of the perennial pan (BĄBEL 2004a). Clastic fine-grained gypsum could also have accumulated at the bottom of the shallow ephemeral (seasonally drying-out) saline pan.

A tentative reconstruction of changes in water level and average pycnocline level in the perennial saline pan is shown in Text-fig. 5. For simplicity, it was assumed (see BĄBEL 2004a for references) that: (1) the changes in water level and average pycnocline level were in phase, (2) the changes in water level were more frequent and rapid than fluctuations of the pycnocline, and (3) the thick selenite beds composed of large crystals devoid of dissolution features and showing continuous growth zoning were deposited in deeper brine than the thin selenite crusts containing smaller crystals (see BĄBEL 2004a, figs 6-7). In this interpretation, the changes in average pycnocline level are basically responsible for the cyclic deposition of the selenite sequences. The thicker selenite beds required a longer duration of the average pycnocline 'highstand' than the thin beds.

The stratigraphic concept explaining the origin of the precise bed-by-bed correlation of selenite sequences by fluctuations in average pycnocline level presented herein (Text-fig. 5) is similar to the high-resolution sequence- and cyclostratigraphic models for long-distance correlation developed by STRASSER (1994) and STRASSER & *al.* (1999). Their models were worked out for shallow carbonate platforms, and are particularly useful in stratigraphic correlation of the flat interiors of such platforms with prevailingly aggradational depositional system (D'ARGENIO & *al.* 1999, p. 372, fig. 7). Because of the limited accommodation the stratigraphic record in such environments is commonly incomplete (STRASSER & *al.* 1999). Also in the model applied herein the aggradational system, typical of salina-type or drawdown basins (WARREN 1999), is assumed. Conversely, however, I assume more complete stratigraphic record, due to higher accommodation typical of such basins (BĄBEL 2004b).

Selenite marker beds h1-h3

Description: Three stacked selenite beds h1-h3 occur in unit SV (Text-figs 3-4). They contain large domal structures composed of honey-coloured sabre crystals (with upward-curved forms). Selenite bed h1 shows a wavy basal surface coinciding with the tops of the large (up to 1 m in diameter) gypsum-microbialite domes in the layer below (Pl. 5, Fig. 1; Appendix, Figs 9A-C). The overlying selenite domes in bed h1 are an apparent continuation of these structures and show slopes composed of long (15-40 cm) sabre crystals which are horizontal and curved upward. The bundles of such sabre crystals growing against each other on the slopes of adjacent domes created characteristic competitive growth structures (see Appendix, Fig. 7, hachure no. 37 in Key to hachure within lithologic columns; and Pl. 5, Fig. 1) useful for recognition and correlation of this bed. The selenite domes from bed h1 have flattened tops which coincide with a flat or slightly wavy base of the overlying bed (h2). The overlying selenite bed h3 displays a flat or slightly wavy base and top (Appendix, Fig. 11). The tops of the selenite beds show dissolution features and in places are covered with fine-grained gypsum.

Interpretation: The beds represent the transition from a shallow perennial saline pan, with microbialite-selenite domes growing at the bottom (now present below h1), to a relatively deep, flat-bottomed perennial pan with a hydrologic regime favourable for selenite crystallisation. Beds h1-h3 represent a sequence of depositional events related to synchronous hydrologic changes, fluctuations of the average pycnocline level, and of water level similar to the b1-b6 sequence (see above, and Text-fig. 5), but occurring in the deeper brine. The beds are isochronous or near-isochronous. The flat-topped selenite domes in bed h1 are the products of selenite growth limited by a constant position of the pycnocline (cf. SCHREIBER 1988, p. 203), as observed in the Messinian gypsum at Eraclea Minoa in Sicily (SCHREIBER 1997).

Remarks: The selenite marker beds h1-h3 within unit SV presumably are coeval with some thick, laterally continuous selenite beds appearing around the isochronous surface Td within the adjacent unit B (Text-figs 3-4). These latter beds show a different fabric and do not contain honey-coloured upward-curved sabre crystals like those in unit SV (compare Appendix, Figs 9 and 10). The selenites from unit B and SV were probably deposited in two separate perennial pans. However, the beds under discussion could have been coeval because the hydrologic regimes and sedimentary events of the adjacent saline pans could have been driven by the same extrinsic, presumably climatic, factors.

Selenite marker beds f1-f3

Description: The laterally continuous selenite beds f1-f3 are intercalated within microcrystalline facies in the upper allochthonous unit of the gypsum sequence in Ukraine (Text-figs 3-4; Pl. 6, Figs 1-2; Appendix, Figs 3, 12-14). They correspond to unit F of KUBICA (1985, 1992) and to layer m (sensu BĄBEL 1996, 1999b), occurring at approximately the same level within allochthonous unit in Poland. As in the case of unit F and layer m in Poland, bed f1 is underlain by clay or directly covers a slightly wavy upper surface of fine-grained gypsum layers, which displays erosion and/or dissolution features. Long, parallel furrows, several cm wide and deep, presumably eroded by strong unidirectional currents, occur directly below bed f1 at Schyrets' quarry and Odaiv (Pl. 6, Fig. 2; Appendix, Figs 13A-B). Bed f1 is about 6 cm-thick and is a very massive selenite crust composed of characteristic conical crystals with morphology and growth structures formed by 'slice-like subcrystals' (see BĄBEL 1987; 1991, pl. 2, fig. 3b; 1999a, fig. 5A). These growth structures are the same as in the giant intergrowths (unit A); however, the crystals do not create intergrowths, albeit they resemble the component crystals of these giant forms. Bed f1 shows a similar fabric and crystal morphology to the palisade selenite layer occurring at the base of gypsum sequences on the Miechów Upland (e.g. at Racławice; Appendix, Fig. 16A; BĄBEL 1991, pl. 2, figs 4-5; pl. 7, fig. 16; ROMAN 1998). The top of bed f1 is a dissolution surface. Bed f2 is a selenite bed similar to f1 but thicker. It contains longer, slightly curved crystals, similar to those from f1, and gypsum microbialite deposits. Bed f2 is covered with a discontinuous layer of clay-gypsum deposits. Bed f3 comprises clusters of typical sabre crystals (see BĄBEL 1999a, figs 5B-C) forming selenite nucleation cones, 0.5-1 m in size (PERYT 1996, see also DRONKERT 1985).

Interpretation: The selenite sequence f1-f3 marks a period of re-establishment of the selenite pan environment in the depositional area of the microcrystalline gypsum facies, which formerly occupied nearly the whole margin of the basin.

Before deposition of selenite beds f1-f3, the saline pans on the basin margin contained calcium-depleted brines or low-salinity waters which only in some areas were able temporarily to precipitate fine-grained gypsum and halite (ROSELL & *al*. 1998, BĄBEL 2005 in press). The peculiar character of these waters or brines, and a low content of calcium ions in particular (BĄBEL 1999b), were responsible for the predominantly clastic deposition in the microcrystalline facies.

Crystallisation of selenite beds f1-f3 was preceded by basin-wide emersion, pedogenesis, local karst and the deposition of sheet-flood clay and clastic gypsum. Ca-depleted water disappeared from the basin margin; it evaporated, seeped into the substrate or drained into deeper areas of the basin as in the lowstand scenario in a salina basin discussed by BĄBEL (2004a, fig. 3). After this emersion, the area was re-connected with the source of new calcium sulphate-enriched brines required for renewed selenite crystallisation. The furrows found below bed f1 at Schyrets' and Odaiv can be interpreted as products of rill erosion during rapid floods of the new brines. After the abrupt rise in water level, brine stratification and a monomictic-polymictic hydrologic regime in the large perennial saline pan became gradually established and selenite deposition started again.

Selenite sequence f1-f3 represents a series of depositional events related to synchronous hydrologic changes, fluctuations in water level and average pycnocline level similar to those in the h1-h3 and b1-b6 sequences (see Text-fig. 5). The f1-f3 beds are also isochronous or near-isochronous.

In the vertical sequence f1-f3, the various crystallographic, growth and morphologic features of the selenite crystals are the same as in the selenite units A to D. It follows that selenites f1-f3 presumably grew in brine having a similar evolution to that obtaining during the deposition of units A-D. This evolution is recorded within a much thinner interval and probably also represents a shorter time interval. Bed f3 passes upward into microcrystalline facies, marking a return to the Ca-depleted brine conditions on the basin margin, as previously after the deposition of unit D (BĄBEL 1999b).

Isochronous surface F1: It is placed at the base of selenite bed f1 and the base of selenite-gypsum microbialite bed m1 in the Nida area (Pl. 6, Figs 1-2; Appendix, Figs 12-13; BĄBEL 1999b).

Isochronous event: It is defined by the establishment of the conditions for permanent gypsum crystallisation on the bottom of the saline pan after the flood of calcium sulphate-enriched brine.

Orange dust marker beds

Description: Orange dusty 'non-plastic' mud (marked Tb in Pl. 2, Figs 1-2; Pl. 3, Fig. 1; and T in Appendix, Figs 6, 8-18) commonly fills in the hollows among the apices of selenite crystals and is incorporated into grass-like selenite beds. It forms a kind of the discontinuous wavy laminae 0.1-3 mm thick. In some places, the laminae contain mainly fine-grained gypsum coloured pale orange by some dispersed material. The bottom and top surfaces of the laminae are relatively sharp and the mud does not show lamination or graded bedding. The mud is similar in colour and appearance to the Badenian tuffites recognised in selenite gypsum by KUBICA (1992, fig. 20). The mud differs from the grey clay intercalations common in gypsum because it is devoid of calcium carbonate (see KUBICA 1992, p. 34). There are no traces of dissolution below the orange mud, whereas grey clay commonly covers dissolution surfaces. Similar orange mud laminae occur in microbialite and microcrystalline gypsum facies, but were not recognised within the giant intergrowths and sabre gypsum facies (Appendix, Figs 4-18).

Interpretation: The mud is interpreted as aeolian dust or, alternatively, as a pyroclastic ash deposit. Aeolian or pyroclastic dust covered the grass-like selenite crystals growing at the bottom of the shallow pan during temporary emersions (Text-fig. 5). The dust was buried when the brine re-flooded the bottom and gypsum crystallisation started again.

Similar orange mud laminae do not occur in the giant- and coarse-crystalline selenite beds typical of deep pans because the dust was not able to settle through the dense, deep and stratified brine. Such dust was transported in the upper water mass and along the pycnocline and dispersed along the shoreline of the pans (see SONNENFELD 1984, pp. 250-253; SONNENFELD & HUDEC 1985). The deposition of aeolian dust particles directly at the bottom of the pan in brine only a few decimetres deep is difficult because the particles are commonly transported in suspension in wind-driven brine sheets and deposited on the marginal evaporite flats from the sinking brines (LONGMORE & *al*. 1986).

Pyroclastic laminae or tuffites are common in the Badenian evaporites (see KRACH 1956, BOBROVNIK 1962, KAMIEŃSKI & GLIŃSKA 1966, DZHINORIDZE & RAEVSKIY 1977). WYSZYŃSKI (1937) recognised seven tuffite laminae within clays intercalated in the middle part of the gypsum and anhydrite deposits N of Stryi. Similar tuffites were found in a borehole core from nearby Opary (KORENEVSKIY & *al*. 1977, p. 67), at Korshiv-Ispas 1 (GURZHIY 1969, p. 112), and at Cherche (KUDRIN 1960). KUBICA (1992) found two to three tuffite layers in the lower autochthonous gypsum unit and up to seven in the upper allochthonous unit. At Wieliczka salt mine only three thin tuffite layers were recognised (WIEWIÓRKA 1979, BUKOWSKI 1999). Abundant Badenian tuffite layers occur directly above and below the evaporites and are used for isochronous stratigraphic correlations (BOBROVNIK 1957, GURZHIY 1969, ALEXANDROWICZ 1997, BUKOWSKI 1999).

Isochronous surfaces Tb, Td *and isochronous events*: Only the orange mud laminae present within bundles of selenite marker beds were chosen as isochronous surfaces (Tb, Td; see Text-figs 4-5, Pl. 2, Figs 1-2; Pl. 3, Fig. 1; Appendix, Figs 3, 8-10) because they are the most easily recognisable and most useful for correlation. The laminae presumably represent aeolian or pyroclastic dust falls which are typical short isochronous events.

Marker bed c

Description: 1-45 cm thick (30 cm on average) layer of fine-grained, snow white to grey, and in places yellow to honey-coloured gypsum appears in a consistent position within the gypsum sections in nearly the whole basin (Text-fig. 4; Pl. 2, Figs 1-2; Pl. 4, Figs 1-2; Appendix, Figs 3, 6A, 8-10, 15A, 18A). The layer commonly shows crenulated microbialite lamination (BĄBEL 1999a, pl. 6, fig. 1), or homogeneous fabric typical of alabastrine facies (PERYT 1996). In some areas a porphyroblastic variety of gypsum is present (Pl. 4, Fig. 2). The base of the layer is not sharp: fine-grained gypsum covers small 'grass-like' selenite lacking dissolution or erosion features. Only locally in the southern Nida area and at Kobeřice is the layer underlain by clay. A 0-5 cm (maximum 20 cm) thick cover of non-laminated dark-grey clay or gypsum-clay deposit occurs at the very sharp top of this layer throughout the entire basin. In the eastern area of the basin, bed c thins and locally disappears, and there only this thin clay layer or discontinuity surface enables correlation (Appendix, Figs 9, 18A). The gypsum below this clay layer or discontinuity is commonly porphyroblastic, yellow-coloured, and contains an admixture of calcium carbonate (Pl. 4, Fig. 2). The clay is commonly overlain with fine-grained microbialite gypsum which in many areas forms two to three thin layers designated as the marker beds d1 and d1' described below (Text-figs 4-5; Pl. 2, Figs 1, 3; Appendix, Figs 6A, 8-10). In the other places, laminated to nodular alabastrine and clastic gypsum occur instead of these beds. In some places, small, flat-bottomed channels are cut into the top surface of bed c, and millimetre to centimetre-size fine-grained gypsum clasts, as well as rounded redeposited crystals, form a kind of lag on this surface (e.g. at Oleshiv S1; Appendix, Fig. 8D). Between the Seret and Zbruch rivers (Text-fig. 2B), the clay overlying layer c is up to 20 cm-thick, locally shows current ripple cross-lamination, and is enriched in tuffaceous material ('bentonitic clay': KLIMCHOUK & *al*. 1995, TURCHINOV 1999).

The correlative value of this layer was recognised by many authors. The bed was first recognised in the Nida area ('key layer': AKERMAN & NIELUBOWICZ 1951; 'fine-grained gypsum layer': NIELUBOWICZ 1961; 'alabaster layer': KRAJEWSKI 1962, p. 86; 'white layer': BOBROWSKI 1963, p. 10). It was designated by WALA as 'layer Ic' (WALA 1961), 'layer c' (WALA 1962, fig. 1; 1963), and then as the formal lithostratigraphic unit (layer) 'alabaster from Gartatowice' (WALA 1980; Appendix, Fig. 6A). Bed c was also noticed in borehole cores in the northern Carpathian Foredeep by KUBICA (1985, p. 41; 1992, p. 24) and was documented along the northern margin of the Foredeep up to the environs of Ivano-Frankivs'k by KASPRZYK (1989a, 1993, figs 3-6 and other papers; 1995a). Bed c was noticed in the Kobeřice area (MÁTL 1981, p. 247; PERYT & *al*. 1997a, b; 1998), and in many Ukrainian outcrops by PERYT (1996, and other papers) and BĄBEL & *al*. (1998). It was redefined as marker bed '1' by PERYT (2001, fig. 10).

Interpretation: Bed c was deposited on a semi-emerged evaporite shoal covered with microbial mats (KASPRZYK 1993; BĄBEL 1996, 1999a) and subjected in some areas to pedogenesis (Text-fig. 5). The shoal was periodically inundated with brine and the microbial mats were encrusted with gypsum and cemented during salinity rises. Homogeneous alabastrine and porphyroblastic gypsum varieties present in bed c could be a product of direct surface or subsurface precipitation from brine sheets (cf. LOGAN 1987, p. 24; PERYT 1996), or be a result of 'meteoric' or vadose diagenesis or pedogenesis (gypsum dissolution and re-precipitation) promoted by rains or run-off water floods (cf. WARREN 1982, MAGEE 1991). In particular, laterally persistent horizons of gypsum porphyroblasts may indicate brine level at the sediment surface (AIGNER & BACHMANN 1989, with references; cf. ARAKEL 1980). It is also possible that subsequently dissolved ephemeral halite crusts or efflorescents could have partially dehydrated an underlying gypsum layer. When the next refreshment occurred, the subsequent hydration produced the alabastrine gypsum (B.C. SCHREIBER, personal communication, October, 2003). The clay, clastic gypsum, and dissolution features found at the top of bed c throughout the basin suggest basin-wide brine dilution probably caused by rains. The clay and clastic gypsum were deposited mainly from meteoric water sheet floods. The top of bed c was subjected to pedogenesis, especially in the eastern area of the basin. Termination of evaporite gypsum precipitation could also have been connected with a cut-off from the source and supply of calcium sulphate-saturated brine into the shoal. When the climate became more arid again the progressive evaporite concentration led to a salinity rise and to renewed deposition of gypsum microbialites on evaporite shoals or in ephemeral pans (beds d1, d1').

Isochronous surface C/D: It is placed at the base of the first clay intercalation or first discontinuity surface at the top of the fine-grained gypsum forming bed c (Text-fig. 4-5; Pl. 2, Figs 1-3; Pl. 4, Figs 1-2; BĄBEL 1996, 1999b).

Isochronous event: It is defined by the onset of basin-wide non-deposition and/or erosion following continuous deposition of fine-grained gypsum (gypsum microbialites) on a vast, flat evaporite shoal. This event was connected with a hydrologic change from the brine-covered or brine-soaked shoal (with the brine saturated in calcium sulphate), into a shoal covered with brackish or meteoric water derived mainly from rains. The event was isochronous or near-isochronous because of the extremely gentle relief.

Remarks: One undesignated alabaster marker bed, very similar to bed c but thinner and less continuous, appears commonly about 1 m below bed c between the Nida area and Baranów Sandomierski in Poland (KUBICA 1992, p. 24). This 0-20 cm thick bed is also covered with clay

(Appendix, Fig. 6, BĄBEL 1999b, fig. 2). A similar bed (or two to three beds) appears locally below bed c at Kobeřice (Appendix, Fig. 15A; PERYT & *al*. 1997a, b). This bed can be roughly correlated with the thick fine-grained microbialite gypsum layer occurring between unit A and marker bed b1 in Ukraine. The alabaster bed can represent a basin-scale shallowing event. The other undesignated alabastrine-porphyroblastic marker bed recognised within unit B in Ukraine (at Pisky, Oleshiv and Palahychi; Appendix, Fig. 10) can also record a similar shallowing and emersion.

Microbialite marker beds

Description: Three 3-8 cm thick, laterally continuous layers of gypsified microbial (cyanobacterial) mats (designated d1) occur just above the clay or discontinuity surface C/D in Ukraine (Text-fig. 4-5; Pl. 2, Figs 1, 3; Appendix, Figs 3, 8-10). Similar layers (d1') appear in the Nida area (Appendix, Fig. 6A). The other microbialite marker beds designated m1 and l1 occur within the upper allochthonous unit in the Nida area (Appendix, Figs 12A, 13A, 16B; BĄBEL 1996; 1999b, pl. 4, fig. 2). All these layers show characteristic crinkled to wavy lamination, which enables their recognition in the field (cf. SHAPIRO & AWRAMIK 2000). This lamination reflects the specific morphology of microbial mats preserved due to their encrustation with tiny gypsum crystals. Some microbialite laminae show a characteristic colour that can be useful for correlation over distances of several kilometres (see symbol no. 38 in Key to symbols in Appendix, Fig. 7, and Appendix, Figs 8D, 8E).

Interpretation: The beds represent specific depositional events associated with the development and gypsification of microbial mats on a flat semi-emerged evaporite shoal or in a very shallow ephemeral pan (except for bed l1, deposited under permanent cover of brine; see BĄBEL 1996). The events presumably required periodic fluctuations in salinity at the beginning of the gypsum saturation stage. Salinity falls favoured the development of specific mat-forming benthic microbial (cyanobacterial) communities, whereas salinity rises led to gypsification of the accreted mats (BĄBEL 1999a, 2004a). The uniform conditions; extremely flat morphology and the identical brine properties favoured the growth of morphologically similar microbial mats, as in the case of the salinity-defined zones of the tidal flats in Abu Dhabi and Sri Lanka (KENDALL & SKIPWITH 1968, GUNATILAKA 1975). Ancient carbonate environments supply examples of individual microbialite beds which continue over distances of more than a hundred kilometres (e.g. HOFFMAN 1967).

Marker bed h

Description: A laterally continuous, 10-50 cm thick intercalation of clastic-microbialite (pedogenic?) gypsum and clay is present in the middle part of unit C-D composed of thick-bedded sabre gypsum facies with vertical crystals (Text-fig. 4; Pl. 5, Fig. 2; Appendix, Figs 3, 6B, 16A, 17). The top of the underlying sabre gypsum bed is commonly eroded and dissolved (corroded). The clastic clay-gypsum sediments display wavy laminations and show features of current deposition (e.g. at Chwałowice and Luchyntsi; Appendix, Figs 6B, 17A) or are homogeneous. Nodular alabastrine gypsum is locally present. Bed h was distinguished in the Nida area by WALA (1962, 1963, 1979; see also KASPRZYK 1994a, figs 3-4; BĄBEL 1999b, fig. 2). It was correlated in borehole cores along the northern margin of the basin up to the environs of Ivano-Frankivs'k by KASPRZYK (1989a, 1993, 1995a) and further east in many outcrops up to Odaiv by PERYT (1996) and PERYT & *al*. (1998). Bed h was redefined as marker bed '2' by PERYT (2001, fig. 10), who correlated this bed with some limestone intercalations occurring in gypsum in the eastern area of the basin (Appendix, Fig. 11A).

Interpretation: Bed h represents interruption of continuous selenite deposition in a deep monomictic and occasionally meromictic pan due to rapid shallowing (cf. KASPRZYK 1993) and destruction of its hydrologic structure, namely a transformation into polymixis characterised by lack of a seasonal or constant pycnocline (see BĄBEL 2004a). The fall in water level progressed to possible emersion and/or restriction in the supply of calcium sulphate-saturated brine to the depositional area. This restriction contributed to the brine dilution. The fall in water level was caused by evaporitic drawdown of the saline pan and/or drainage of its brine to other deeper areas of the basin. The microbialite and clastic gypsum comprising bed h was deposited in shallow ephemeral and temporary brackish pans or on semi-emerged evaporite shoals (cf. PERYT 2001). The clay accumulated mainly from sheet-floods of run-off water generated by rains.

Isochronous surface G/H: It is placed at the discontinuity surface at the base of layer h, below the lowermost clastic-microbialitic gypsum or clay, and directly over the tops of selenite crystals in the underlying layer (Pl. 5, Fig. 2; BĄBEL 1996, 1999b, fig. 2).

Isochronous event: The event is defined by the arrest of continuous selenite deposition in deep perennial saline pans or subbasins. The event was presumably promoted by the rapid fall in water level, and followed the modelled scenario of a lowstand condition in a salina basin (BĄBEL 2004a, figs 2-3).

High energy events

Two types of basin-scale high-energy events were recognised in the sections studied.

The first one is the deposition of unique gypsum stromatolitic domes composed of 'clastic' gypsum grains (see Appendix, symbols no. 19 and 25 in Key to symbols in Fig. 7, and Figs 6A, 10A-B; BĄBEL 1999a, pl. 7, fig. 2). They differ from the commonest gypsum microbialites, which are created by in situ gypsification of microbial mats in a low-energy environment (see BĄBEL 1996). The gypsum domes accreted by trapping and binding of gypsum grains by cyanobacterial mats, alternatively with mat gypsification and the growth of thin selenite crusts, in a way described by BĄBEL (1999a). These stromatolites were found in the northern Nida area in Poland (KWIATKOWSKI 1970, 1972; BĄBEL 1999a, b) and in the environs of Rohatyn in Ukraine. Both occurrences appear within the same interval of the section: 1.5-3.5 m above marker bed c (Appendix, Figs 6A, 10A-B). The appearance of these unique stromatolites was controlled by specific local conditions (e.g. HOFFMAN 1967; SHAPIRO & AWRAMIK 2000) and was probably diachronous (see sections in the Nida area). These stromatolites recorded a series of depositional events related to frequent strong storms and wind waves sweeping gypsum grains over the microbial (cyanobacterial) domes covering the leeside shoals of the shallow saline pans.

The other high-energy events are recorded at Zavallia and Kudrintsy, and are represented by 0.1-0.3 m thick gypsarenite layers sandwiched within gypsified microbial mat deposits (and porphyroblastic gypsum) typical of the flat semi-emerged evaporite shoals (Appendix, Fig 18B). The wave and current ripples on the top surfaces of the gypsarenite suggest a tempestite origin of these layers. The events were probably connected with strong wind tides and stormy weather. Brine was pushed by wind from saline pans onto surrounding flat evaporite shoals, and the soft, loose gypsum substrate was reworked by storm waves and currents (cf. AIGNER & BACHMANN 1989). The cover of clastic gypsum was deposited during the waning phase of the storm and created a local marker bed.

CYCLIC SEDIMENTATION

The Badenian gypsum deposits show evidence of cyclic sedimentation at various scales. Growth zoning of gypsum crystals, lamination of gypsum microbialites and the pattern of layering of selenite beds are the most noticeable features. The salina model of sedimentation (BĄBEL 2004a, b) suggests the following possible reasons for the cyclicity.

Millimetre-scale crystal growth zoning in selenite beds constitutes the lowest-order cyclicity. It seems that the zones recorded mostly seasonal (year, month, weeks) periods of mixis in stratified monomictic (to polymictic) pans, as discussed before. It is likely that some very regular zoning reflected an annual cycle, with each growth zone representing mixis associated with a dry season lowstand (BABEL 2004a).

Lamination of gypsified microbial (cyanobacterial) mats is another type of the lowest-order cyclicity. The lamination could reflect periodic floods of brine sheets on evaporite shoals, followed by gypsification of cyanobacterial mats, like in the wet majanna flats in the MacLeod salina in Australia (LOGAN 1987). Such floods could have been driven by winds or by the temporary fluctuations (rises) in water level that are characteristic of any salina basin. Alternatively, the lamination could reflect a seasonal cycle of gypsification of cyanobacterial mats covering the margins of a monomictic-polymictic pan. Such gypsification could take place during a period of mixis, exactly like in the case of the growth zones of selenite beds. Annual cycles of gypsum precipitation and cyanobacterial mat growth were observed in the monomictic Solar Lake in Sinai (ECKSTEIN 1970, COHEN & *al*. 1977).

The centimetre- to metre-scale layering of selenite beds can be generally interpreted as a reflection of fluctuations in the water level and average pycnocline level in saline pans occupying a salina basin. This interpretation follows the models for selenite deposition developed earlier (BĄBEL 2004a, figs 6-7; cf. HARDIE & EUSTER 1971, fig. 24) and environmental reconstructions of selenite facies by other authors (e.g. WARREN 1982, and references in BĄBEL 2004a). The suggested interpretation assumes that, in the relatively shallow water and flat-bottomed pans, these fluctuations could produce sequences of isochronous or near-isochronous selenite marker beds reflecting periods of the average pycnocline 'highstand' (see Text-fig. 5). In the deeper pans, with the large bottom areas staying permanently below the pycnocline, the accretion of selenites was continuous and they did not record the small-scale fluctuations in water level and pycnocline level that were recorded in the shallow pans.

Thus, the vertical sequence of the units: A-B-C-D (giant-gypsum intergrowths [unbedded or thick-bedded selenites]/grass-like gypsum [thin-bedded selenites]/sabre-gypsum [thick-bedded selenites]; Text-figs 3-4) is interpreted as reflecting large-scale fluctuations in water level in a salina basin: highstand/lowstand/highstand cycle. The distribution of the bedding suggests that the lower-order water-level changes are superimposed on this larger cycle. The smallest-scale changes were recorded only in the lowstand grass-like facies, whereas they are not visible in the in the giant intergrowths and sabre facies. The thickest (15-30 cm), laterally continuous selenite beds within the grass-like facies (unit B) appear to occur in separate bundles (such as selenite sequence b1-b6; Text-fig. 4; Pl. 2, Figs 1-3), showing patterns involving some repetition of beds ('stacking patterns' or 'stratification cycles'; see SCHWARZACHER 2000), suggesting that they perhaps recorded some subordinate larger rises in water level and pycnocline level during the general lowstand (cf. Text-fig. 5). Some subordinate larger-scale fluctuations are recorded by 0.4-1.5 m layering intervals in the sabre facies. The apparent and laterally extensive discontinuities between the main sabre gypsum layers within unit C-D (e.g. Appendix, Fig. 17) could represent some larger drops in pycnocline level and water level during a more general highstand. The lack or scarcity of such layering in the giant intergrowths (the lower and middle part of unit A; Appendix, Figs 6A, 8, 15A) can be explained either by a lack of similar drops in pycnocline level and water level, or by deposition in relatively deeper brine than in the case of the sabre gypsum unit, i.e. permanently below the average pycnocline level. Rapid drops in water level associated with relatively long-term emersions are reflected by breaks in the normal sedimentary record and are represented by intervals enriched in clay around isochronous surfaces C/D, G/H (and similarly: F1).

The nature and duration of all these presumed cyclic or periodic water level changes require further study; however, the most simple and most probable factor is climatic control. The interpretation presented above is simplified and should be treated as a working hypothesis. The suggested climate control can be complicated or even completely obliterated by changes in inflow/outflow ratio in the salina basin, as discussed in BĄBEL (2004b, with references). Nevertheless, similar cycles in many Messinian selenite basins (RICHTER-BERNBURG 1973, SCHREIBER & *al*. 1976, fig. 14; ROUCHY 1982, DRONKERT 1985, SCHREIBER 1997, ROSELL & *al*. 1998) and in lake systems around the world, (e.g. GLENN & KELTS 1991) are interpreted as climatically driven. Cycles similar to the highstand/lowstand/highstand sequence recorded by units A-B-C-D are interpreted as related to global climatic changes promoted by orbital cycles (e.g. KRIJGSMAN & *al*. 2001, ROVERI & *al*. 2004). The absence of such cycles in the eastern area of the basin, where gypsum microbialites predominate, can be explained by sedimentation on a majanna-type flat in a salina basin (BĄBEL 2005 in press).

FINAL REMARKS

In this paper, the event stratigraphic and high-resolution methodology was applied to the primary shallow-water gypsum deposits of a large salina-type basin comprising mainly evaporite shoal facies (represented typically by fine-grained gypsum) and saline pan facies (represented by selenites). This approach has revealed some new possibilities in isochronous correlation of such evaporite deposits.

In the basin studied, some individual beds were correlated precisely over distances of tens to hundreds of kilometres, albeit they were deposited in very shallow to semi-emerged environments (0-5 m in depth) susceptible to erosion. Such bed-by-bed correlation was possible because of the extremely gentle depositional relief in the basin and the specific type of evaporite deposition, typical of the salina basins, which was aggradation, i.e. vertical accretion of gypsum sediments, controlled mainly by water level, water-table level and by fluctuations in the average pycnocline level (WARREN 1999). Due to the flat relief, the changes in water level or pycnocline level were recorded nearly instantaneously throughout the area. Such fluctuations can be very rapid in a salina basin (especially in comparison with typical sea-level changes) and therefore the depositional or erosional record of such short events can be used for isochronous or near-isochronous correlation.

The individual selenite beds, in particular, were correlated over great distances and were interpreted as isochronous or near-isochronous deposits. The best for correlation were thin (5-30 cm) selenite beds with intercalations of fine-grained gypsum (commonly creating grass-like structures), which represent deposits of the evolving shallow and flat-bottom saline pans. Each selenite bed is a record of the average pycnocline level highstand whereas the intercalated fine-grained gypsum represents a pycnocline and water level drop or emersion. In contrast to these well-bedded, grass-like selenites, the metres-thick, poorly-bedded selenite units with scarce dissolution surfaces and fine-grained gypsum intercalations do not show precise bed-by-bed correlation in the basin. These selenites were deposited in deeper saline pans in which the average pycnocline level drops were recorded by bedding planes (i.e. by intercalations of fine-grained gypsum or dissolution surfaces) only in the shallow slope areas or swells (BĄBEL 1999a, fig. 3). In the deeper parts of these pans, permanently below the average pycnocline level, the continuous gypsum crystal growth did not produce any pronounce bedding. Nevertheless, the growth zoning in crystals from such selenite beds can be correlated throughout the basin and used for precise isochronous correlation in the same manner as varves or tree-rings.

Precise long-distance correlation is known from several different evaporite basins (e.g. AIGNER & BACHMANN 1989); so far the most precise isochronous high-resolution correlation was achieved within laminated sulphates that were presumably deposited in relatively deep meromictic basins below the permanent pycnocline level (RICHTER-BERNBURG 1985, KIRKLAND 2003). The present paper demonstrates that similar correlation is possible in the gypsum evaporites representing the very shallow environments of a salina basin: saline pans no more than a few metres deep and semi-emerged evaporite shoals. The best deposits for isochronous correlation are the primary selenite deposits.

Acknowledgements

This publication would not have been possible without the help of Andrii BOGUCKI, University of Lviv, whose encouragement, experience, organisational support and direct assistance in the field permit effective fieldwork during a dozen or so expeditions to Ukraine in 1994-2002. I am greatly indebted to families: BIALKOVS'KII from Melnitsa Podilska, IVAS'KEVICH from Burshtyn, MADER from Chortkiv, NAVAL'KOVSKII from Horodenka, DMYTRUK from Kalush, TYCHOLIZ from Tlumach, PIKOV'SKII from Bedrykivtsi, whose hospitality and organisational help enabled me to carry out my fieldwork in vast areas of gypsum exposures in Ukraine. I also thank Viktor BULHAKOV, Yaroslav and Roman DMYTRUK, Hala and Vasyl TYCHOLIZ, Katerina VINDHOL'TS, Svitlana VIZNA, Petro VOLOSHIN, and Andrii YATSYSHYN for assistance in the field. In particular, I thank the speleologists Sergei EPIFANOV from Ternopil, Volodymyr GALAICHUK from Borschiv and Igor MALAVSKII from Lviv, for guidance and assistance in visiting gypsum caves in Podillia, as well as Pavel KONEČNÝ, Petro MARTINEC and Anna ŚWIERCZEWSKA – for help in visiting the Kobeřice quarry in Czech Republic. Sofia HRYNIV, Stepan KORIN, Volodymyr KOVALEVICH, Genadii PANOV, Oleg PETRICHENKO, Borys SEREBRODOLSKII, Igor TURCHINOV supplied valuable information concerning the geology of the Badenian gypsum deposits in Ukraine. Finally I thank the reviewers of this paper, Andrzej GĄSIEWICZ, Stefano LUGLI, B. Charlotte SCHREIBER, Ireneusz WALASZCZYK, and Christopher J. WOOD for their valuable comments and correction of the English, which greatly improved this text. This research was supported by the Polish Scientific Committee (KBN) grant 6 P04D 038 09 realised in 1996-1998 and by funds of the Institute of Geology of the University of Warsaw.

REFERENCES

AIGNER, T. & BACHMANN, G.H. 1989. Dynamic stratigraphy of evaporite-to-red bed sequence, Gipskeuper (Triassic), southwest German Basin. *Sedimentary Geology*, **62**, 5-25.

AKERMAN, K. & NIELUBOWICZ, R. 1951. Short description of principal industrial gypsum and anhydrite beds in Poland. *Przemysł Chemiczny*, **7**, 537-544. [*In Polish with English abstract*]

ALEXANDROWICZ, S.W. 1997. Lithostratigraphy of the Miocene deposits in the Gliwice area (Upper Silesia, Poland). *Bulletin of the Polish Academy of Sciences*, *Earth Sciences*, **45**, 167-179.

ANDERSON, A.T.JR. 1984. Probable relations between plagioclase zoning and magma dynamics, Fuego Volcano, Guatemala. *American Mineralogists*, **69**, 660-676.

ANDERSON, R.Y., DEAN, W.E., BRADBURY, J.P. & LOVE, D. 1985. Meromictic lakes and varved lake sediments in North America. *U.S. Geological Survey Bulletin*, **1607**, 1-18.

ANDREYEVA-GRIGOROVICH, A.S., OSZCZYPKO, N., SAVITSKAYA, N.A., ŚLĄCZKA, A. & TROFIMOVICH, N.A. 2003. Correlation of Late Badenian salts of the Wieliczka, Bochnia and Kalush areas (Polish and Ukrainian Carpathian Foredeep). *Annales Societatis Geologorum Poloniae*, **73**, 67-89.

ARAKEL, A.V. 1980. Genesis and diagenesis of Holocene evaporitic sediments in Hutt and Leeman Lagoons, Western Australia. *Journal of Sedimentary Petrology*, **50**, 1305-1326.

BĄBEL, M. 1987. Giant gypsum intergrowths from the Middle Miocene evaporites of southern Poland. *Acta Geologica Polonica*, **37**, 1-20.

— 1991. Crystallography and genesis of the giant intergrowths of gypsum from the Miocene evaporites of Poland. *Archiwum Mineralogiczne*, **44**, 103-135. Warszawa.

— 1996. Wykształcenie facjalne, stratygrafia oraz sedymentacja badeńskich gipsów Ponidzia. *In*: P.H. KARNKOWSKI (*Ed*.), Analiza basenów sedymentacyjnych a nowoczesna sedymentologia. Materiały **5** Krajowego Spotkania Sedymentologów, pp. B1-B26. Warszawa.

— 1999a. Facies and depositional environments of the Nida Gypsum deposits (Middle Miocene, Carpathian Foredeep, southern Poland). *Geological Quarterly*, **43**, 405-428.

— 1999b. History of sedimentation of the Nida Gypsum deposits (Middle Miocene, Carpathian Foredeep, southern Poland). *Geological Quarterly*, **43**, 429-447.

— 1999c. Two possible saline cyclothems in the Badenian evaporites of the Carpathian foreland basin. *Biuletyn Państwowego Instytutu Geologicznego*, **387**, 87-88.

— 2000. Anisotropic development of equivalent gypsum crystal faces promoted by chiral organic compounds. *In*: N.P YUSHKIN, V.P. LUTOEV, M.F. SAMOTOLKOVA, M.V. GAVRILIUK & G.V. PONOMAREVA (*Eds*), Mineralogy and life: biomineral homologies. **3** International Seminar "Mineralogy and life", pp. 132-133. *Geoprint*; Syktyvkar.

— 2004a. Models for evaporite, selenite and gypsum microbialite deposition in ancient saline basins. *Acta Geologica Polonica*, **54**, 219-249.

— 2004b. Badenian evaporite basin of the northern Carpathian Foredeep as a drawdown salina basin. *Acta Geologica Polonica*, **54**, 313-337.

— 2005 in press. Selenite - gypsum microbialite facies and sedimentary evolution of the Badenian evaporite basin of the northern Carpathian Foredeep. *Acta Geologica Polonica*, **55**.

BĄBEL, M. & BOGUCKIY, A. 1999. Basin-wide isochronic correlation of the Badenian shallow-water gypsum strata in Ukraine, Poland and the Czech Republic. *Biuletyn Państwowego Instytutu Geologicznego*, **387**, 89-90.

BĄBEL, M., BOGUCKIY, A. & VOLOSHIN, P. 1998. Isochronic correlation of the Miocene evaporites of Carpathian Foredeep over a distance of several hundred kilometres. *In*: **15** IAS Congress (Alicante, Spain), Abstracts, pp. 161-162. *Publicaciones de la Universidad de Alicante*, *Compobell*, *S.L.*; Murcia.

BJÖRCK, S., WOHLFARTH, B. & POSSNERT, G. 1995. [14]C AMS mesurements from the Late Weichselian part of the Swedish Time Scale. *Quaternary International*, **27**, 11-18.

BOBROVNIK, D.P. 1957. Volcanic tuffs revealed in some places of the South-Western borders of the Russian platform. *Geologicheskiy Sbornik Lvovskovo Geologicheskovo Obshchestva* [*Geological Review of the Lvov Geological Society*], **4**, 143-154. [*In Russian*]

— 1962. Mineralogy of gypsum-anhydrite from the sulphur deposits in the Precarpathians. *Mineralogical Sbornik*, *Lvov Geological Society*, **16**, 261-272. [*In Russian with English summary*]

BOBROWSKI, W. 1963. Gypsum in the eastern bank of the Nida river valley. *Biuletyn Instytutu Geologicznego* (not numbered), pp. 1-29. [*In Polish with English summary*]

BUKOWSKI, K. 1999. Comparison of the Badenian saliferous series from Wieliczka and Bochnia in the light of new data. *Prace Państwowego Instytutu Geologicznego*, **168**, 43-56. [*In Polish with English summary*]

CATUNEANU, O. 2002. Sequence stratigraphy of clastic systems: concepts, merits, and pitfalls. *Journal of African Earth Sciences*, **35**, 1-43.

CODY, A.M. & CODY, R.D. 1991. Chiral habit modification of gypsum from epitaxial-like adsorption of stereospecific growth inhibitors. *Journal of Crystal Growth*, **113**, 508-519.

COHEN, Y., KRUMBEIN, W.E., GOLDBERG, M. & SHILO, M. 1977. Solar Lake (Sinai). 1. Physical and chemical limnology. *Limnology and Oceanography*, **22**, 597-608.

D'ARGENIO, B., FERRERI, V., RASPINI, A., AMODIO, S. & BUONOCUNTO, F.P. 1999. Cyclostratigraphy of a carbonate platform as a tool for high-precision correlation. *Tectonophysics*, **315**, 357-384.

DRONKERT, H. 1985. Evaporite models and sedimentology of Messinian and Recent evaporites. *GUA Papers of Geology*, Ser. **1**, No. **24**, 1-283. Utrecht.

DZHINORIDZE, N.M. & RAEVSKIY, V.I. 1977. Basic peculiarities of the Tortonian salt formation of the Carpathian region. *In*: A.L. YANSHIN & M.A. ZHARKOV (*Eds*), Problems of salt formation, v. **1**, pp. 257-261. *Nauka*, *Sibirskoe Otdelenie*; Novosibirsk. [*In Russian*]

ECKSTEIN, Y. 1970. Physicochemical limnology and geology of a meromictic pond on the Red Sea shore. *Limnology and Oceanography*, **15**, 363-372.

EINSELE, G. 1998. Event stratigraphy: recognition and interpretation of sedimentary event horizons. *In*: P. DOYLE & M.R. BENNETT (*Eds*), Unlocking the stratigraphical record: Advances in modern stratigraphy, pp. 145-193. *John Wiley & Sons Ltd*.; Chichester.

EINSELE, G., CHOUGH, S.K. & SHIKI, T. 1996. Depositional events and their records – an introduction. *Sedimentary Geology*, **104**, 1-9.

ERNST, G., SCHMID, F., SEIBERTZ, E., KELLER, S. & WOOD, C.J. 1983. Event-Stratigraphie im Cenoman und Turon von NW-Deutschland. *Zitteliana*, **10**, 531-554. München.

FERSMAN, A.J. 1919. On mineralogical and geological investigations of the Saki lake. *In*: D.S. BELYANKIN (*Ed*.), Academician A. J. Fersman, Collected works, v. **1**, pp. 809-822. *Izdatelstvo Akademii Nauk USSR*; Moscow 1952. [*In Russian*]

GARLICKI, A. 1968. Autochthonous salt series in the Miocene of the Carpathian Foredeep, between Skawina and Tarnów. *Biuletyn Instytutu Geologicznego*, **215**, 5-77. [*In Polish with English summary*]

— 1979. Sedimentation of Miocene salts in Poland. *Geological Transactions* [*Prace Geologiczne*, *Polska Akademia Nauk*, *Oddział w Krakowie*], **119**, 1-67. [*In Polish with English summary*]

— 1994. Comparison of salt deposits in Upper Silesia and Wieliczka (southern Poland). *Przegląd Geologiczny*, **42**, 752-753. [*In Polish with English summary*]

GĄSIEWICZ, A. & CZAPOWSKI, G. 1995. Cykliczność sedymentacji utworów ewaporatowych badenu zapadliska przedkarpackiego – dyskusja. *Przegląd Geologiczny*, **43**, 335-338.

GEISLER-CUSSEY, D. 1986. Approche sédimentologique et géochimique des mécanismes générateurs de formations évaporitiques actuelles et fossiles. Marais salants de Camargue et du Levant espagnol, Messinien mediterraneen et Trias lorrain. *Sciences de la Terre*, *Mémoires*, **48**, 1-268. Nancy.

GLENN, C.R. & KELTS, K. 1991. Sedimentary rhythms in lake deposits. *In*: G. EINSELE & A. SEILACHER (*Eds*), Cycles and events in stratigraphy, pp. 188-221. *Springer*; Berlin.

GRISSINO-MEYER, H.D. 2005. Ultimate tree-ring pages. http://web.utk.edu/~grissino/

GUNATILAKA, A. 1975. Some aspects of the biology and sedimentology of laminated algal mats from Mannar Lagoon, north-west Ceylon. *Sedimentary Geology*, **14**, 275-300.

GURZHIY, D.V. 1969. Lithology of Forecarpathian molasses, pp. 1-204. *Naukova Dumka*; Kiev. [*In Russian*]

HARDIE, L.A. & EUGSTER, H.P. 1971. The depositional environment of marine evaporites: a case for shallow, clastic accumulation. *Sedimentology*, **16**, 187-220.

HOFFMAN, P. 1967. Algal stromatolites: use in stratigraphic correlation and paleocurrent determination. *Science*, **157**, 1043-1045.

KAMIEŃSKI M. & GLIŃSKA, S. 1966. On tuffites with halite from the salt mine of Bochnia. *Archiwum Mineralogiczne*, **26**, 77-89. [for 1965] [*In Polish with English summary*]

KASPRZYK, A. 1989a. Lithology of the Miocene sulfate deposits in the Staszów region. *Kwartalnik Geologiczny*, **33**, 241-268. [*In Polish with English summary*]

— 1989b. Content of strontium in Miocene gypsum rocks of the Staszów area. *Przegląd Geologiczny*, **37**, 201-207. [*In Polish with English summary*]

— 1993. Lithofacies and sedimentation of the Badenian (Middle Miocene) gypsum in the northern part of the Carpathian Foredeep, southern Poland. *Annales Societatis Geologorum Poloniae*, **63**, 33-84.

— 1994a. Distribution of strontium in the Badenian (Middle Miocene) gypsum deposits of the Nida area, southern Poland. *Geological Quarterly*, **38**, 497-512.

— 1994b. Cyclicity of sedimentation of the Badenian evaporate deposits in the Carpathian Foredeep (southern Poland). *Przegląd Geologiczny*, **42**, 349-356.

— 1995a. Correlation of sulphate deposits of the Carpathian Foredeep at the boundary of Poland and Ukraine. *Geological Quarterly*, **39**, 95-108.

— 1995b. Cykliczność sedymentacji utworów ewaporatowych badenu zapadliska przedkarpackiego – replika. *Przegląd Geologiczny*, **43**, 339-341.

— 2003. Sedimentological and diagenetic patterns of anhydrite deposits in the Badenian evaporite basin of the Carpathian Foredeep, southern Poland. *Sedimentary Geology*, **158**, 167-194.

KASPRZYK, A. & ORTÍ, F. 1998. Palaeogeographic and burial controls on anhydrite genesis: the Badenian basin in the Carpathian Foredeep (southern Poland, western Ukraine). *Sedimentology*, **45**, 889-907.

KAUFFMAN, E.G. 1988. Concepts and methods of high-resolution event stratigraphy. *Annual Review of Earth and Planetary Sciences*, **16**, 605-654.

KAUFFMAN, E.G., ELDER, W.P. & SAGEMAN, B.B. 1991. High-resolution correlation: a new tool in chronostratigraphy. *In*: G. EINSELE & A. SEILACHER (*Eds*), Cycles and events in stratigraphy, pp. 795-819. *Springer*; Berlin.

KENDALL, C.G.S.C. & SKIPWITH, P.A.D'E. 1968. Recent algal mats of a Persian Gulf lagoon. *Journal of Sedimentary Petrology*, **38**, 1040-1058.

KHRUSHCHOV, D.P. & PETRICHENKO, O.I. 1979. Evaporite formations of Central Paratethys and conditions of their sedimentation. *Annales Géologiques des Pays Helléniques*, *Tome hors série*, No. **2**, 595-612. Athens.

KIRKLAND, D.W. 2003. An explanation for the varves of the Castile evaporites (Upper Permian), Texas and New Mexico, USA. *Sedimentology*, **50**, 899-920.

KLIMCHOUK, A.B., TURCHINOV, I.I. & ANDREJCHOUK, V.N. 1995. Structural prerequisites of speleogenesis in gypsum in the Western Ukraine, pp. 1-105. *Ukrainian Speleological Association*; Kiev. [*In Russian with English summary*]

KORENEVSKIY, S.M., ZAHAROVA, V.M. & SHAMAHOV, V.A. 1977. Miocene halogenic formations of Carpathian Foreland. *Trudy Vsesoyuznovo Nauchno-Issledovatelnovo Geologicheskovo Instituta*, *Novaya Ser*., **271**, 1-248. *Nedra*; Leningrad.

KRACH, W. 1956. The faunistic analysis of the Miocene profile in Krywałd in Upper Silesia. *Biuletyn Instytutu Geologicznego*, **107**, 123-144. [*In Polish with English summary*]

KRAJEWSKI, R. 1962. O budowie i powstaniu złoża siarki w Piasecznie. *Wszechświat*, No. **4**, 85-91. Kraków.

KREUTZ, S. 1925. Sur la protection de la nature inanimée. *Ochrona Przyrody*, No. **5**, 58-68. Kraków. [*In Polish*]

KRIJGSMAN, W., FORTUIN, A.R., HILGEN, F.J. & SIERRO, F.J. 2001. Astrochronology for the Messinian Sorbas basin (SE Spain) and orbital (precessional) forcing for evaporite cyclicity. *Sedimentary Geology*, **140**, 43-60.

KUBICA, B. 1985. The chemical series. *In*: K. PAWŁOWSKA (*Ed*.), Geology of the Tarnobrzeg native sulphur deposit. *Prace Instytutu Geologicznego*, **114**, 34-54. [*In Polish with English summary*]

— 1992. Lithofacial development of the Badenian chemical sediments in the northern part of the Carpathian Foredeep. *Prace Państwowego Instytutu Geologicznego*, **133**, 1-64. [*In Polish with English summary*]

— 1994. Lithogeophysical correlation of the Badenian chemical deposits of the Carpathian Foredeep (southern Poland). *Przegląd Geologiczny*, **42**, 759-765. [*In Polish*]

KUDRIN, L.N. 1955. The Upper Tortonian gypsum of the south-west margin of Russian Platform. *Uchenye Zapiski Lvovskovo Gosudarstvennovo Universiteta im*. *Ivana Franko*, *Ser*. *Geologicheskaya*, **35**, 129-161. [*In Russian*]

— 1960. On the Upper-Tortonian bar between the salt-bearing basin and the open sea within the limits of the south-western outlying districts of the Russian Platform. *Doklady Akademii Nauk SSSR*, **131**, 909-912. [*In Russian*]

KWIATKOWSKI, S. 1970. Origin of alabasters, intraformational breccias, folds and stromatolites in Miocene gypsum of Southern Poland. *Bulletin de l'Académie Polonaise des Sciences*, *Sér*. *Sciences Géologiques et Géographiques*, **18**, 37-42.

— 1972. Sedimentation of gypsum in the Miocene of southern Poland. *Prace Muzeum Ziemi*, **19**, 3-94. Warszawa. [*In Polish with English summary*]

LACROIX, A. 1897. Le gypse de Paris et les minéraux qui l'accompagnent (première contribution a la minéralogie du basin de Paris). *Nouvelles Archives du Muséum d'Histoire Naturelle*, *Paris*, *Sér*. **3**, **9**, 1-296.

LADYZHENSKIY, N.P. & ANTIPOV, V.I. 1961. Geological structure and gas- and oil-bearing of the Soviet Forecarpathians, pp. 1-267. *Gostoptechizdat*; Moscow. [*In Russian*]

LOGAN, B.W. 1987. The MacLeod evaporite basin, western Australia. Holocene environments, sediments and geological evolution. *AAPG Memoir*, **44**, pp. 1-140. Tulsa.

LONGMORE, M.E., LULY, J.G. & O'LEARY, B.M. 1986. Cesium-137 redistribution in the sediments of the playa, Lake Tyrrel, northwestern Victoria. II. Pattern of cesium-137 and pollen redistribution. *Palaeogeography*, *Palaeoclimatology*, *Palaeoecology*, **54**, 197-218

MAGEE, J.W. 1991. Late Quaternary lacustrine, groundwater, aeolian and pedogenic gypsum in the Prungle Lakes, southeastern Australia. *Palaeogeography*, *Palaeoclimatology*, *Palaeoecology*, **84**, 3-42.

MÁTL, V. 1981. Ložiska sádrovce opavské pánve. *Geologický Průzkum*, **23**, 346-350. Praha.

MEYERS, W.J. 1978. Carbonate cements: their regional distribution and interpretation in Mississippian Limestones of southwestern New Mexico. *Sedimentology*, **25**, 371-400.

NIELUBOWICZ, R. 1961. Remarks concerning the stratigraphy of several Miocene gypsum layers in the west zones of Subcarpathian Depression. *Cement-Wapno-Gips,* **16**/**26**, 68-77. Kraków. [*In Polish with French abstract*]

NIEMCZYK, J. 1988. Cyclothems in Miocene Evaporite Seriers on the Carpathian border between Broniszów and Mała. *Zeszyty Naukowe AGH*, **1118**, *Geologia*, *Kwartalnik*, **12**, 109-115. [for 1986] [*In Polish with English summary*]

— 1995. Geological section at Krzyżanowice near Pińczów as a base for lithostratigraphy of the Gypsum Formation of the Nida region (Southern Poland). *Geologia*, *Kwartalnik AGH*, **21**, 183-196. [*In Polish with English abstract*]

NOWAK, T.W. & POŁTOWICZ, S. 2000. Miocene deposits at Broniszów, Glinik and Mała area (the Middle Carpathians). *Geologia*, *Kwartalnik AGH*, **26**, 375-396. [*In Polish with English summary*]

NYSTUEN, J.P. 1998. History and development of sequence stratigraphy. *In*: F.M. GRADSTEIN, K.O. SANDVIK & N.J. MILTON (*Eds*), Sequence stratigraphy – concepts and applications. *Norwegian Petroleum Society*, *Special Publication*, **8**, pp. 31-116. *Elsevier*; Amsterdam.

OREN, A. 1999. Microbiological studies in the Dead Sea: future challenges toward the understanding of life at the limit of salt concentrations. *Hydrobiologia*, **405**, 1-9.

ORTÍ CABO, F., PUEYO MUR, J.J., GEISLER-CUSSEY, D. & DULAU, N. 1984. Evaporitic sedimentation in the coastal salinas of Santa Pola (Alicante, Spain). *Revista d'Investigacions Geologiques*, **38**-**39**, 169-220.

PERYT, T.M. 1996. Sedimentology of Badenian (middle Miocene) gypsum in eastern Galicia, Podolia and Bukovina (West Ukraine). *Sedimentology*, **43**, 571-588.

— 2000. Resedimentation of basin centre sulphate deposits: Middle Miocene Badenian of Carpathian Foredeep, southern Poland. *Sedimentary Geology*, **134**, 331-342.

— 2001. Gypsum facies transitions in basinal-marginal evaporites: middle Miocene (Badenian) of west Ukraine. *Sedimentology*, **48**, 1103-1119.

PERYT, T.M., HAŁAS, S., KAROLI, S. & PERYT, D. 1997a. Isotopic record of environmental changes during deposition of Badenian (Middle Miocene) gypsum at Kobeřice near Opava (Czech Republic). *Przegląd Geologiczny*, **45**, 807-810. [*In Polish with English summary*]

PERYT, T.M., JASIONOWSKI, M., KAROLI, S., PETRICHENKO, O.I., POBEREGSKI, A.V. & TURCHINOV, I.I. 1998. Correlation and sedimentary history of the Badenian gypsum in the Carpathian Foredeep (Ukraine, Poland, and Czech Republic). *Przegląd Geologiczny*, **46**, 729-732. Warszawa.

PERYT, T.M., KAROLI, S., PERYT, D., PETRICHENKO, O.I., GEDL, P., NARKIEWICZ, W., ĎURKOVIČOVÁ, J. & DOBIESZYŃSKA, Z. 1997b. Westernmost occurrence of the Middle Miocene Badenian gypsum in central Paratethys (Kobeřice, Moravia, Czech Republic). *Slovak Geological Magazine*, **3**, 105-120.

PERYT, T.M., SZAFRAN, J. JASIONOWSKI, M., HALAS, S., PERYT, D., POBEREZHSKYY, A., KAROLI, S. & WÓJTOWICZ, A. 2002. S and O isotope composition of the Badenian (Middle Miocene) sulphates in the Carpathian Foredeep. *Geologica Carpathica*, **53**, 391-398.

PETRICHENKO, O.I., PERYT, T.M. & POBEREGSKY, A.V. 1997. Pecularities of gypsum sedimentation in the Middle Miocene Badenian evaporite basin of Carpathian Foredeep. *Slovak Geological Magazine*, **3**, 91-104.

PITTET, B. & STRASSER, A. 1998. Long-distance correlation by sequence stratigraphy and cyclostratigraphy: examples and implications (Oxfordian from the Swiss Jura, Spain, and Normandy). *Geologische Rundschau*, **86**, 852-874.

POBEREZHSKYY, A.V. 2000. The physical-chemical parameters of conditions of gypsum sedimentation in the Badenian evaporite basin of the Carpathian Foredeep. *Geologiia i Geochimiia Goryuchikh Kopalyn*, **4**, 38-55. Lviv. [*In Ukrainian with English summary*]

POŁTOWICZ, S. 1993. Palinspastic palaeogeography reconstruction of Badenian saline sedimentary basin in Poland. *Zeszyty Naukowe AGH*, **1559**, *Geologia*, *Kwartalnik*, **19**, 174-178, 203-233. [*In Polish with English summary*]

PRYSJAZHNJUK, V.A. 1998. Tyrassian suite of Precarpathian region. *Geologichnii Zhurnal*, [*Geological Journal*, *National Academy of Sciences of Ukraine*], No. **1**-**2**, 130-136. Kiev.

RICHTER-BERNBURG, G. 1973. Facies and paleogeography of the Messinian evaporites on Sicily. *In*: C.W. DROOGER (*Ed*.), Messinian events in the Mediterranean, pp. 124-141. *North-Holland Publishing Company*; Amsterdam.

— 1985. Zechstein-Anhydrite. Fazies and Genese. *Geologisches Jahrbuch*, **A**, **85**, 1-85.

RODRÍGUEZ-ARANDA, J.P., ROUCHY, J.M., CALVO, J.P., ORDÓÑEZ, S. & GARCÍA DEL CURA, M.A. 1995. Unusual twinning features in large primary gypsum crystals formed in salt lake conditions, middle Miocene, Madrid Basin, Spain – palaeoenvironmental implications. *Sedimentary Geology*, **95**, 123-132.

ROMAN, A. 1998. Wykształcenie i sedymentacja badeńskich gipsów okolic Racławic na Wyżynie Miechowskiej, pp. 1-69. *MSc Thesis*; University of Warsaw.

RÖGL, F. 1999. Mediterranean and Paratethys. Facts and hypotheses of an Oligocene to Miocene paleogeography (short overview). *Geologica Carpathica*, **50**, 339-349.

ROSELL, L., ORTÍ, F., KASPRZYK, A., PLAYA, E. & PERYT, T.M. 1998. Strontium geochemistry of Miocene primary gypsum: Messinian of southeastern Spain and Badenian of Poland. *Journal of Sedimentary Research*, **68**, 63-79.

ROUCHY, J.M. 1982. La genèse des évaporites messiniennes de Méditerrannée. *Mémoires du Muséum National d'Histoire Naturelle*, *Sér*. C, *Sciences de la Terre*, **50**, pp. 1-267. Paris.

ROVERI, M., LANDUZZI, A., BASSETTI, M.A., LUGLI, S., MANZI, V., RICCI-LUCCHI, F. & VAI, G.B. 2004. The record of Messinian events in the Northern Apennines Foredeep Basins. Field trip guide book, **B19**, pp. 1-48. **32** International Geological Congress, Florence, Italy. *APAT*; Roma.

SCHREIBER, B.C. 1988. Subaqueous evaporite deposition. *In*: B.C. SCHREIBER (*Ed*.), Evaporites and hydrocarbons, pp. 182-255. *Columbia University Press*; New York.

— 1997. Field trip to Eraclea Minoa: Upper Messinian. *In*: International Conference on Neogene Mediterranean Paleoceanography (Erice, Italy), Excursion Guidebook, pp. 72-80. *Societa Geologica Italiana*, Milano; *ESCO Secretariat*, Zürich.

SCHREIBER, B.C., CATALANO, R. & SCHREIBER, E. 1977. An evaporitic lithofacies continuum: latest Miocene (Messinian) deposits of Salemi Basin (Sicily) and a modern analog. *In*: J.H. FISHER (*Ed*.), Reefs and evaporites – concepts and depositional models. *Studies in Geology*, **5**, pp. 169-180. *American Association of Petroleum Geologists*; Tulsa.

SCHREIBER, B.C., FRIEDMAN, G., DECIMA, A. & SCHREIBER, E. 1976. Depositional environments of Upper Miocene (Messinian) evaporite deposits of the Sicilian Basin. *Sedimentology*, **23**, 729-760.

SCHWARZACHER, W. 2000. Repetitions and cycles in stratigraphy. *Earth-Science Reviews*, **50**, 51-75.

SHAPIRO, R.S. & AWRAMIK, S.M. 2000. Microbialite morphostratigraphy as a tool for correlating Late Cambrian-Early Ordovician sequences. *Journal of Geology*, **108**, 171-180.

SONNENFELD, P. 1984. Brines and evaporites, pp. 1-613. *Academic Press Inc*.; Orlando.

SONNENFELD, P. & HUDEC, P.P. 1985. Origin of clay films in rock salt. *Sedimentary Geology*, **44**, 113-120.

STRASSER, A. 1994. Milankovitch cyclicity and high-resolution sequence stratigraphy in lagoonal-peritidal carbonates (Upper Tithonian-Lower Berriasian, French Jura Mountains). *In*: P.L. DE BOER & D.G. SMITH (*Eds*), Orbital forcing and cyclic sequences. *Special Publication of the International Association of Sedimentologists*, **19**, pp. 285-301. *Blackwell*; Oxford.

STRASSER, A., PITTET, B., HILLGÄRTNER, H. & PASQUIER, J.-B. 1999. Depositional sequences in shallow carbonate-dominated sedimentary systems: concepts for a high-resolution analysis. *Sedimentary Geology*, **128**, 201-221.

TRASHLIEV, S. 1969. Conditions and duration of the building up of the evaporite formation in the Tortonian in north-western Bulgaria. *Bulletin of the Geological Institute*, *Ser. Metallic and Non-metallic Mineral Deposits* [*Izvestiya na Geologicheskiya Institut*, *Ser. Rudni i Nerudni Polezni Iskopaemi*], **13**, 143-156. Sofia. [*In Bulgarian with English summary*]

TURCHINOV, I.I. 1999. The Badenian (Middle Miocene) gypsum section in Kryvche (Podolia, west Ukraine). *Biuletyn Państwowego Instytutu Geologicznego*, **387**, 70-74.

WALA, A. 1961. Litologia mioceńskiej serii ewaporatów w okolicy Pińczowa. *Sprawozdania z Posiedzeń Komisji*, *Polska Akademia Nauk*, *Oddział w Krakowie*, No. **1**-**6**, 275-280.

— 1962. Charakterystyka petrograficzna profili serii gipsowej w okolicy Buska, Wiślicy i Gartatowic oraz próba korelacji ich z profilem w Gackach koło Pińczowa. *Sprawozdania z Posiedzeń Komisji*, *Polska Akademia Nauk*, *Oddział w Krakowie*, No. **1**-**6**, 269-271.

— 1963. Korelacja litostratygraficzna serii gipsowej obszaru nad nidziańskiego. *Sprawozdania z Posiedzeń Komisji*, *Polska Akademia Nauk*, *Oddział w Krakowie*, No. **7**-**12**, 530-532. [for 1962]

— 1979. Badania litologiczne mioceńskich warstw gipsowych i ilastych z wierceń w rejonie Winiar. *In*: Sprawozdanie z prac badawczych mioceńskiej serii gipsowej w obszarze Niecki Nidy, zał. 4, pp. 1-31. *Unpublished*. Archiwum Przedsiębiorstwa Geologicznego. Kraków.

— 1980. Litostratygrafia gipsów nidziańskich (fm). *In*: Sympozjum naukowe „Gipsy niecki nidziańskiej i ich znaczenie surowcowe", pp. 5-10. Kraków.

WARREN, J.K. 1982. The hydrological setting, occurrence and significance of gypsum in late Quaternary salt lakes in South Australia. *Sedimentology*, **29**, 609-637.

— 1999. Evaporites. Their evolution and economics, pp. 1-438. *Blackwell Sci*.; Oxford.

WIESE, F. & KRÖGER, B. 1998. Evidence for a shallowing event in the Upper Turonian (Cretaceous) *Mytiloides scupini* Zone of northern Germany. *Acta Geologica Polonica*, **48**, 265-284.

WIEWIÓRKA, J. 1979. Tuffit conductive levels as found in the Wieliczka salt mine. *Sprawozdania z Posiedzeń Komisji*, *Polska Akademia Nauk*, *Oddział w Krakowie*, **21**/**1**, 176-178. [for 1977]

WYSZYŃSKI, O.W. 1937. Wiercenia poszukiwawcze koncernu „Małopolska" w Wowni. *Przemysł Naftowy*, **12**, 88-92. Lwów.

Manuscript submitted: 10th October 2003
Revised version accepted: 20th November 2004

PLATE 1

Growth zoning defining isochronous surface A in giant gypsum intergrowths; correlated dark zones and one dark-white zone (marked 3) are numbered as in Appendix, Figs 4-5; Góry Wschodnie S2, Poland (Fig. 1) and Kasova Hora W, Ukraine (Fig. 2)


?
?
5
4
2
1

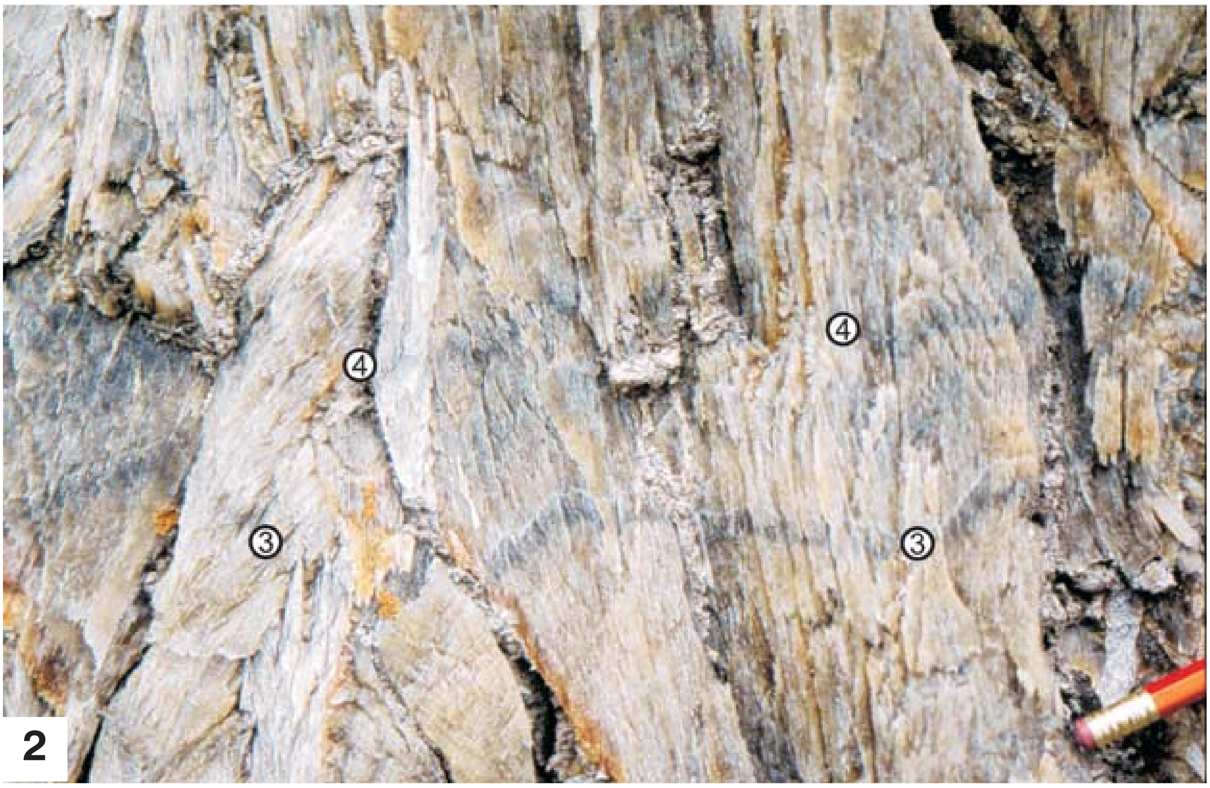
4
4
3
3
2

PLATE 2

Stratigraphy and selenite sequences near marker bed c; units lettered as in Text-figs 4-5; Oleshiv: outcrop N of Palahychi N4 (Fig. 1), Pidkamin' N (Fig. 2) and Podillia (Fig. 3)

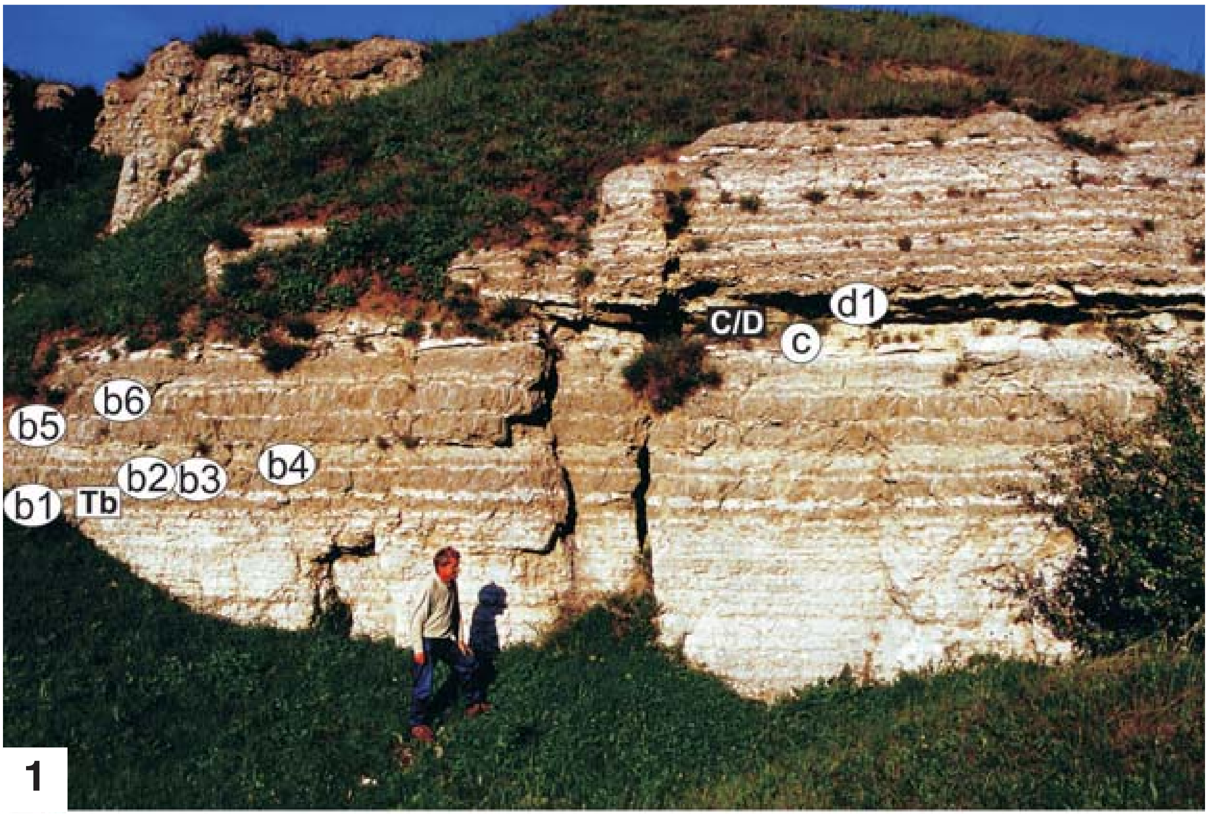
d1
C/D
c
b6
b5
b4
b2
b3
b1
Tb
1

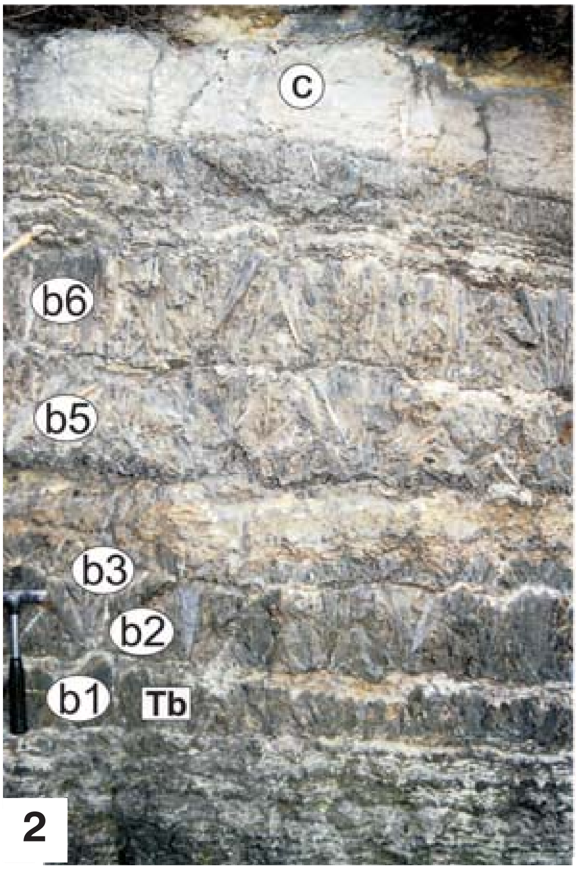
c
b6
b5
b3
b2
b1
Tb
2


C/D
d1
3

PLATE 3

1 – Grass-like selenites intercalating gypsum microbialite and clastic deposits at Mezhyhirtsi; stratigraphic units lettered as in Text-figs 4-5

2 – Grass-like selenite bed covered with fine-grained gypsum showing brecciated and spotted structure which is interpreted as a pedogenic feature (P); a single gypsified cyanobacterial mat is seen as a white band (arrowed) within selenite crust; unit B, Borków

1

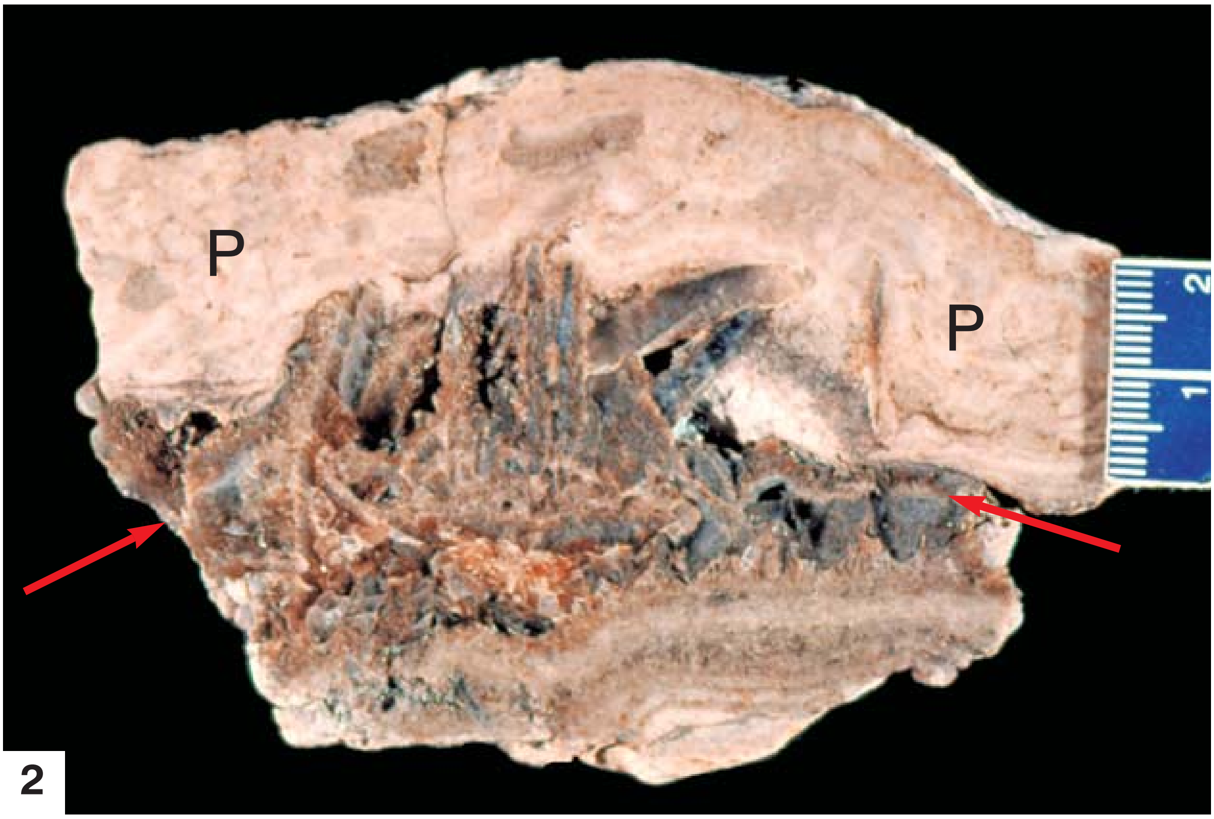

2

PLATE 4

Stratigraphy and selenite sequences below marker bed c; units lettered as in Text-fig. 4; note large selenite-gypsum microbialite domes; Ozerna cave (Fig. 1) and Tovtry (Fig. 2)

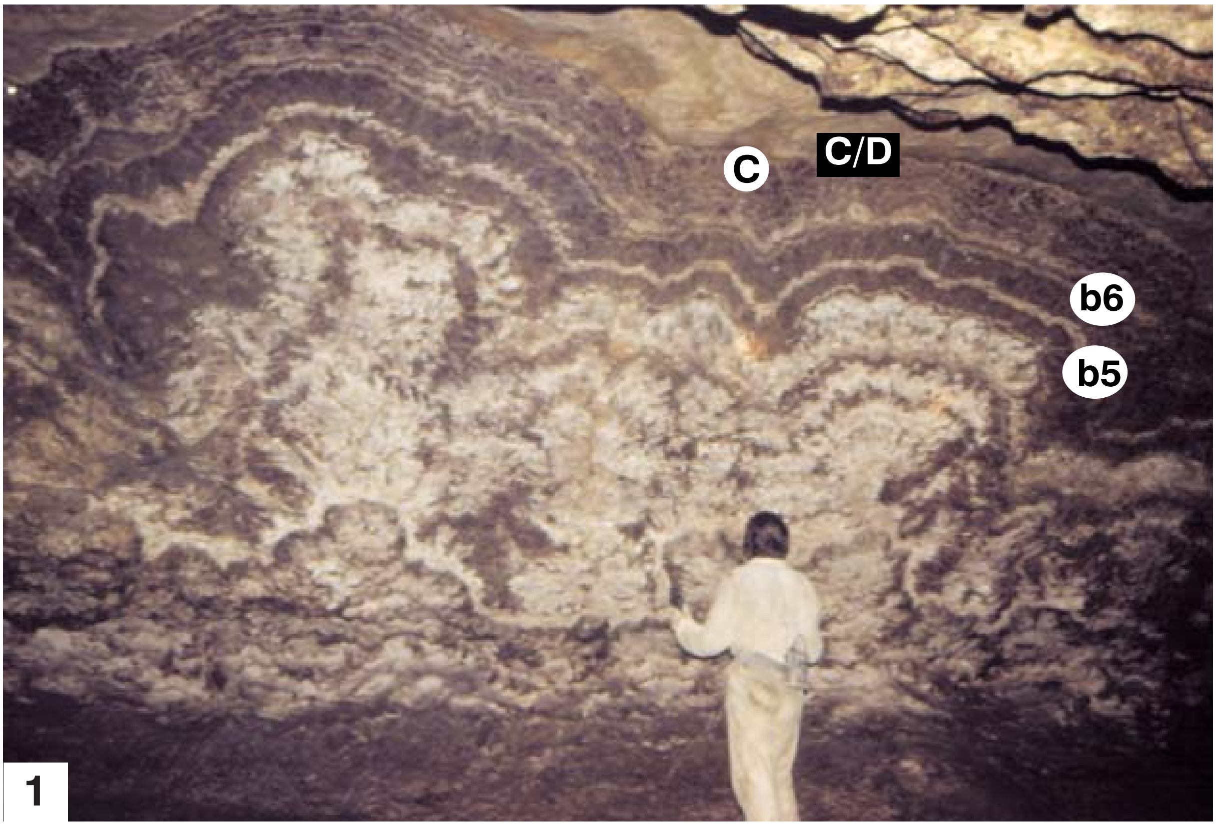

1

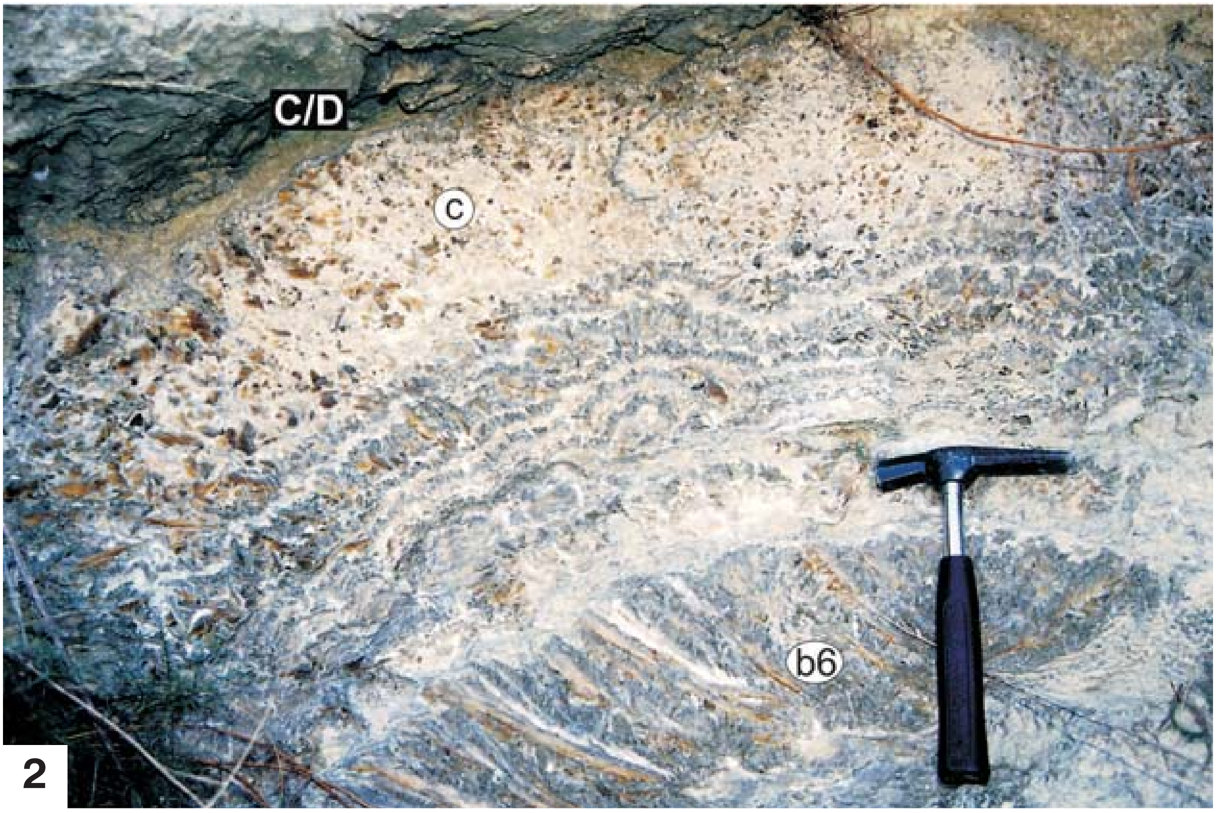

2

PLATE 5

1 – Sequence of selenite marker beds h1-h3 at Verenchanka; note various-scale domal structures composed of grass-like gypsum and characteristic competitive growth structures (arrowed) between bundles of sabre crystals growing on slopes of the adjacent domes in bed h1

2 – Marker bed h and isochronous surface G/H within sabre selenite unit C-D at Podillia; the hammer head is 2.3 cm across

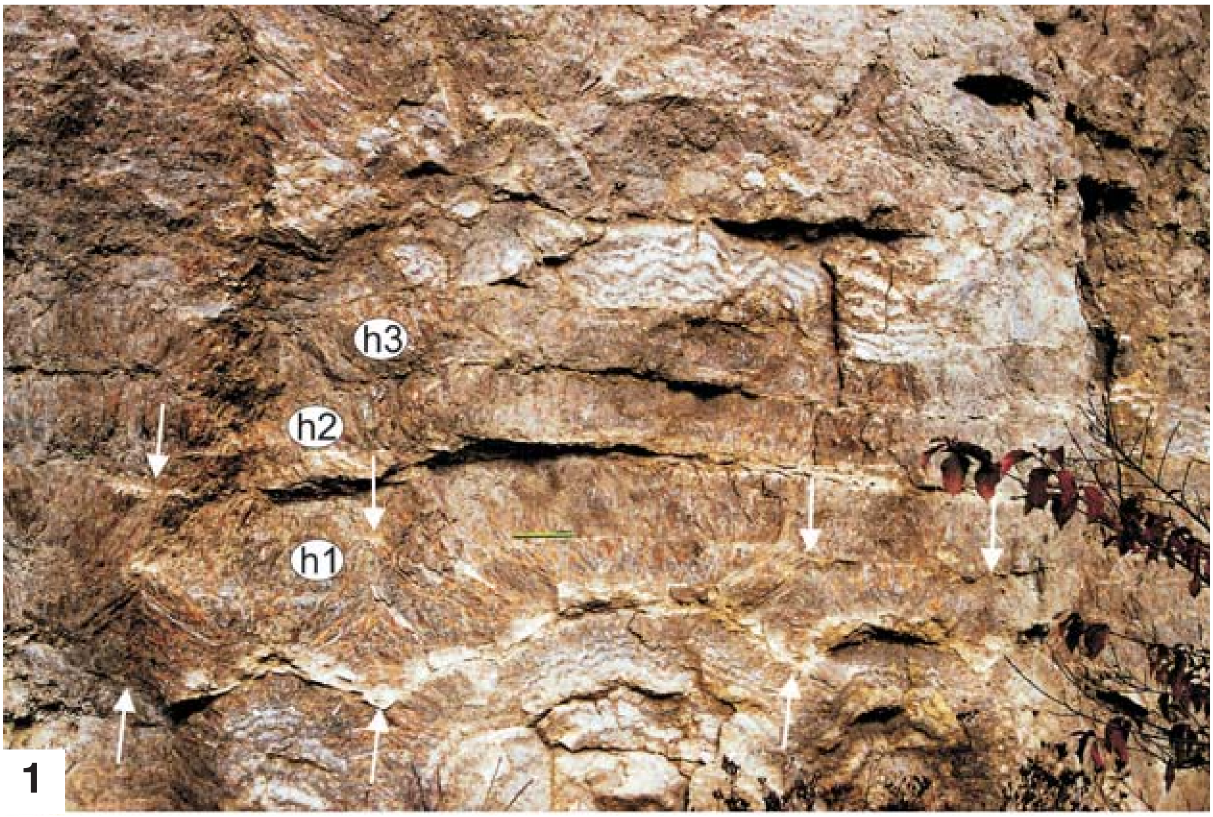
h3
h2
h1
1

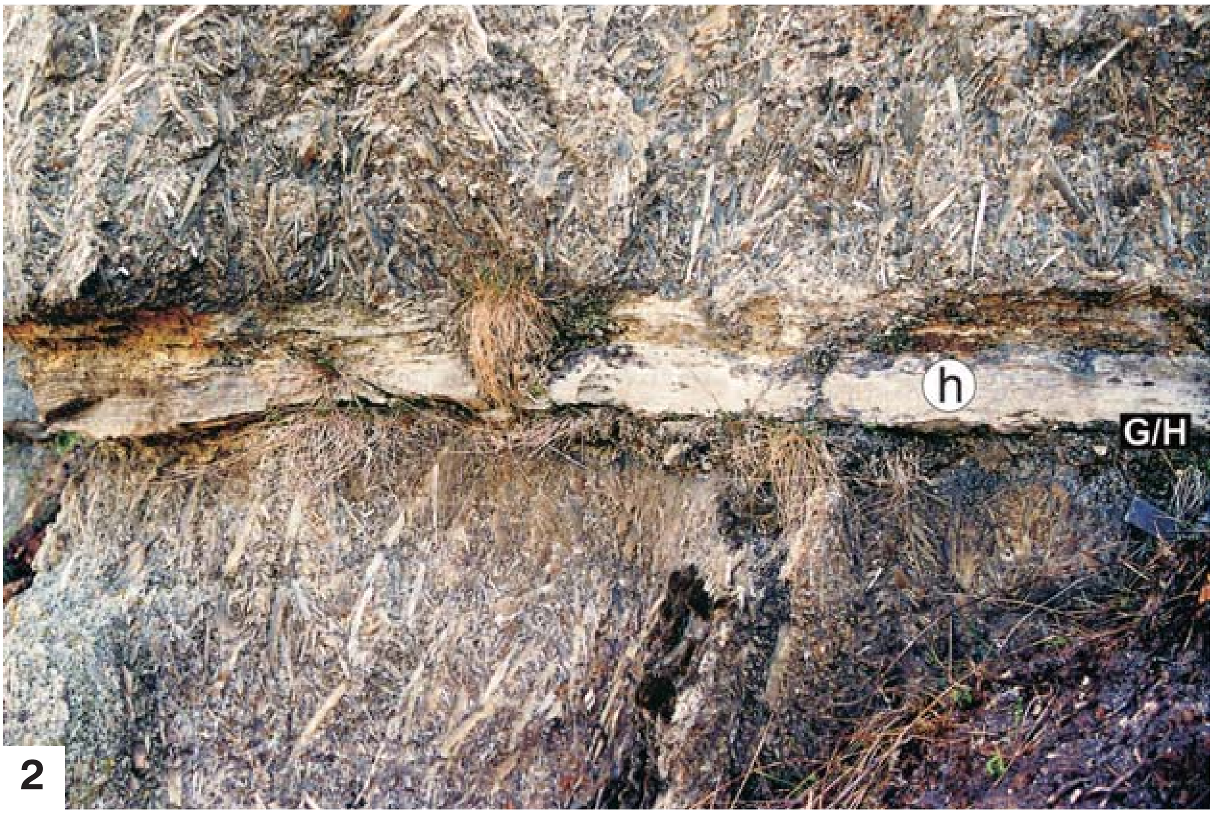
h
G/H
2

PLATE 6

Sequence of selenite marker beds f1-f3 and isochronous surface F1; Palahychi S1 (Fig. 1) and Odaiv (Fig. 2)

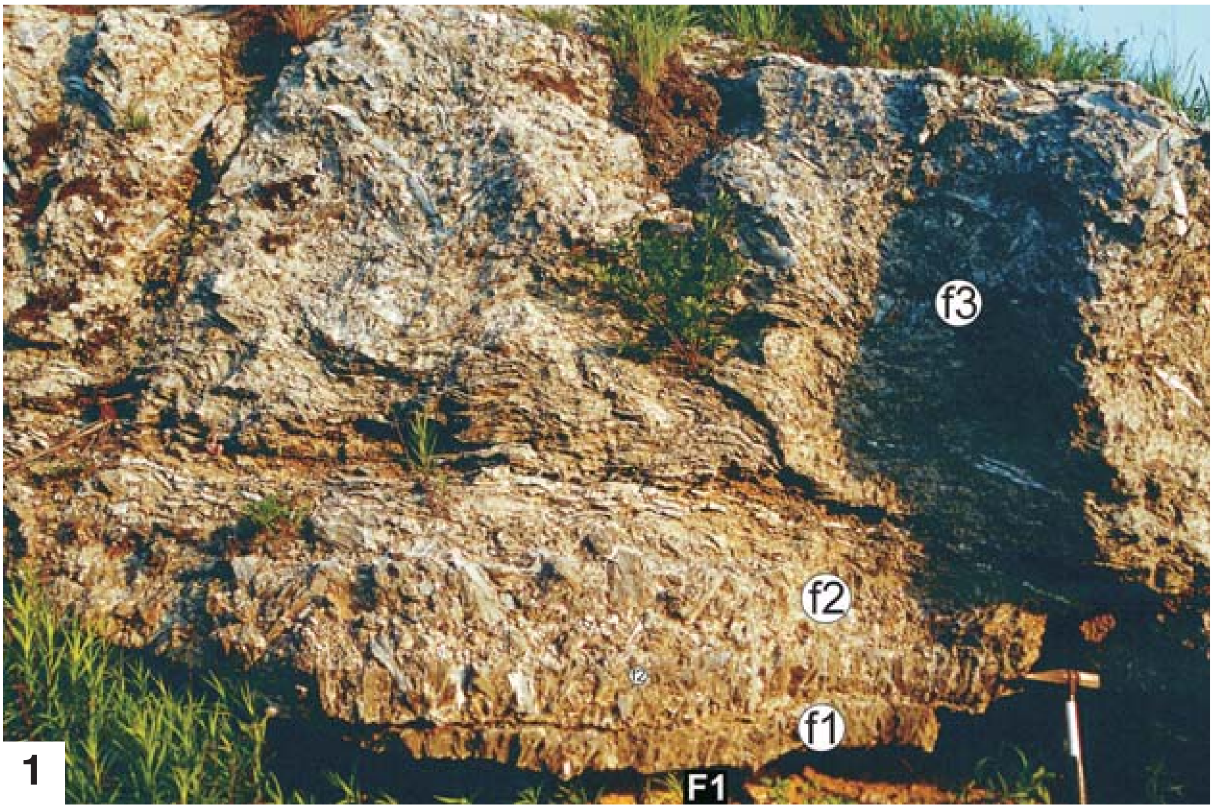
f3
f2
f1
F1
1

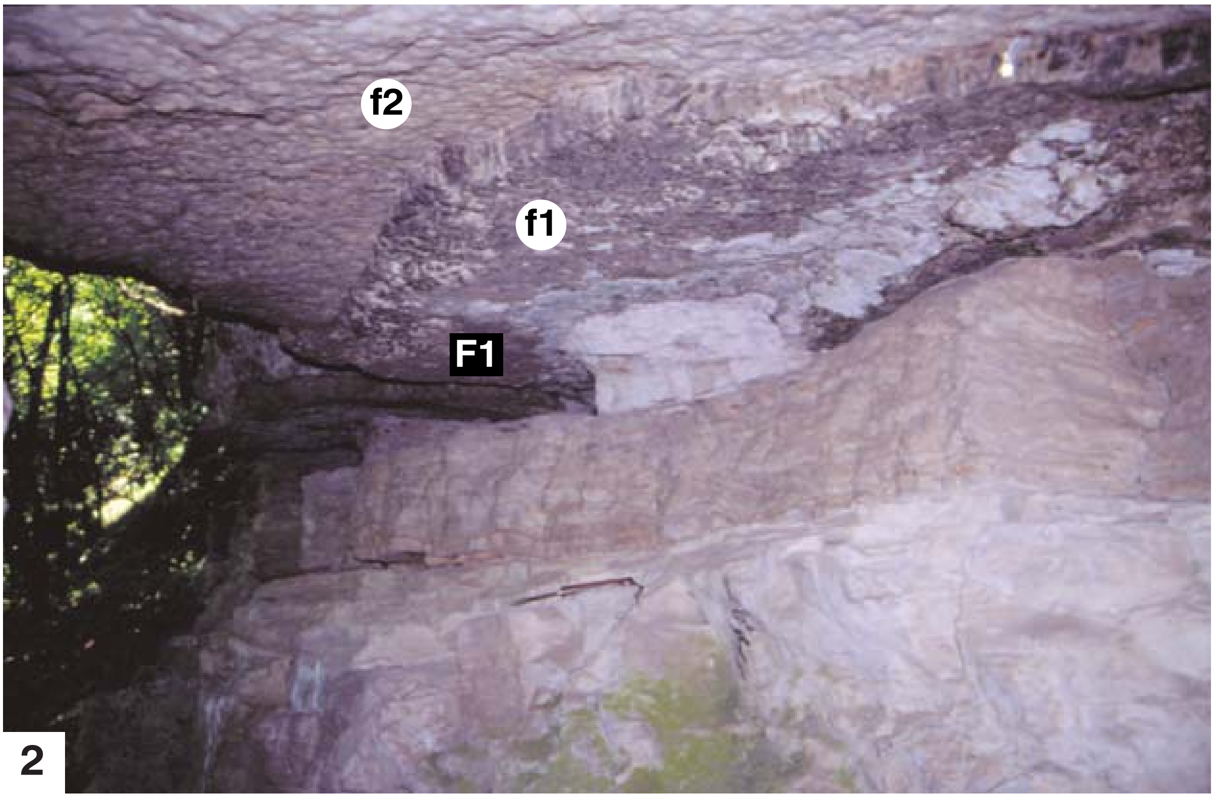
f2
f1
F1
2

MACIEJ BĄBEL

Event stratigraphy of the Badenian selenite evaporites (Middle Miocene) of the northern Carpathian Foredeep

Acta Geologica Polonica, Vol. 55 (2005), No. 1

On-Line Appendix

World Wide Web Address:

http://www.geo.uw.edu.pl/agp/table/appendixes/55-1/

Warszawa 2005

Table 1. List of studied localities

Localities in Ukraine

In English	*In Ukrainian*	*In Russian*	*In Polish* [*In Romanian*]	
Anadoly	Анадолы	Анадолы	[Anadol]	Fig. 1, map 26; Figs 2, 18A-B
Borschiv	Борщів	Борщев	Borszczów	Fig. 1, map 24; Figs 2, 18A-B
Bratyshiv	Братишів	Братышев	Bratyszów	Fig. 1, map 16; Figs 2, 8E, 10E
Chortova Hora	Чортова Гора	Чертова Гора	Czortowa Góra	Fig. 1, map 10; Figs 2, 8B
Chun'kiv	Чуньків	Чуньков	Czinkeu [Cinčau]	Fig. 1, map 23; Figs 2, 9C, 11B
Hannusivka	Ганнусівка	Ганнусовка	Hanusowce	Fig. 1, map 15; Figs 2, 12B, 13B, 14B
Harasymiv	Гарасимів	Герасимов	Harasimów	Fig. 1, map 18; Figs 2, 8E, 10E, 17D
Hlushkiv	Глушків	Глушков	Głuszków	Fig. 1, map 20; Figs 2, 12C, 13C, 14B
Holovchyntsi	Головчинці	Головчинцы	Hołowczyńce	Fig. 1, map 21; Figs 2, 9B, 11A
Isakiv	Ісаків	Ісаков	Isaków	Fig. 1, map 17; Figs 2, 10E, 12C, 13C, 14B, 17D
Kasova Hora	Касова Гора	Касова Гора	---	Fig. 1, map 10, Figs 2, 5, 8C
Kolokolyn	Колоколин	Колоколин	Kołokolin	Fig. 1, map 9; Figs 2, 5, 10B, 12B, 13B, 14A
Kostryzhivka	Кострижівка	Кострижевка	Kostryżówka	Fig. 1, map 23; Figs 9B, 11A
Krasiiv	Красіїв	Красиев	Krasiejów	Fig. 1, map 14; Figs 2, 8C, 10C, 17C
Kryvche	Кривче	Кривче	Krzywcze	Fig. 1,map 24; Figs 2, 9D, 11C
Kudryntsi	Кудринці	Кудринцы	Kudryńce	Fig. 1, map 25; Figs 2, 18A-B
Kuropatnyky	Куропатники	Куропатники	Kuropatniki	Fig. 1, map 10; Figs 12B, 17B
Lany	Лани	Ланы	Łany	Fig. 1, map 13, Figs 2, 8C, 10C
Lokitka	Локітка	Локотка	Łokutki	Fig. 1, map 16; Figs 2, 10E
Luchyntsi	Лучинці	Лучинцы	Łuczyńce	Fig. 1, map 10; Figs 2, 12B, 13B, 17A
Mamalyha	Мамалига	Мамалыга	Mamałyga [Mamaliga]	Fig. 1, map 27; Figs 2, 9D, 18A-B
Medynia	Mединя	Mединя	Medynia	Fig. 1, map 12; Figs 2, 8C, 10B-C, 17C
Mezhyhirtsi	Межигірці	Межигорцы	Międzyhorce	Fig. 1, map 13; Figs 2, 8C, 10C, 17C
Mlynky, cave	Млинки, печера	Млынки, пещера	---	Fig. 1, map 22; Figs 2, 18A-B
Naberezhne	Набережне	Набережное	---	Fig. 1, map 10; Figs 2, 8C, 10B
Nahoriany	Нагоряни	Нагоряны	Nagórzany	Fig. 1, map 19; Figs 2, 9A, 11A
Nyrkiv	Нирків	Нирков	Nyrków	Fig. 1, map 19; Figs 2, 9A, 11A
Obelnytsia	Обельниця	Обельница	Obelnica	Fig. 1, map 10; Fig. 17B
Odaiv	Одаїв	Одаев	Odaje	Fig. 1, map 16; Figs 2, 12C, 13B, 14B, 17D
Oleshiv	Олешів	Олешев	Oleszów	Fig. 1, map 16; Figs 2, 5, 8D, 10C, 12C, 17C
Optymistychna, cave	Оптимістична, печера	Оптимистическая, пещера	---	Fig. 1, map 24; Figs 2, 9D, 11C
Ozeriany	Озеряни	Озеряни	Jezierzany	Fig. 1, map 10; Figs 2, 8B, 10B, 17B
Ozerna, cave	Озерна, печера	Озерная, пещера	---	Fig. 1, map 24; Figs 2, 9C, 11C
Palahychi	Палагичі	Палагичи	Pałahicze	Fig. 1, map 16; Figs 2, 8D, 10D-E, 12C, 13B, 17D
Pidkamin'	Підкамінь	Подкамень	Podkamień	Fig. 1, map 8; Figs 2, 8B, 10A, 12B, 13A
Pisky	Піски	Пески	Piaski	Fig. 1, map 6; Figs 2, 8A, 10A, 12A, 13A, 17A
Podillia	Поділля	Подолье	Podole	Fig. 1, map 10; Figs 2, 5, 8B, 10B, 17C
Pryozerne	Приозерне	Приозерное	Psary	Fig. 1, map 8; Figs 2, 5
Radians'ke Zahiria	Радянське Загір'я	Радянськое Загорье	---	Fig. 1, map16; Fig. 8E
Repuzhyntsi	Репужинці	Репужинцы	Repużyńce	Fig. 1, map 19; Figs 2, 9A, 11A
Rohatyn	Рогатин	Рогатин	Rohatyn	Fig. 1, map 10; Figs 2, 5, 8B
Sarnyky	Сарники	Сарники	Sarnki	Fig. 1, map 10; Fig. 17C
Skov'iatyn	Сков'ятин	Сковятин	Skowiatyn	Fig. 1, map 24; Figs 2, 9D, 11C, 18A-B
Schyrets'	Щирець	Щирец	Szczerzec, Szczyrec	Fig. 1, map 6; Figs 2, 5, 8A, 10A, 12A, 13A, 14A
Stal'nivtsi	Стальнівці	Стальновцы	[Stalinesti]	Fig. 1, map 27; Figs 2, 18A-B
Tovtry	Товтри	Товтры	Toutry [Tauteni]	Fig. 1, map 23; Figs 2, 9C, 11B
Ustechko	Устечко	Устечко	Uścieczko	Fig. 1, map 19; Figs 2, 9A, 11A, 12C, 13C, 17D
Velyka Holda	Велика Холда	---	Góra Korosty	Fig. 1, map 10; Figs 2, 8B, 10B, 17B
Verenchanka	Веренчанка	Веренчанка	Werenczanka [Vranceni]	Fig. 1, map 23; Figs 2, 9C, 11B
Verteba, cave	Вертеба, печера	Вертеба, пещера	Werteba, jaskinia	Fig. 1, map 24; Figs 2, 9C, 11C
Vikniany (Bilohirka)	Вікняни (Білогірка)	Викняни (Белогорка)	Okniany	Fig. 1, map 16; Figs 2, 8E, 10E
Voinyliv	Войнилів	Войнилов	Wojniłów	Fig. 1, map 11; Figs 2, 12B, 13B, 14B
Yahodivka	Ягодівка	Фрага	Fraga	Fig. 1, map 8; Figs 2, 10A, 17A
Yunashkiv	Юнашків	Юнашков	Junaszków	Fig. 1, map 10; Figs 2, 17B
Zahirochko	Загірочко	Загорочко	Zagóreczko	Fig. 1, map 7; Figs 2, 12B, 13A, 14A, 17A
Zavallia	Завалля	Завалье	Zawale	Fig. 1, map 25; Figs 2, 18A-B
Zhalybory	Жалибори	Жалиборы	Żelibory	Fig. 1, map 10; Figs 2, 8C
Zveniachyn	Звенячин	Звенячин	Zwiniacze	Fig. 1, map 23; Figs 2, 9B, 11B

Localities in Poland

Bilczów	Fig. 1, map 5; Fig. 4B
Biniatki	Fig. 1, map 5; Fig. 4A
Bogucice-Skałki	Fig. 1, map 5; Fig. 4B
Borków	Fig. 1, map 5; Figs 6A-B, 8A, 10A, 12A, 13A, 14A, 16A-B, 17A
Broniakówka	Fig. 1, map 3; Figs 15A-B
Bronina	Fig. 1, map 5; Fig. 4A
Chotel Czerwony	Fig. 1, map 5; Fig. 4C
Chotel Czerwony-Zagórze	Fig. 1, map 5; Fig. 4B
Chotelek Zielony	Fig. 1, map 5; Fig. 4A
Chwałowice	Fig. 1, map 5; Figs 4A, 6A-B
Czernica [Czernitz *in German*]	Fig. 1, map 2; Figs 15A-B
Gacki	Fig. 1, map 5; Fig. 4B
Galów	Fig. 1, map 5; Fig. 4A
Gartatowice	Fig. 1, map 5; Figs 6A-B
Gorysławice	Fig. 1, map 5; Fig. 4C
Góry Wschodnie	Fig. 1, map 5; Fig. 4C
Leszcze	Fig. 1, map 5; Fig. 4B
Łagiewniki	Fig. 1, map 5; Fig. 4A
Łatanice	Fig. 1, map 5; Fig. 4B
Marzęcin	Fig. 1, map 5; Fig. 4B
Owczary	Fig. 1, map 5; Fig. 4A
Podgaje	Fig. 1, map 4; Fig. 16A
Przęślin	Fig. 1, map 5; Fig. 4C
Racławice	Fig. 1, map 4; Figs 16A-B
Sielec Rządowy	Fig. 1, map 5; Fig. 4C
Skorocice	Fig. 1, map 5; Fig. 4B
Stawiany	Fig. 1, map 5; Figs 6A-B
Wola Zagojska	Fig. 1, map 5; Fig. 4B

Localities in Czech Republic and Moldova

Kobeřice, Czech Republic	Fig. 1, map 1; Figs 15A-B
Kriva, Criva; Moldova	Fig. 1, map 27; Figs 18AB

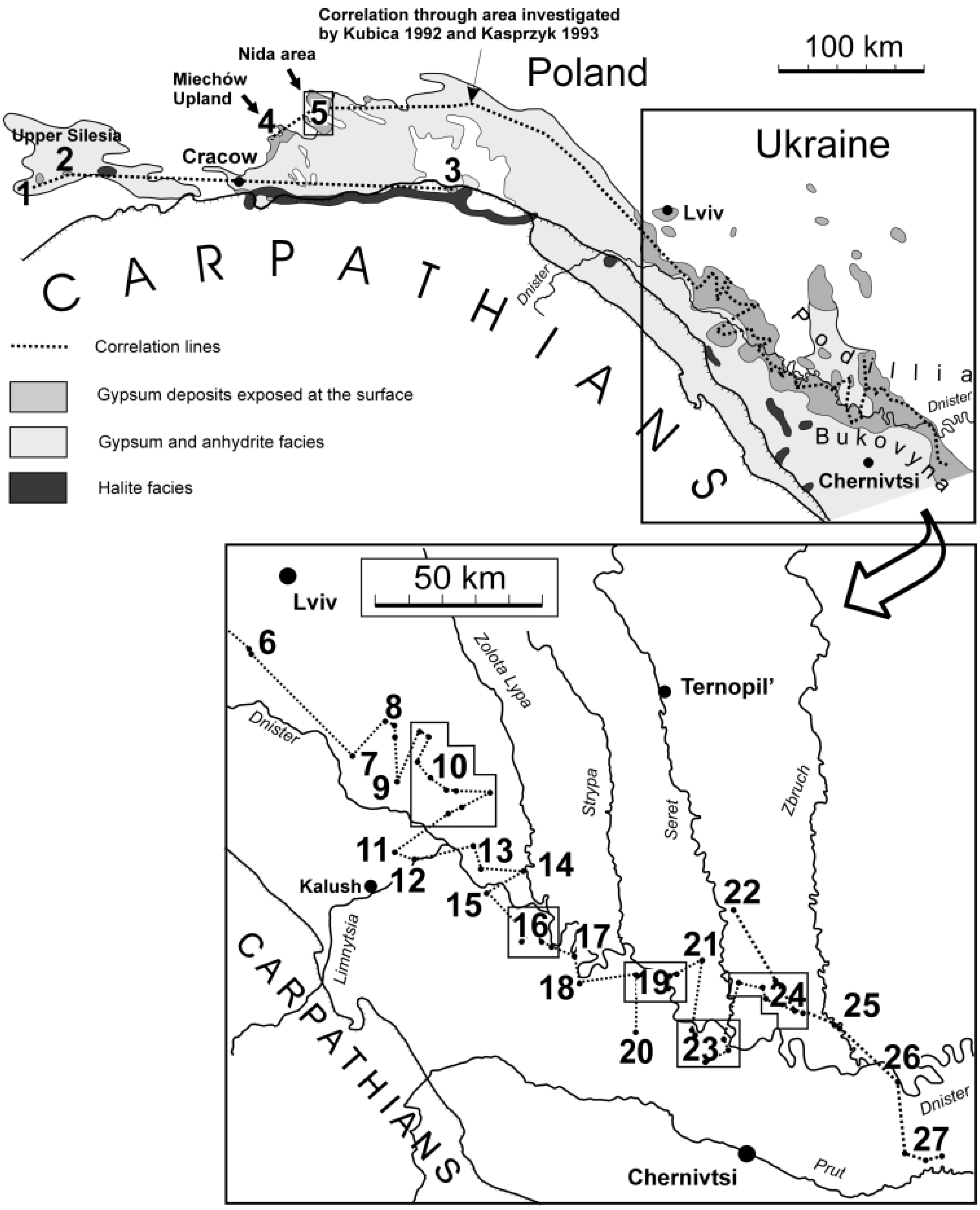

Fig. 1. Distribution of studied gypsum outcrops in the Badenian (Middle Miocene) evaporite basin in the northern Carpathian Foredeep in Ukraine, Poland, Czech Republic (at Kobeřice, area marked by 1) and Moldova (at Kriva, area marked 27); geological map after ATLAS GEOLOGICZNY GALICYI 1885-1914, GARLICKI 1979, PANOW & PŁOTNIKOW 1996, and other sources; studied areas are numbered from 1 to 27 and shown on separate detailed maps illustrating distribution of studied sections along the correlation lines

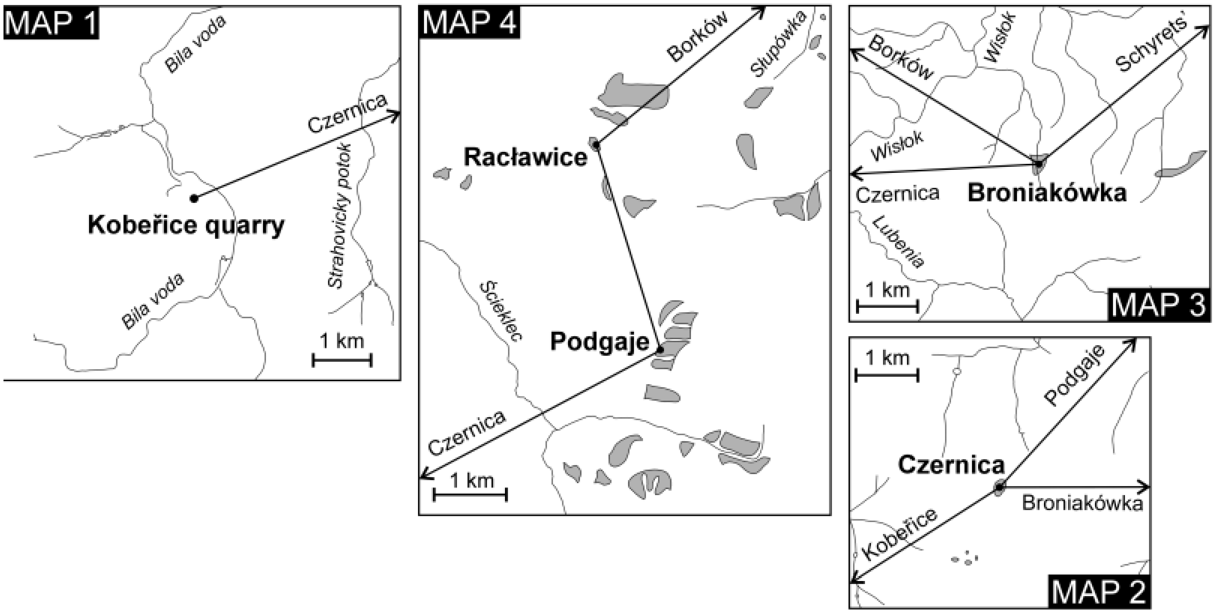

Fig. 1. Continued. Detailed maps showing distribution of studied gypsum outcrops; Badenian gypsum deposits exposed at the surface are shadowed; map 2 after SARNACKA 1956; map 3 after KUCIŃSKI & NOWAK 1967; map 4 after ROMAN 1998, WALCZOWSKI 1984, WOIŃSKI 1989

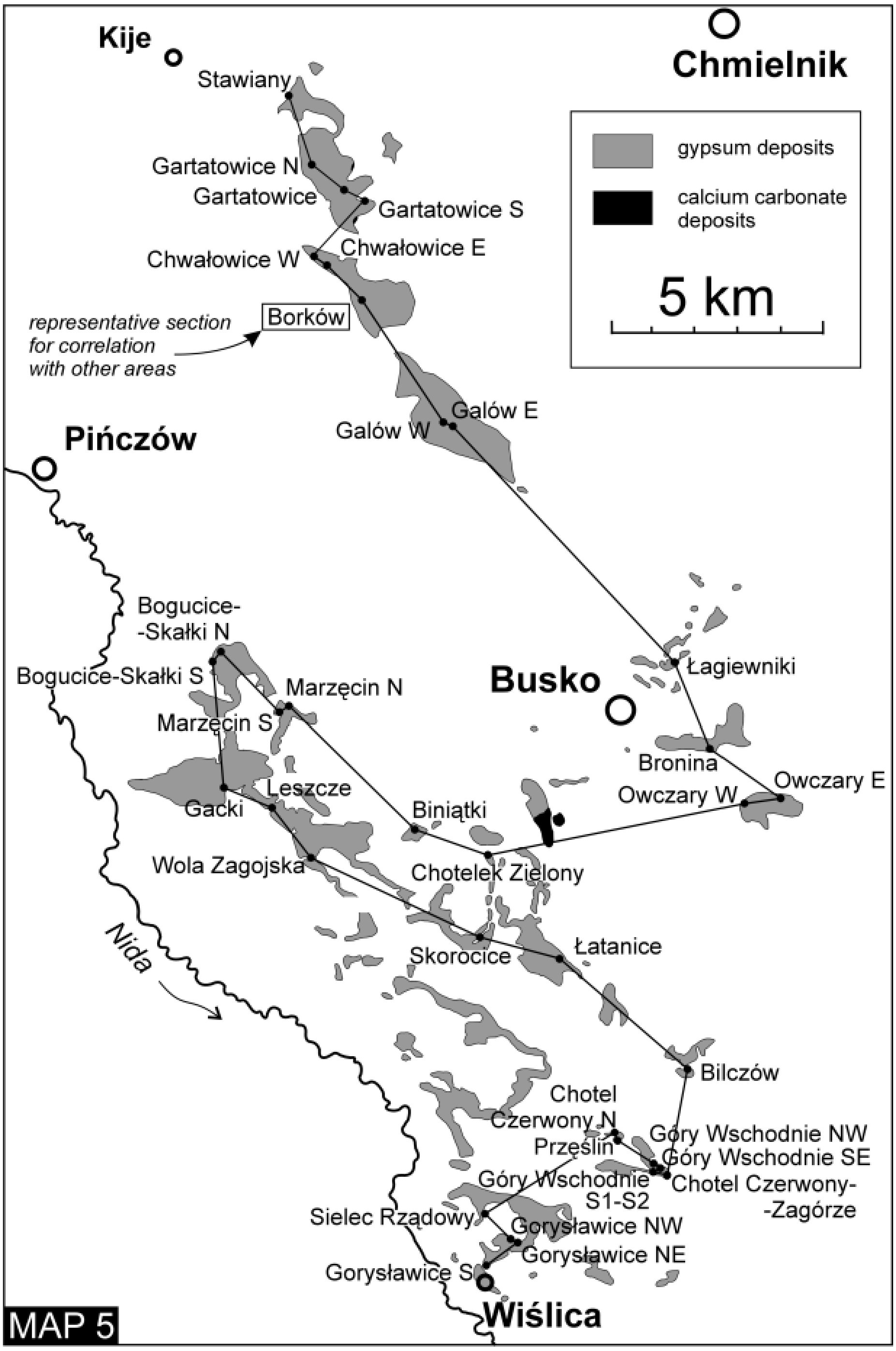

Fig. 1. Continued. Detailed map showing distribution of studied gypsum outcrops; after many sources cited in BĄBEL 2002, fig. 7

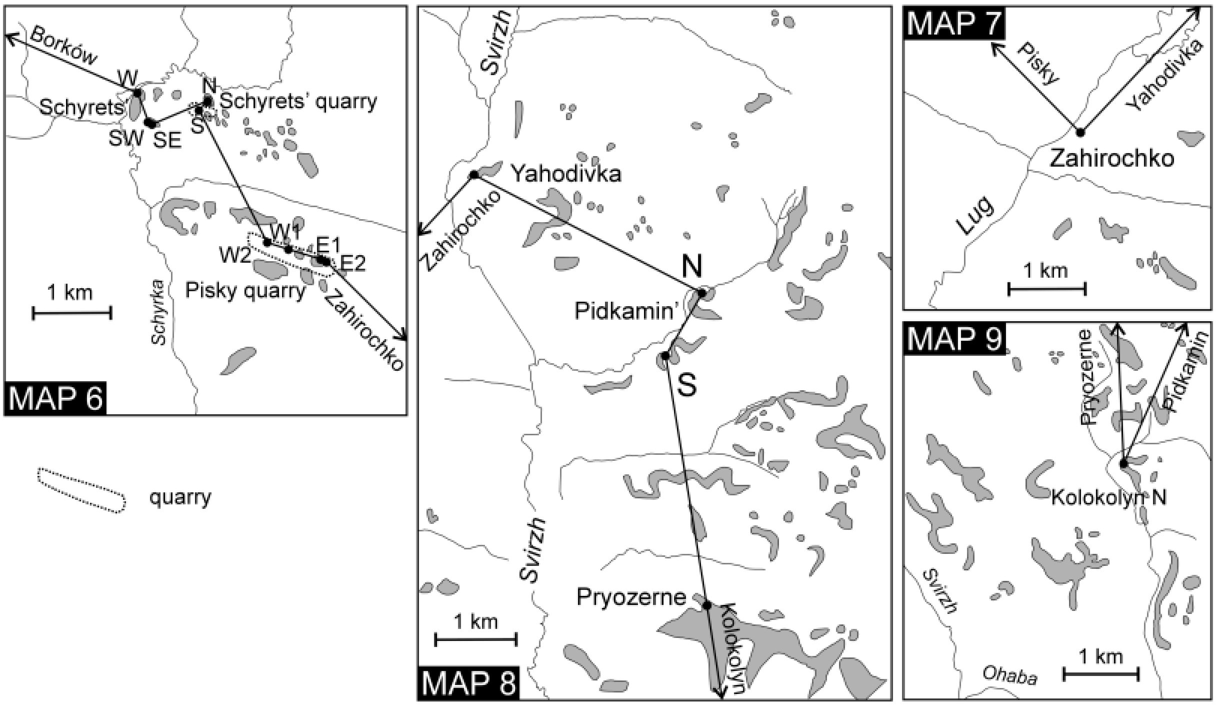

Fig. 1. Continued. Detailed maps showing distribution of studied gypsum outcrops; Badenian gypsum deposits exposed at the surface are shadowed; map 6 after TEISSEYRE 1894-1895; map 7 after TEISSEYRE 1895; maps 8-9 after TEISSEYRE 1892-1893

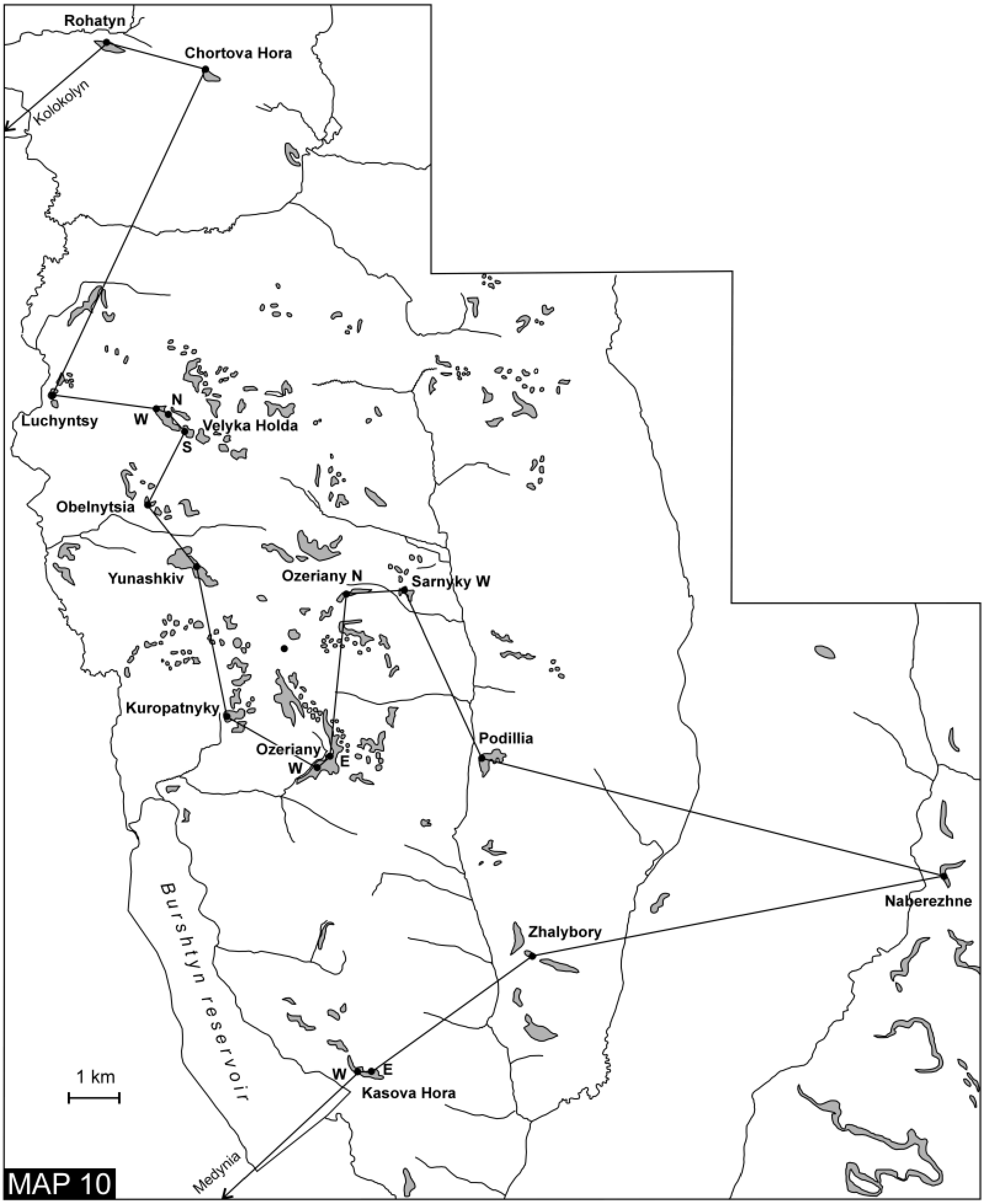

Fig. 1. Continued. Detailed map showing distribution of studied outcrops; Badenian gypsum deposits exposed at the surface are shadowed; after BIENIASZ 1885a, 1898b; TEISSEYRE 1892-1893, 1896

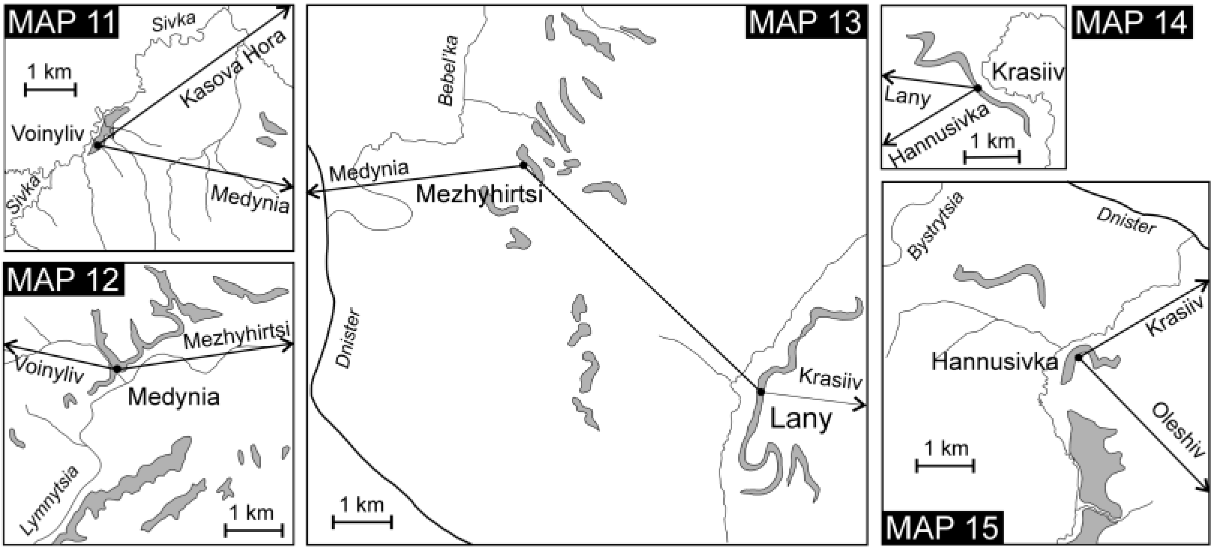

Fig. 1. Continued. Detailed maps showing distribution of studied gypsum outcrops; Badenian gypsum deposits exposed at the surface are shadowed; maps 11-12 after TEISSEYRE 1896; map 13 after BIENIASZ 1885a, TEISSEYRE 1896; map 14 after BIENIASZ, 1885a; map 15 after TEISSEYRE 1896, ŁOMNICKI 1905b

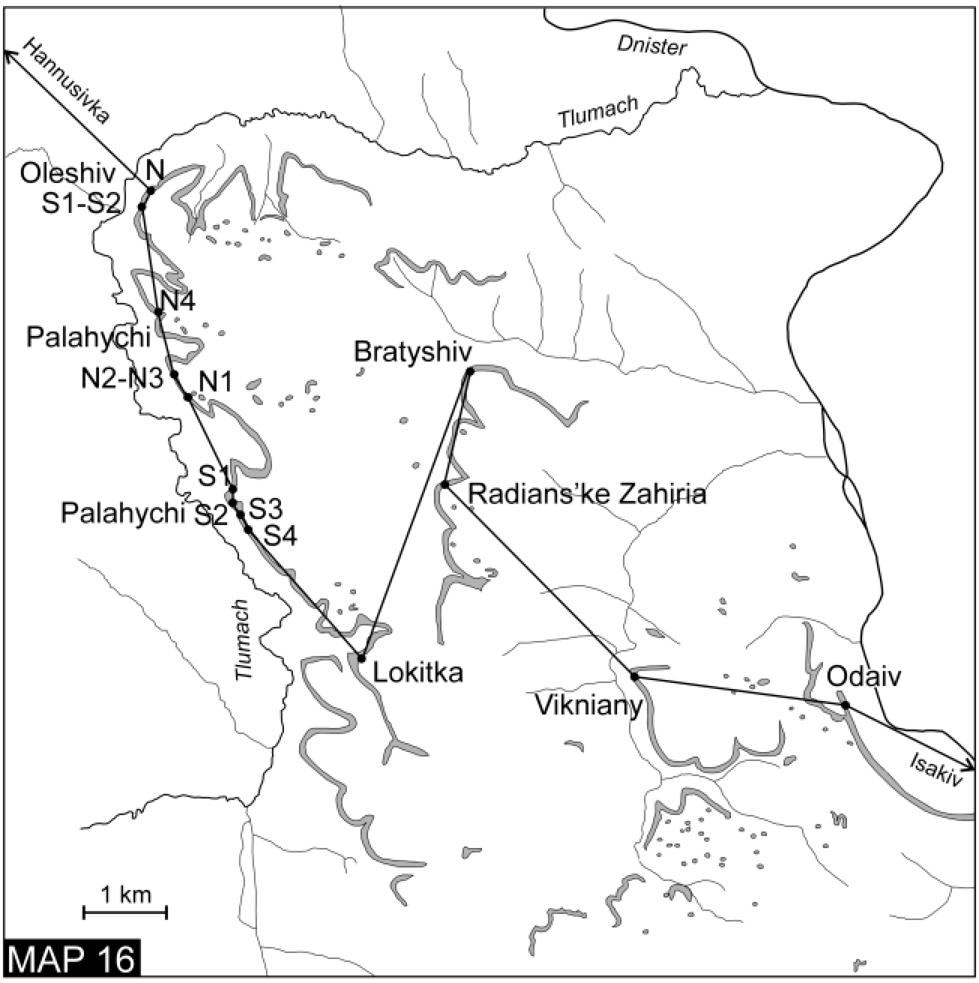

Fig. 1. Continued. Detailed map showing distribution of studied gypsum outcrops; Badenian gypsum deposits exposed at the surface are shadowed; after BIENIASZ 1885b

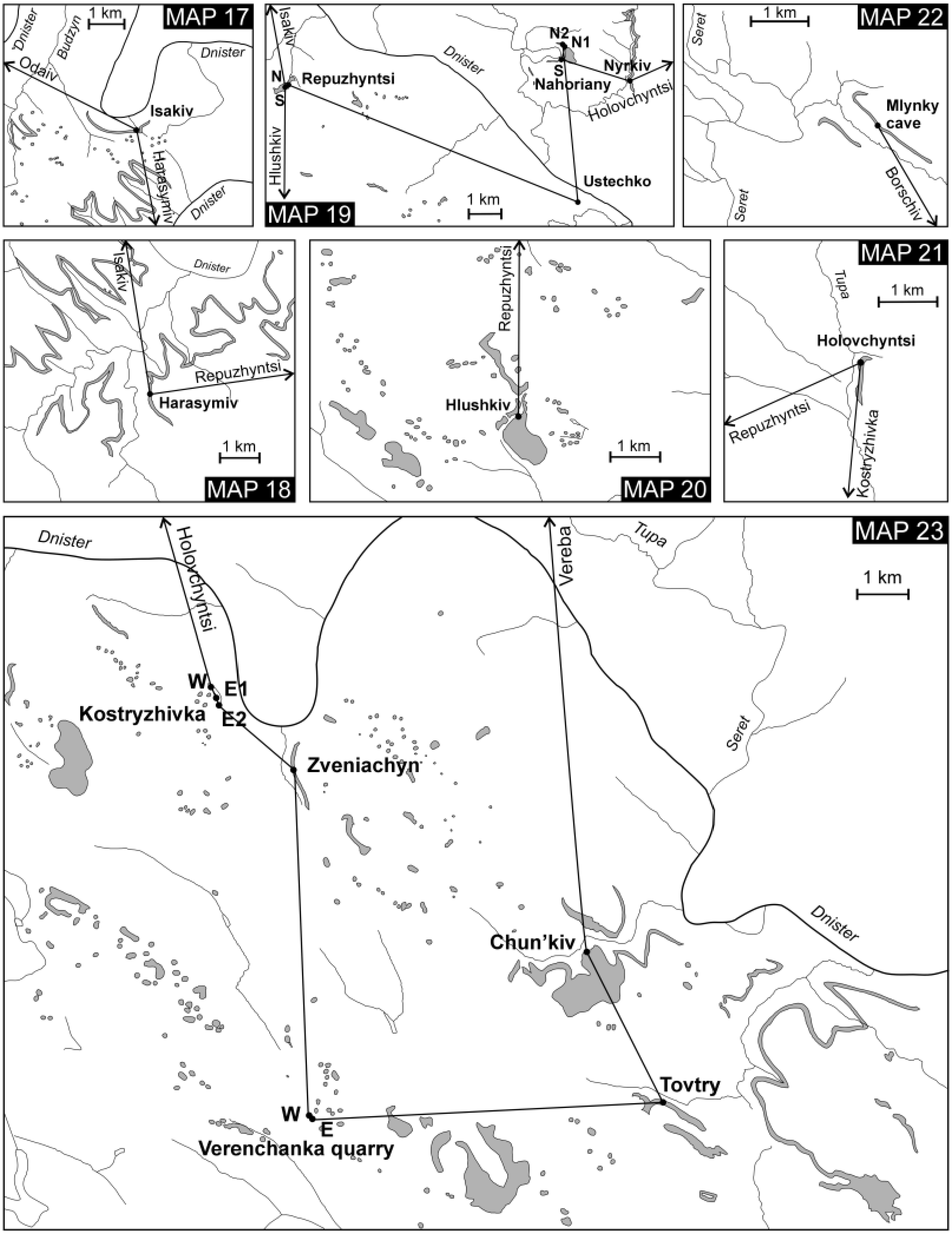

Fig. 1. Continued. Detailed maps showing distribution of studied gypsum outcrops; Badenian gypsum deposits exposed at the surface are shadowed; map 17 after BIENIASZ 1885b; map 18 after BIENIASZ 1885b, ŁOMNICKI 1905a; modified; map 19 after ALTH 1885a; map 20 after ALTH 1885b; map 21 after ALTH 1885a; supplemented; map 22 after BIENIASZ 1898a; map 23 after ALTH 1885b

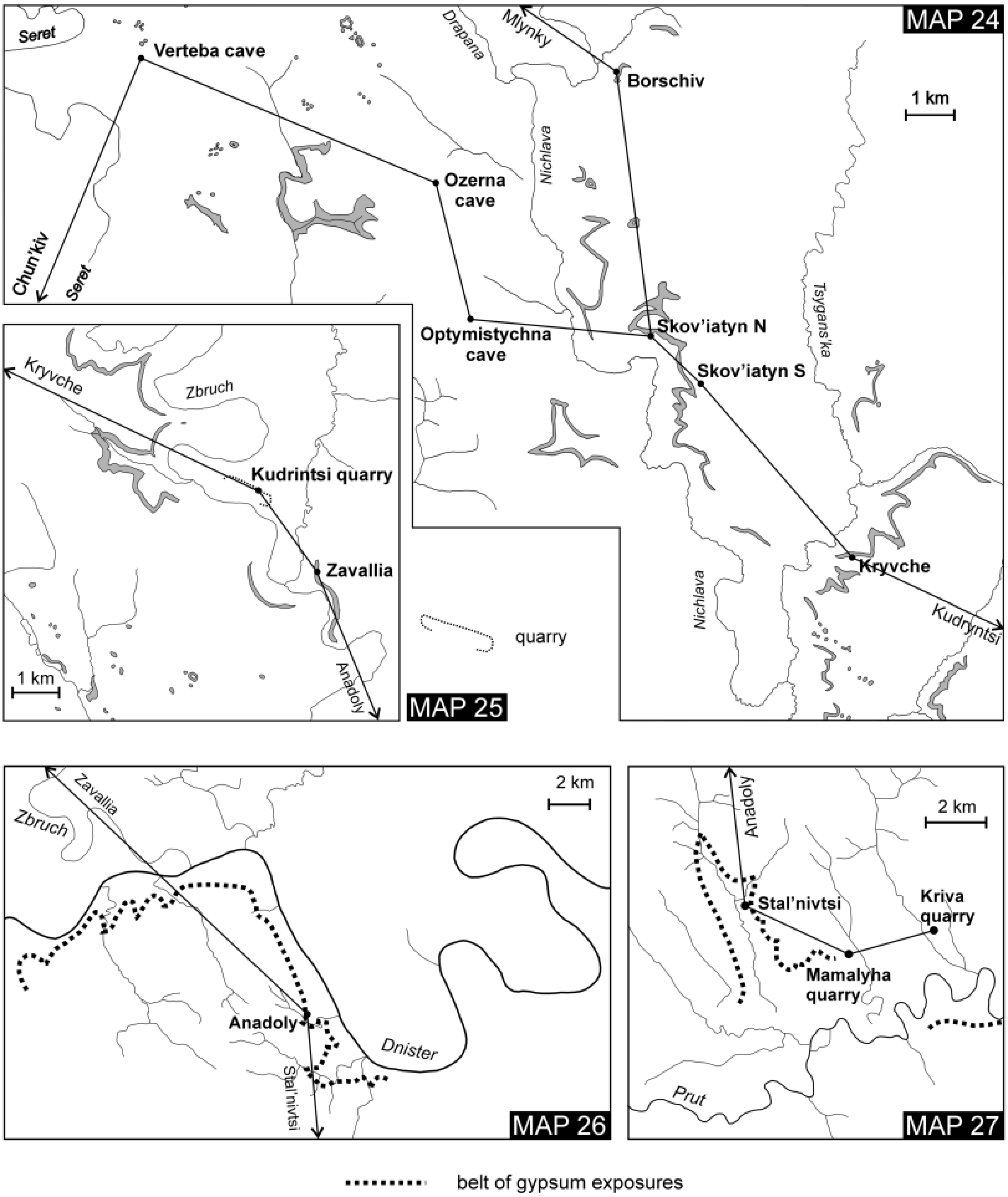

Fig. 1. Continued. Detailed maps showing distribution of studied gypsum outcrops; Badenian gypsum deposits exposed at the surface are shadowed (except for maps 26, 27); map 24 after BIENIASZ 1898a, c; map 25 after BIENIASZ 1898c; maps 26-27 after MACOVEI & ATANASIU 1931

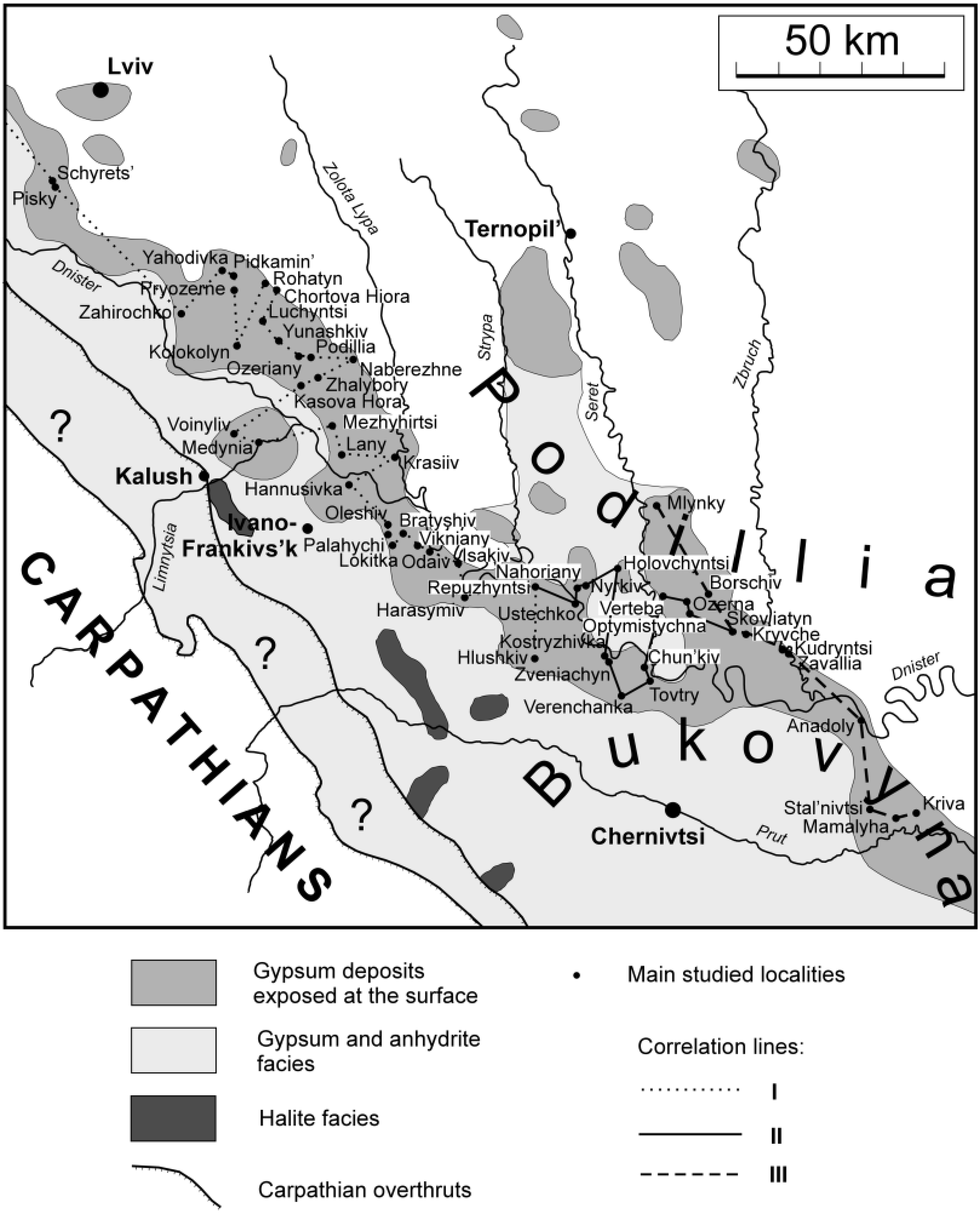

Fig. 2. Distribution of studied gypsum outcrops and correlation lines in the Badenian (Middle Miocene) evaporite basin in the northern Carpathian Foredeep in Ukraine and north Moldova (locality Kriva; bottom right); after ATLAS GEOLOGICZNY GALICYI 1885-1914, OLSZEWSKI 1911, PANOW & PŁOTNIKOW 1996 and other sources (see Fig. 1, maps 6-27 in this Appendix and BĄBEL 2004)

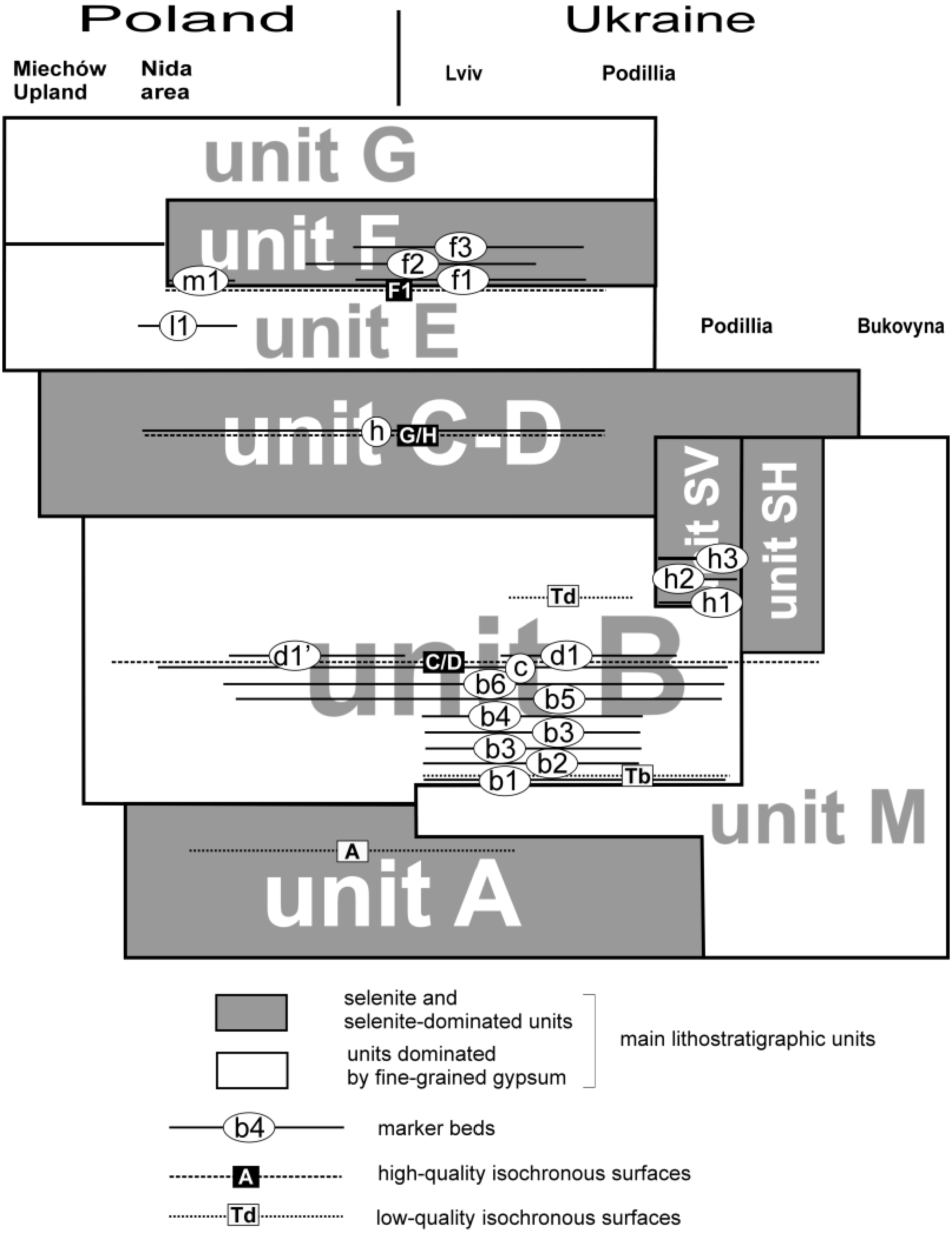

Fig. 3. Stratigraphy of the Badenian gypsum evaporites in the northern Carpathian Foredeep along the correlation line 4-27 (Miechów Upland-Bukovyna) shown in Fig. 1

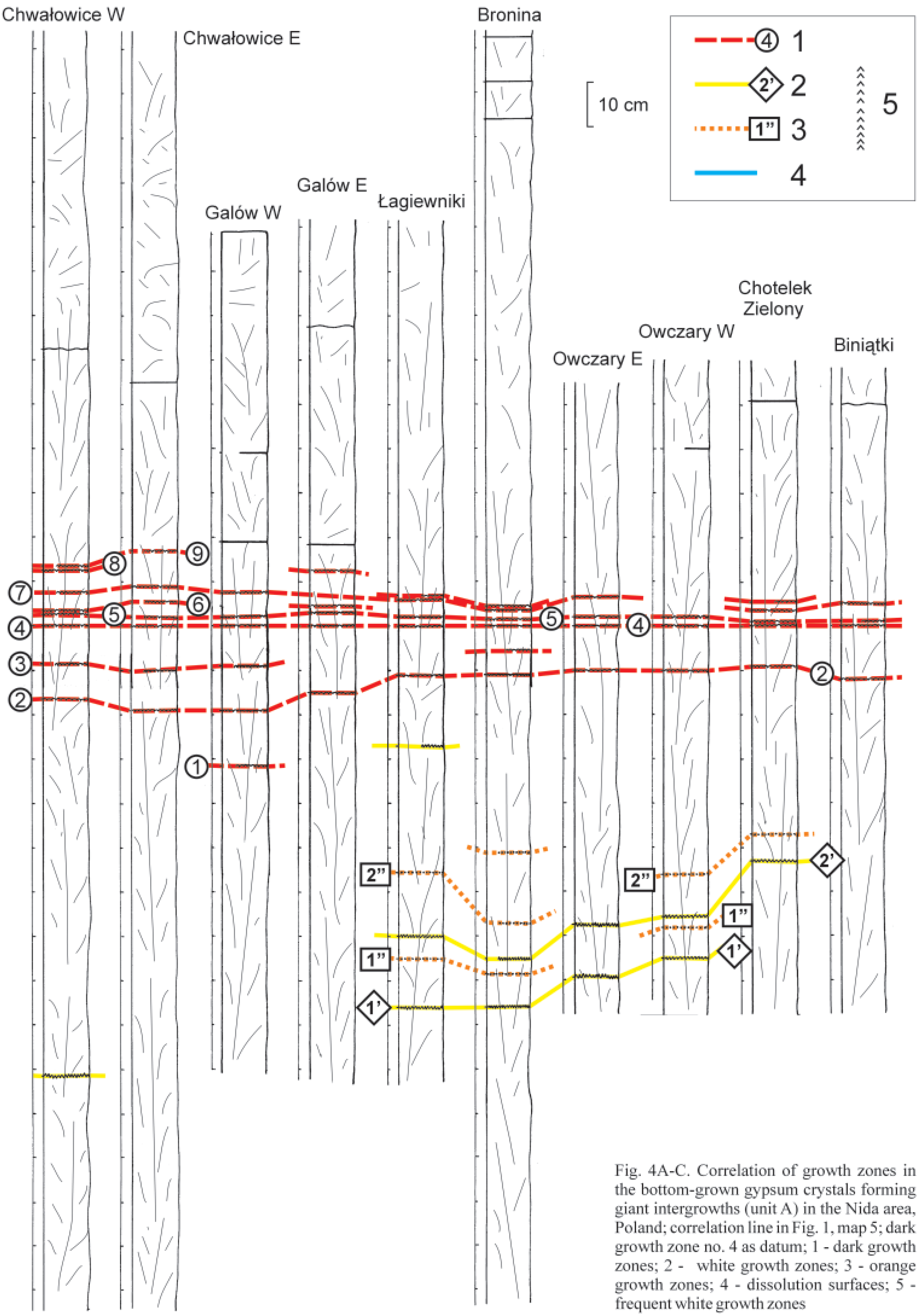

Fig. 4A-C. Correlation of growth zones in the bottom-grown gypsum crystals forming giant intergrowths (unit A) in the Nida area, Poland; correlation line in Fig. 1, map 5; dark growth zone no. 4 as datum; 1 - dark growth zones; 2 - white growth zones; 3 - orange growth zones; 4 - dissolution surfaces; 5 - frequent white growth zones

FIGURE 4A

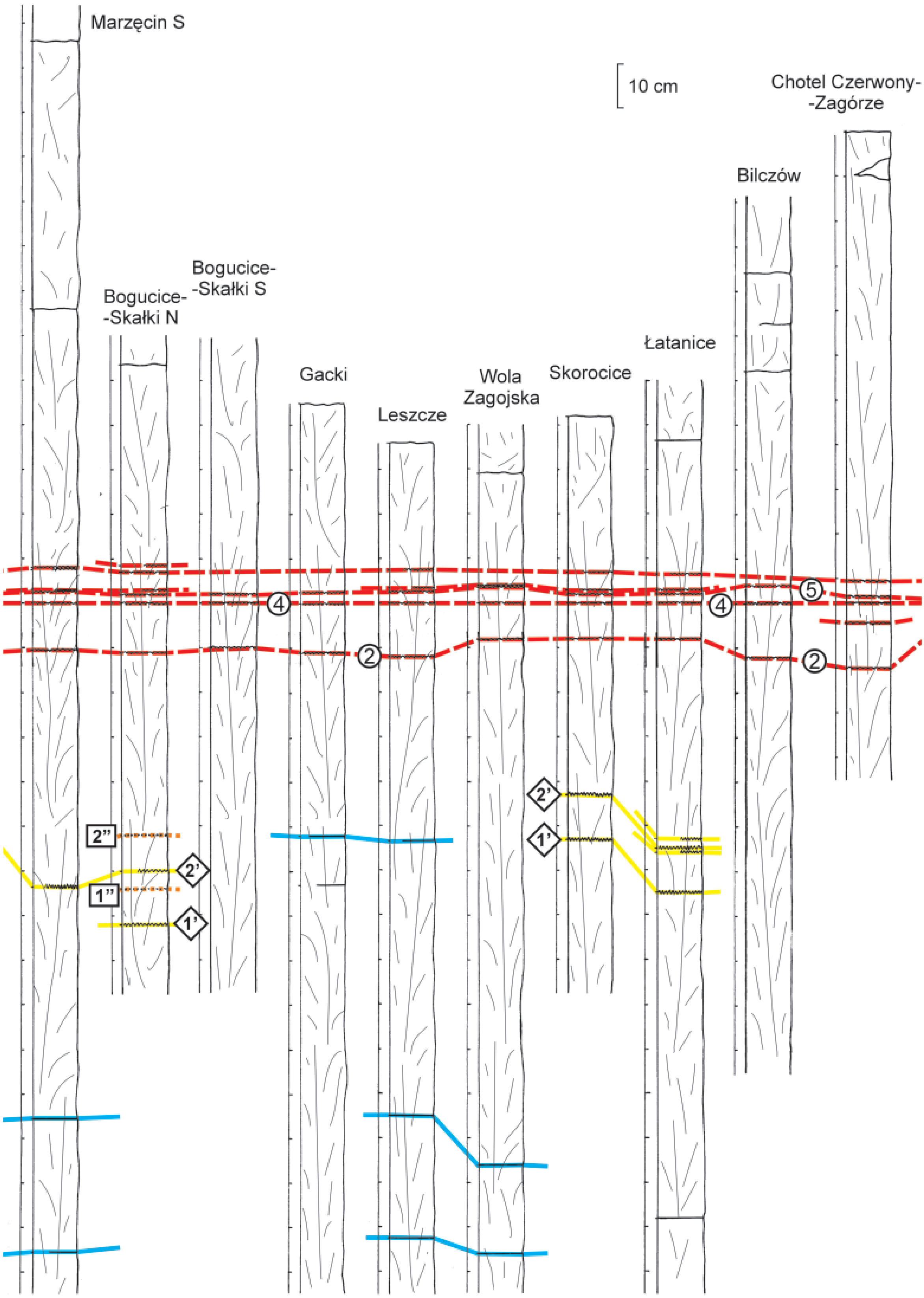

FIGURE 4B

Fig. 4A-C. Continued

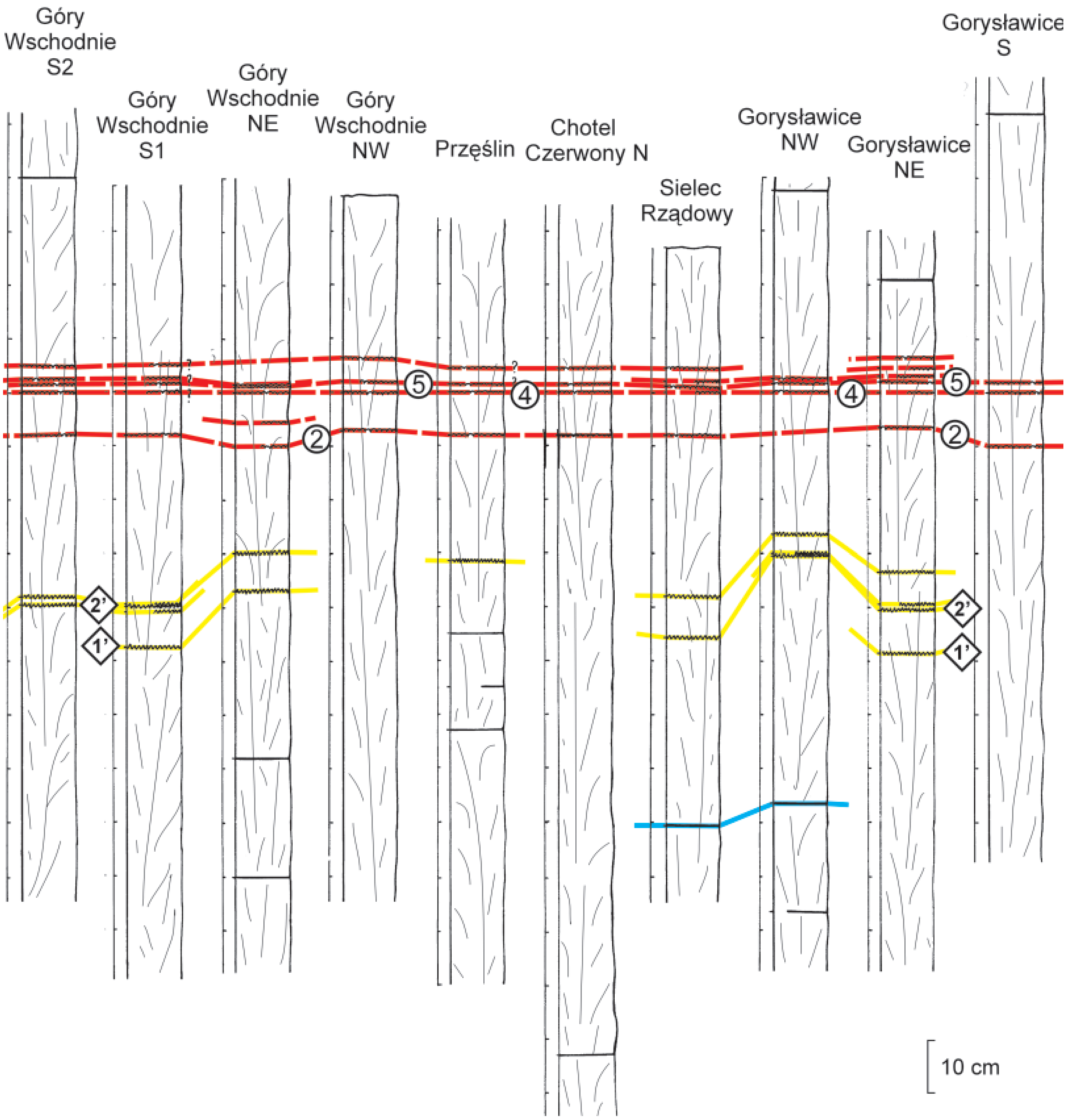

FIGURE 4C

Fig. 4A-C. Continued

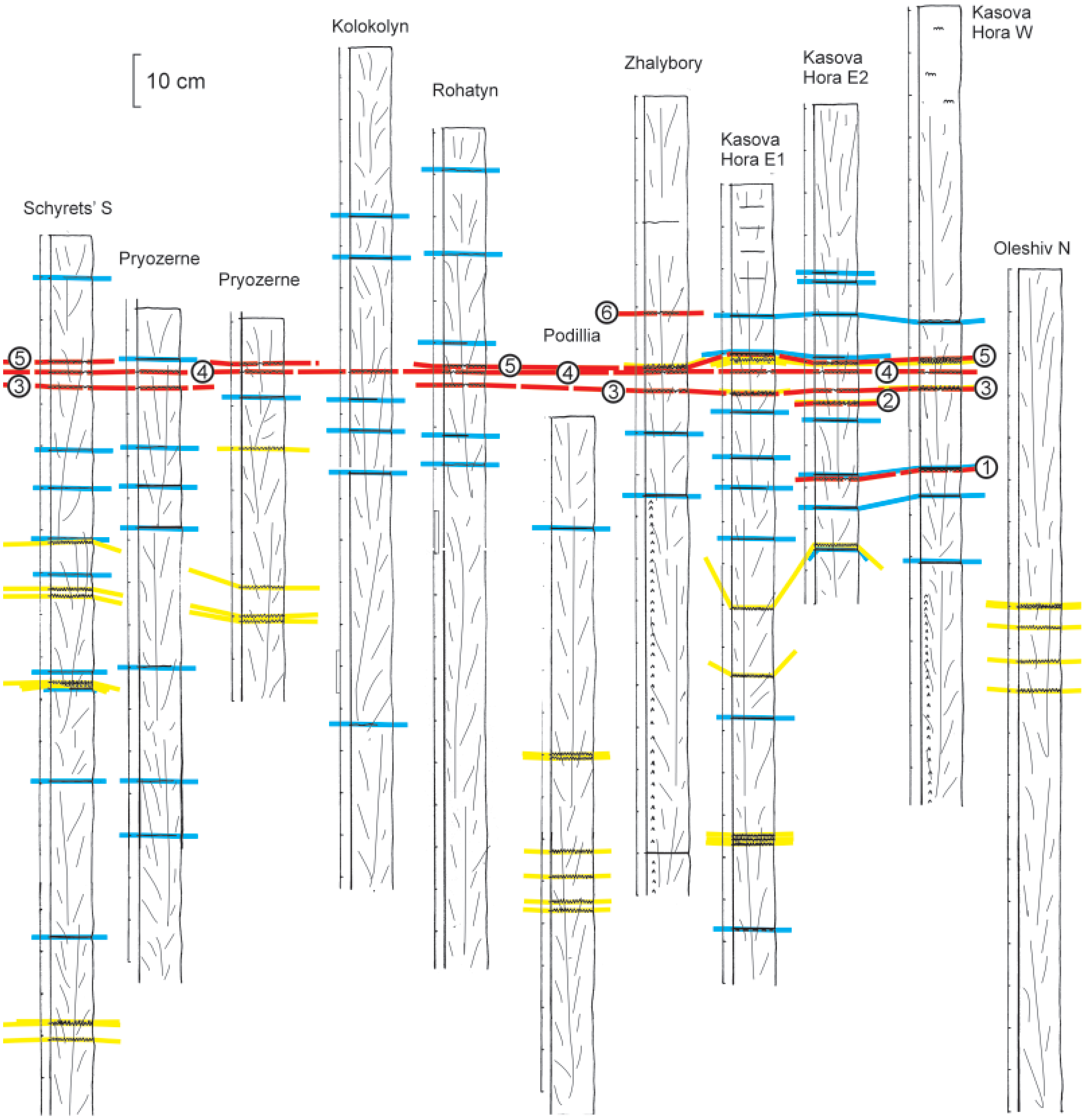

Fig. 5.

Correlation of growth zones in the giant gypsum intergrowths (unit A) in Ukraine; correlation line I in Fig. 2; dark growth zone no. 4 as datum; see Fig. 4A for explanation of symbols

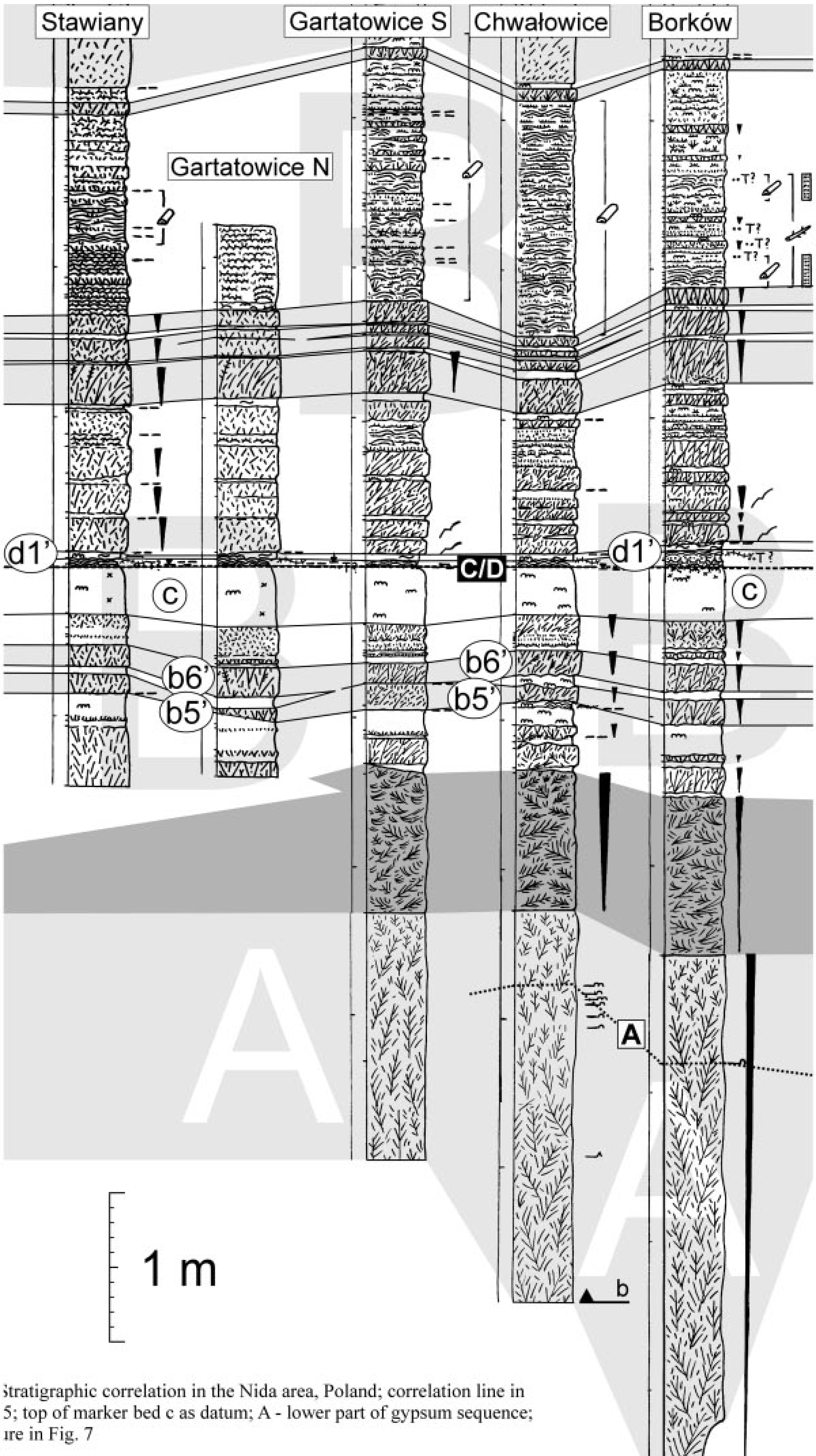

Stratigraphic correlation in the Nida area, Poland; correlation line in
5; top of marker bed c as datum; A - lower part of gypsum sequence;
ıre in Fig. 7

FIGURE 6A

Fig. 6. Continued.
B - middle part of gypsum sequence;
key to hachure in Fig. 7

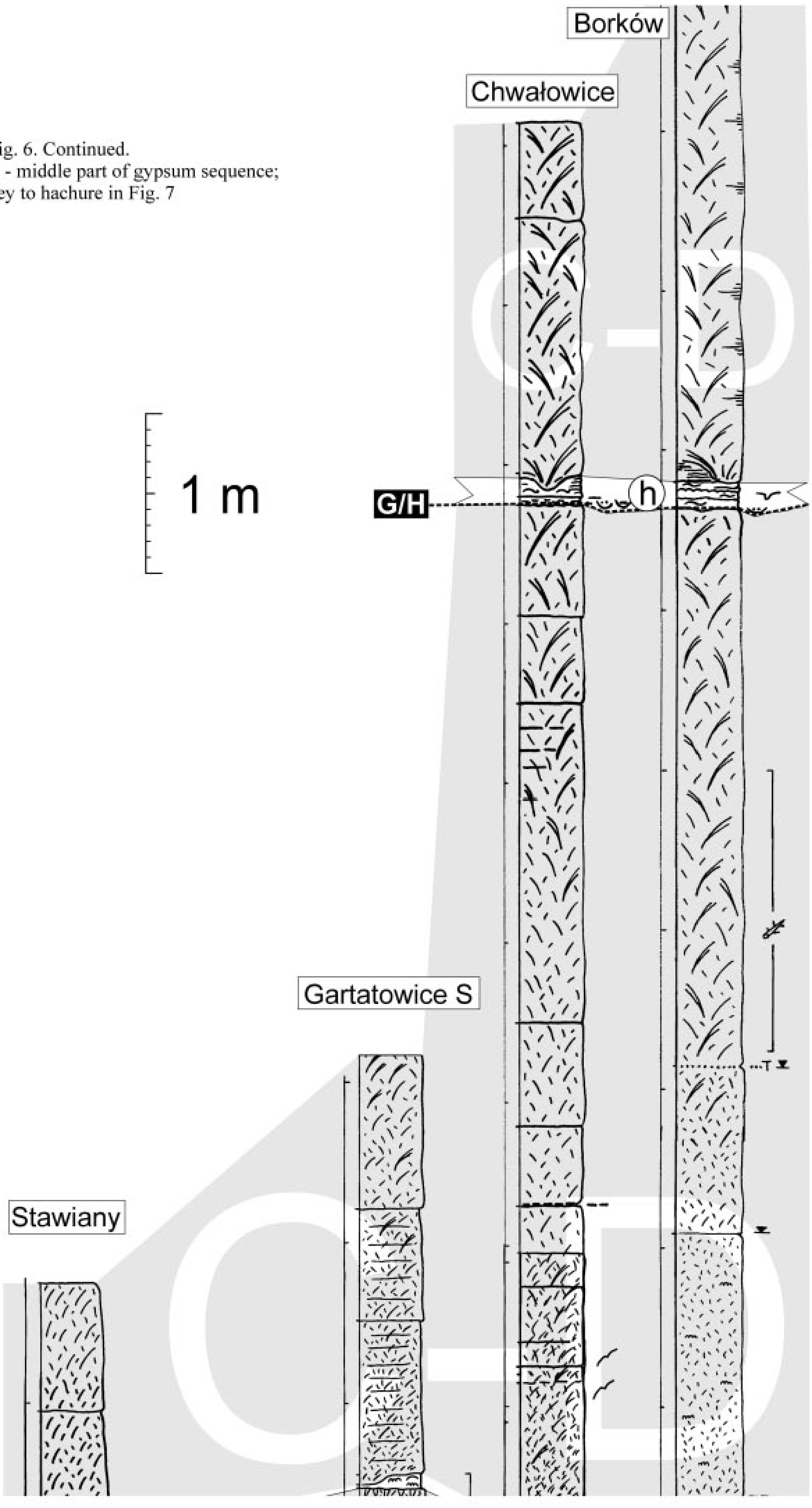

FIGURE 6B

Fig. 6A-B. Continued

Selenite components:

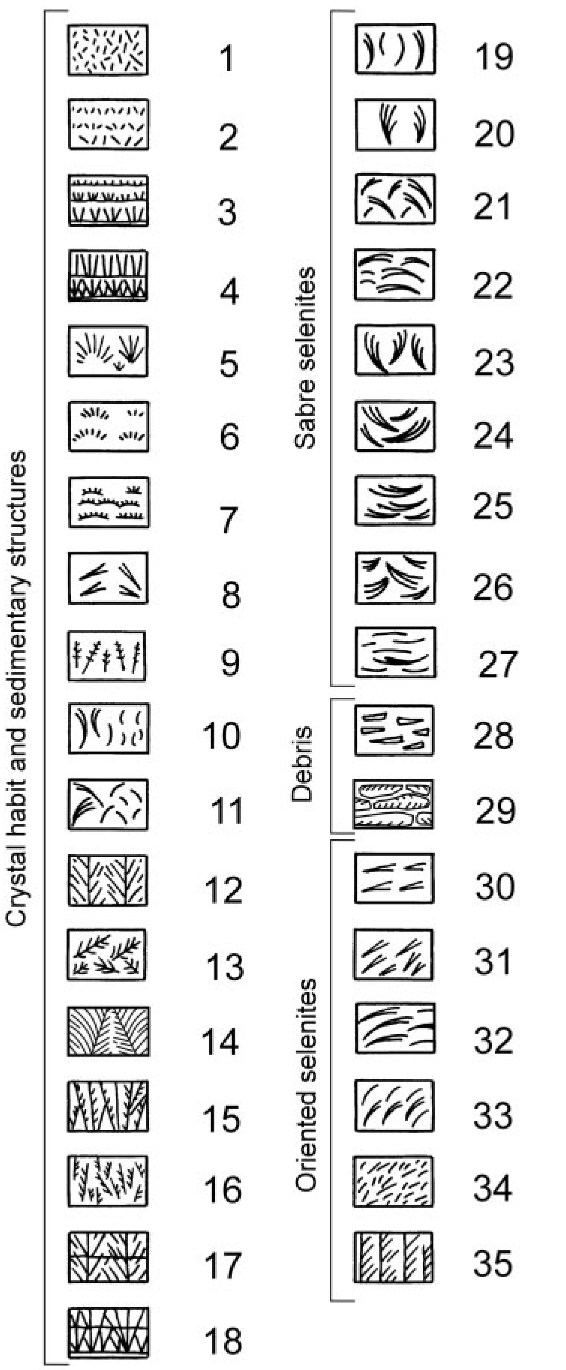

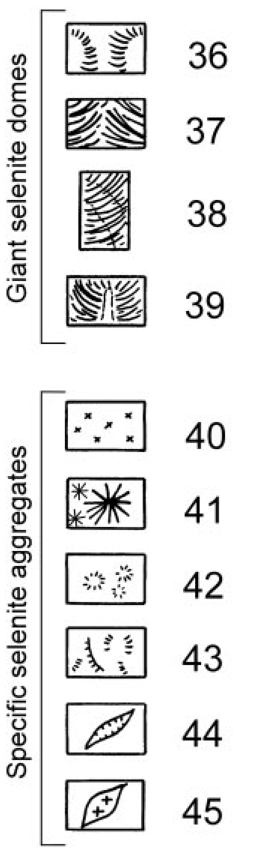

Fig. 7. Explanations of hachure and symbols for Figs 6, 8-18.
Key to hachure within lithologic columns: **1-45 - Selenite components (hachure reflects arrangement, sizes, and shapes of crystals):** 1 - randomly scattered, straight rod-like crystals: short (left) and long (right); 2 - rows of rod-like crystals creating grass-like structures without a sharp base: short crystals (top), long crystals (bottom); 3 - rows of rod-like crystals showing grass-like structures and with a flat base: short crystals (top), long crystals (bottom); 4 - straight grass-like crystals showing palisade-parallel (top) and palisade-radial structure (bottom); 5 - radial or fan-like aggregates of straight crystals grown from point centres (right) and overgrowing fine-grained gypsum dome (left); 6 - rows of small grass-like crystals without a sharp base grown on fine-grained gypsum domes; 7 - rows of small grass-like crystals with a sharp base grown on fine-grained gypsum domes; 8 - intergrowths of straight crystals showing "swallow tail" habit; 9 - aggregates of crystals resembling palm-tree leaves; 10 - vertically oriented single sabre crystals: long (left) and short (right); 11 - obliquely-oriented short sabre crystals (right) and aggregates of split long sabre crystals (left); 12 - vertically-oriented giant gypsum intergrowths showing segmented or chevron structure; 13 - obliquely- and subhorizontally-oriented giant gypsum intergrowths; 14 - subvertically-oriented giant intergrowths showing enlarged upper component crystals; 15 - palisade of large subvertical crystals similar to component crystals of the giant intergrowths, showing characteristic flat crystal surface and growth structures created by slice-like subcrystals (BĄBEL 1999, fig. 5); 16 - small crystals similar to component crystals of the giant intergrowths (with characteristic flat crystal surface and growth structures created by slice-like subcrystals; BĄBEL 1999, fig. 5); 17 - flat horizontal synsedimentary dissolution surface within giant gypsum intergrowths showing syntaxial growth over this surface; 18 - flat horizontal synsedimentary dissolution surface within radial aggregates of the grass-like crystals showing syntaxial growth over this surface; 19-27 - single and split sabre crystals variably oriented in relation to horizontal surface: 19-20 vertical and subvertical crystals (19) and aggregates of split crystals (20); 21 - obliquely-oriented and horizontally-curved crystals; 22 - horizontally-oriented and downward-curved crystals; 23-24 - obliquely-oriented and upward-curved crystals; 25 - horizontally-oriented and upward-curved crystals; 26 - downward-oriented and horizontally-curved crystals; 27 - horizontally-oriented (flat laying), downward- and upward-curved crystals; 28 - redeposited horizontally-laying clasts of crystals within fine-grained gypsum matrix (selenite debris flow facies); 29 - accumulation of in situ broken, abraded and dissolved crystals (selenite debris facies); 30-35 - crystals showing concordant orientation of apices; 30 - subhorizontally oriented subparallel intergrowths; 31 - obliquely-oriented subparallel intergrowths; 32 - horizontally-oriented subparallel sabre crystals; 33 - obliquely-oriented subparallel sabre crystals; 34 - obliquely-oriented subparallel short rod-like crystals; 35 - giant intergrowths with enlarged and subparallel component crystals; 36-39 - gypsum domes with slopes composed of horizontal and upward-curved sabre crystals: 36 - short sabre crystals on slopes of small (<0.5 m) gypsum domes; 37 - long sabre crystals on slopes of large (0.5-2 m) selenite domes; 38 - long sabre crystals on slopes of giant (several m) selenite domes; 39 - sabre crystals on slopes of vertically-elongated domes resembling columns or trunks (TURCZYNOW & ANDRIJCZUK 1995); 40 - gypsum porphyroblasts and aggregates of porphyroblasts ; 41 - radial aggregates of crystals; 42 - concentric groups of centrifugally-oriented of crystals; 43 - small grass-like crystals covering-vertically or sub vertically-oriented substrate; 44 - druse- or geode-like aggregates of centripetally-oriented crystals; 45 - large (up to 1 m) transparent and honey crystals filling-in giant druse-like pores or caverns

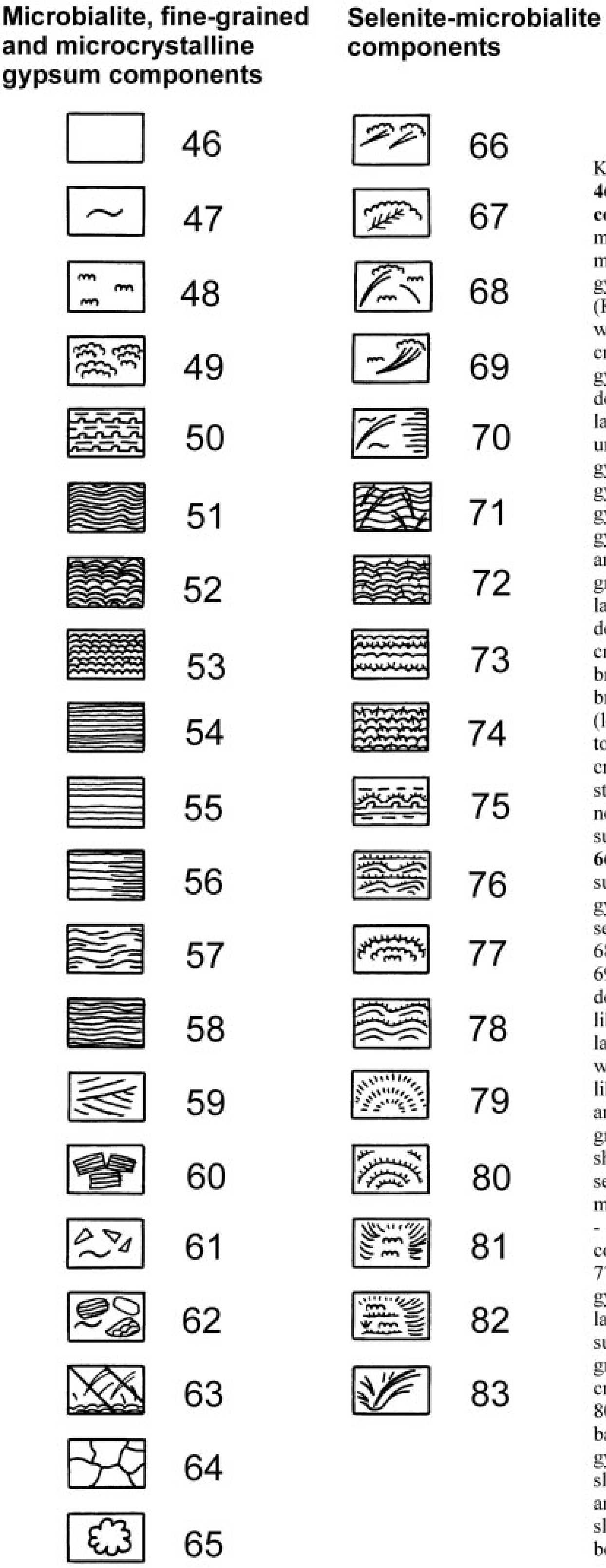

Fig. 7. Continued.

Explanations of hachure and symbols for Figs 6, 8-18.

Key to hachure within lithologic columns:

46-65 - Microbialite, fine-grained and microcrystalline gypsum components: 46 - fine-grained homogeneous gypsum (alabaster when massive and white), or other non-differentiated fine-grained or microcrystalline gypsum; 47 - fine-grained or microcrystalline gypsum showing banded or spotted structure, or with relic lamination (KWIATKOWSKI 1972); 48 - fine-grained (alabaster-like) gypsum with traces of gypsified crenulated microbial mats; 49 - gypsified crenulated microbial mats creating small domal structures; 50 - gypsified microbial mats creating small (< 5 cm) ball-like "alabaster" domes (BĄBEL 1996; 1999, pl. 5, fig. 2) intercalated with clay laminae; 51 - wavy laminated gypsum representing gypsified smooth undulating microbial mats; 52 - wavy laminated gypsum representing gypsified smooth microbial mats creating domal structures; 53 - gypsum microbialite showing crenulated lamination representing gypsified crenulated microbial mats; 54 - flat thin (< 1 mm) laminated gypsum; 55 - flat thick (1-10 mm) laminated gypsum; 56 - fine-grained and microcrystalline gypsum with obscured flat lamination; 57 - fine-grained and microcrystalline gypsum showing obscured wavy lamination; 58 - wavy thin-laminated gypsum showing soft-sediment deformation folds; 59 - fine-grained gypsum showing inclined and cross-stratification; 60 - breccias of laminated gypsum; 61 - gypsum breccias with alabaster clasts and alabaster matrix; 62 - gypsum breccias with alabaster-like matrix and rounded clasts of laminated (left), microbialite (right, bottom), and homogeneous gypsum (right, top); 63 - secondary alabaster with ghosts and relics of primary sabre crystals; 64 - secondary alabaster with homogeneous and nodular structure; 65 - megaspheroids: large (up to 0.5 m) displacive balls or nodules of secondary alabaster with cauliflower-like external surfaces.

66-83 - Selenite-microbialite components: 66 - small isolated subhorizontal intergrowths showing "swallow tail" habit within gypsum microbialite deposits; 67 - large isolated intergrowth with segmented or chevron structure within gypsum microbialite deposits; 68 - single isolated sabre crystals within gypsum microbialite deposits; 69 - aggregate of split sabre crystals within gypsum microbialite deposits; 70 - isolated sabre crystal within homogeneous (alabaster-like) gypsum with relic lamination; 71 - sabre crystals within wavy laminated gypsum microbialite deposits; 72 - short rod-like crystals within wavy laminated gypsum microbialite deposits; 73 - small grass-like crystals covering surfaces of gypsified crenulated microbial mats and intercalating gypsum microbialite deposits; 74 - small isolated grass-like crystals scattered within gypsum microbialite deposits showing crenulated lamination; 75 - small (< 10 cm) microbialite-selenite domes, formed by grass-like crystals covering the ball-like microbialite "alabaster" domes, sandwiched between clay laminae; 76 - large (up to 30 cm high) laminated microbialite-selenite domes composed of clastic gypsum laminae and grass-like gypsum laminae; 77 - laminated microbialite-selenite domes, composed of clastic gypsum laminae and grass-like gypsum laminae, intercalated with flat laminae of grass-like gypsum; 78 - gypsum dome with cauliflower surface created by gypsified crenulated microbial mats covered with grass-like crystals; 79 - gypsum dome composed of rows of radiating crystals, without sharp base, intercalated with fine-grained gypsum; 80 - gypsum dome composed of rows of grass-like crystals with sharp base intercalated with fine-grained gypsum; 81 - selenite dome with gypsum microbialite core and horizontally oriented sabre crystals on slopes; 82 - selenite dome with core composed of gypsum microbialite and grass-like gypsum and horizontally oriented sabre crystals on slopes; 83 - selenite nucleation cone (DRONKERT 1985) created by bottom-grown sabre crystals

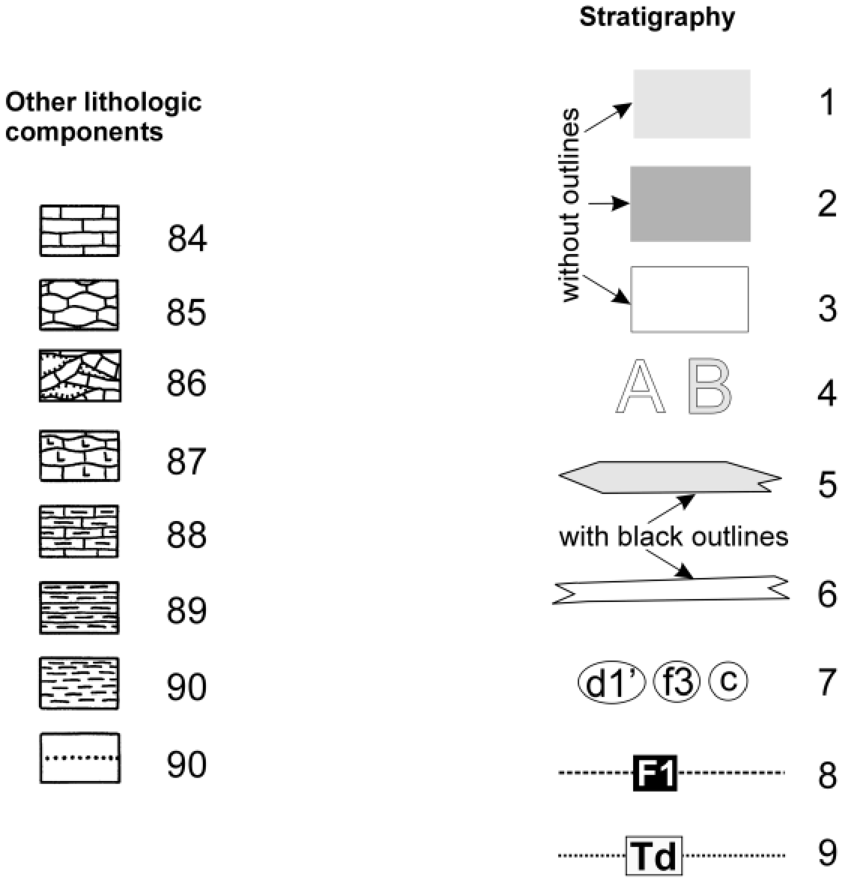

Fig. 7. Continued.
Explanations of hachure and symbols for Figs 6, 8-18

Key to hachure within lithologic columns:

84-90 - Other lithologic components: 84 - limestone (non-differentiated); 85 - wavy bedded limestone; 86 - brecciated limestone with calcite druses; 87 - lithothamnian (red-algal) limestone; 88 - marly limestone; 89 - marly clay; 90 - clay and gypsum-clay deposit; 91 - orange dusty clay

Key to stratigraphic symbols:

1-4 - lithostratigraphic units and/or facies; 1 -selenite and selenite-dominated lithostratigraphic units (and/or facies) composed of vertical crystals; 2 - selenite and selenite-dominated lithostratigraphic units (and/or facies) composed of horizontal crystals; 3 - non-selenite lithostratigraphic units (and/or facies) mainly composed of fine-grained gypsum; 4 - designations of lithostratigraphic units; 5-6 - marker beds; 5 - selenite or selenite dominated marker beds; 6 - m`arker bed composed of fine-grained gypsum; 7 - designations of marker beds; 8 - high-quality isochronous surfaces; 9 - low-quality isochronous surfaces

Key to symbols showing selected features

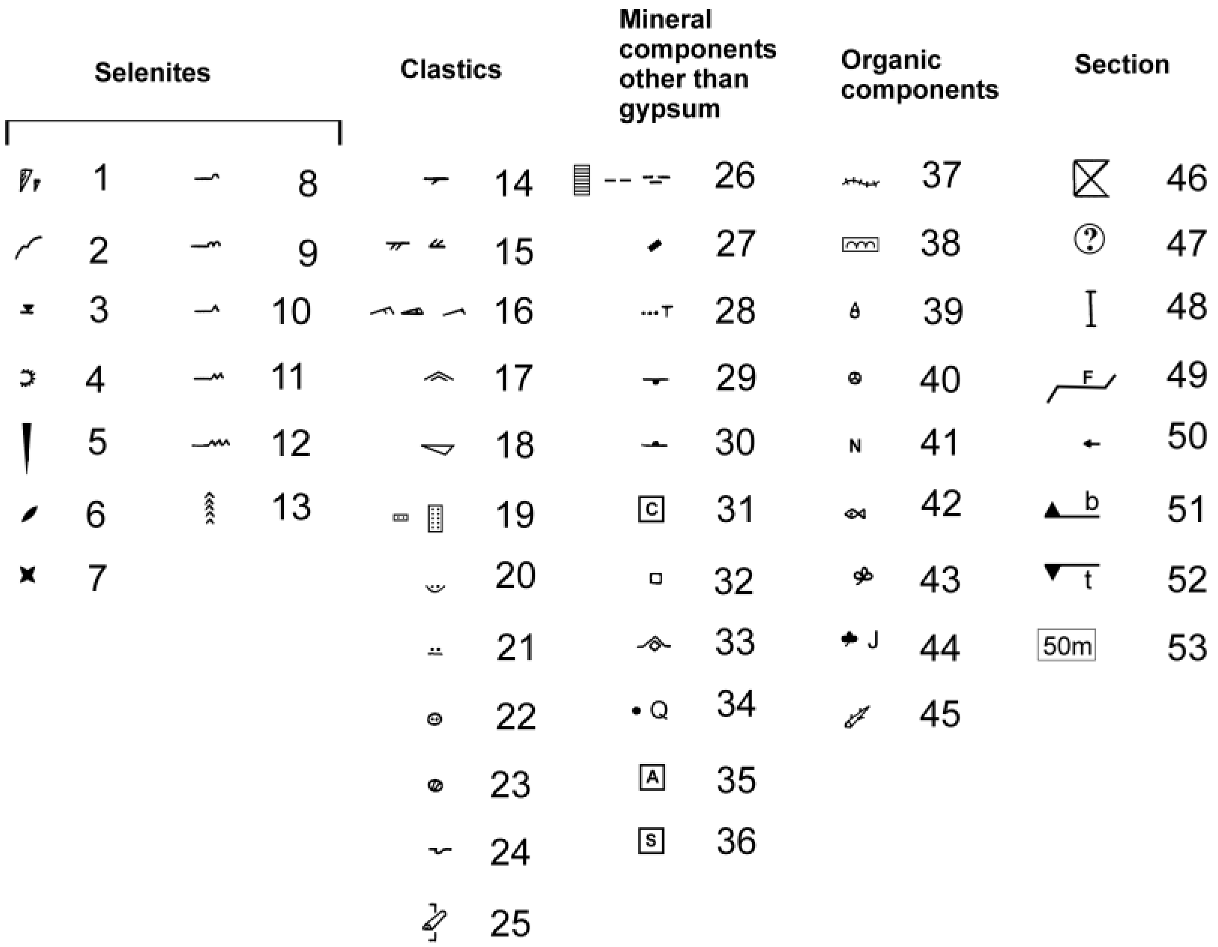

Fig. 7. Continued. Explanations of hachure and symbols for Figs 6, 8-18.

Key to symbols outside lithologic columns:

1-13 - Features of selenite; 1 - crystals showing characteristic flat surface with growth structures created by slice-like subcrystals (see BĄBEL 1999, fig. 5A); 2 - sabre crystals broken due to compaction; 3 - synsedimentary dissolution surface; 4 - small selenite-microbialite domes covered with crystals from one side due to action of brine current (BĄBEL 2002); 5 - large inter- and intracrystalline pores; 6 - single lenticular crystals (>0.5 cm in size); 7 - aggregates of crystals resembling "desert roses" (>0.5 cm in size); 8-13 - growth zones of giant intergrowths; 8-9 - dark growth zones (up to 0.5 cm thick) created by inclusions of organic matter; 8 - single dark growth zone; 9 - two adjacent dark growth zones; 10-13 - white growth zones (ca. 1 mm thick) created by tiny mineral inclusions; 10 - single white growth zone; 11 - two adjacent white growth zones; 12 - three adjacent white growth zones; 13 - frequent white growth zones;

14-26 - Features of clastics; 14 - erosion surface; 15 - low-angle cross stratification (left) and high-angle cross stratification (centre and right); 16 - current ripples; 17 - wave ripples; 18 - loaded current ripples; 19 - sugar-like clastic gypsum; 20 - small channels filled with sugar-like clastic gypsum; 21 - laterally continuous laminae of sugar-like clastic gypsum; 22 - intraclasts of fine-grained gypsum; 23 - intraclasts of large broken, abraded and dissolved gypsum crystals; 24 - slump and soft-sediment deformation folds; 25 - laterally elongated laminated microbialite-selenite domes composed of sugar-like clastic gypsum laminae (KWIATKOWSKI 1972; BĄBEL 2002);

26-36 - Mineral components other than gypsum; 26 - clay intercalation and clay showing perfect, flat, mm-scale lamination (left); 27 - clast of clay; 28 - orange dust or dusty clay interpreted as aeolian or pyroclastic deposit; 29 - top of the gypsum bed encrusted with calcite; 30 - base of the gypsum bed encrusted with calcite; 31 - intercalation or admixture of calcium carbonate; 32 - traces of, and gypsum pseudomorphs after dissolved halite crystals; 33 - solution subsidence deformation and breccias related to halite dissolution; 34 - quartz and quartzite pebbles (< 2 cm in size); 35 - traces of anhydrite laths (< 2 mm in length); 36 - small sulphur nodules;

37-45 - Organic components; 37 - thin (1-3 mm) wavy microbial mat gypsified and encrusted with lenticular gypsum crystals; 38 - gypsified crenulated microbial mats showing dark colour significant for local correlation; 39 - thin-walled gastropods and/or molluscs; 40 - foraminifers; 41 - nannoplankton; 42 - fish remnants; 43 - plant remains; 44 - jet; 45 - fragments of lignite, tree trunks, and tree branches encrusted and covered with gypsum crystals;

46-52 - Features of section; 46 - covered parts of the section; 47 - unknown distance between parts of the section; 48 - poorly exposed parts of the section; 49 - mechanical contacts (faults, shear surfaces related to landslides or slumps); 50 - horizontal discontinuity surfaces significant for local correlation; 51 - well exposed base surface of the gypsum section; 52 - well exposed top surface of the gypsum section; 53 - distance between sections

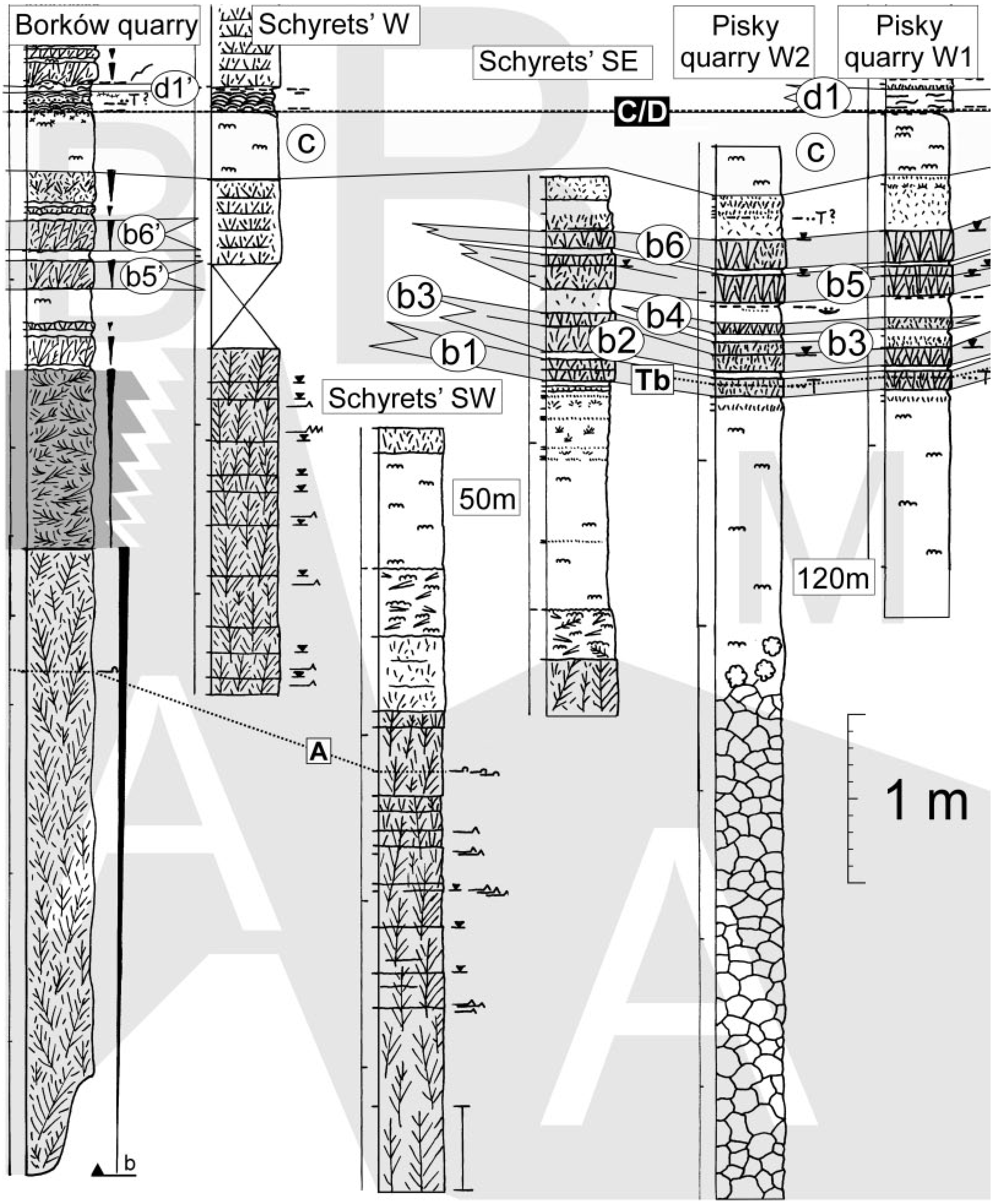

FIGURE 8A

Fig. 8A-E. Stratigraphic correlation in Ukraine; lowermost part of the gypsum sequence below marker bed c; correlation line I in Fig. 2; top of bed c as datum; key to hachure in Fig. 7

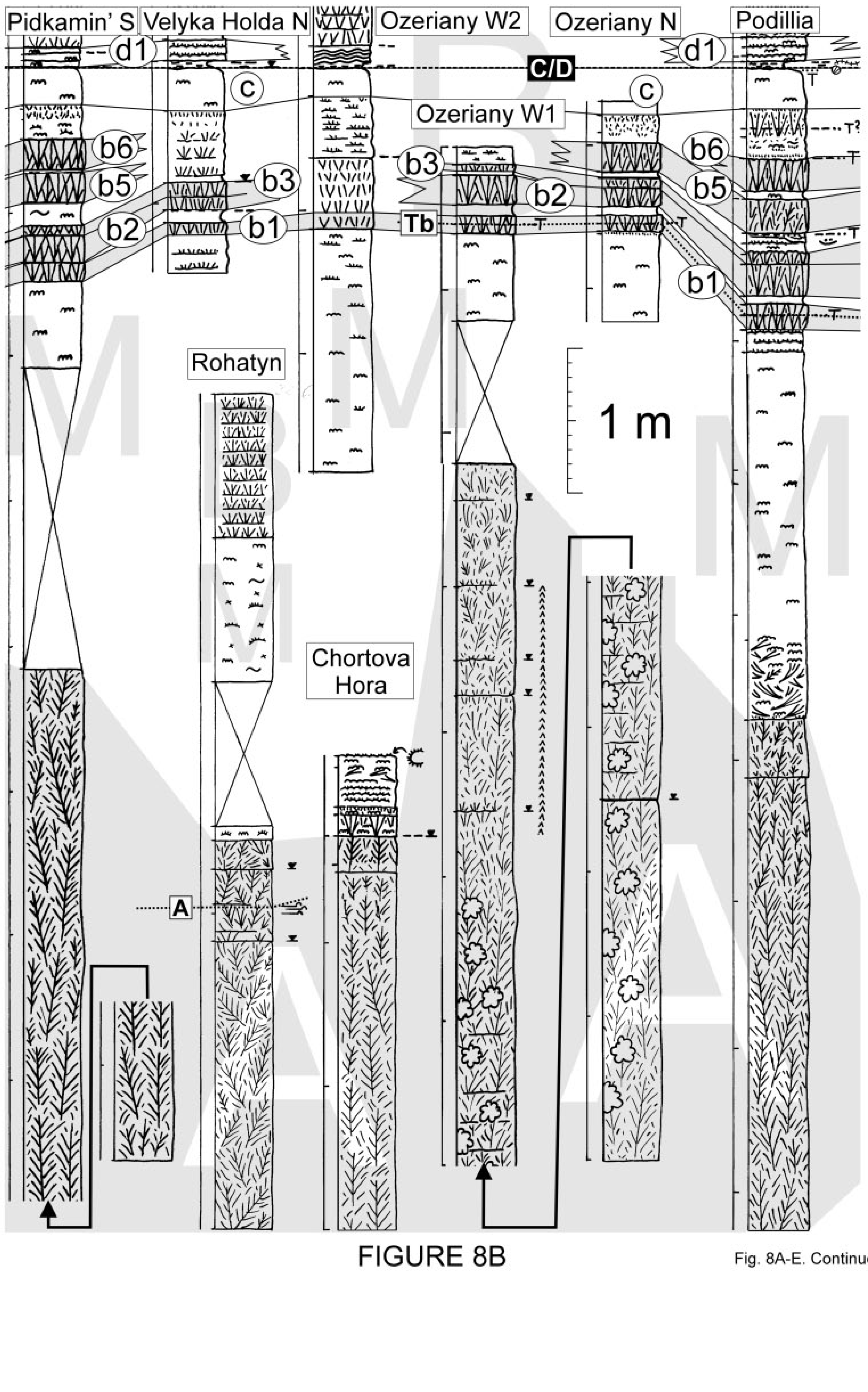

FIGURE 8B

Fig. 8A-E. Continued

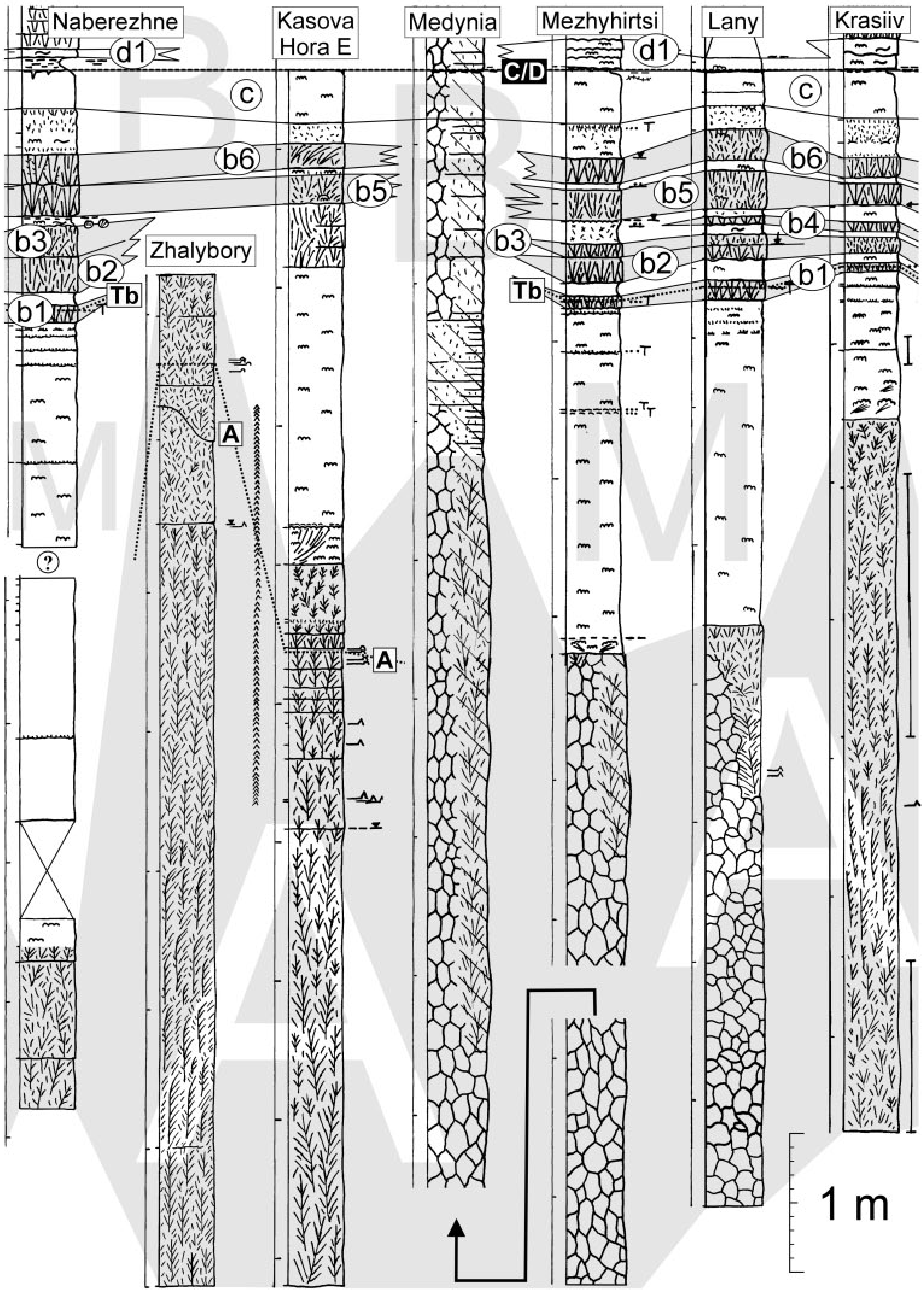

FIGURE 8C

Fig. 8A-E. Continued

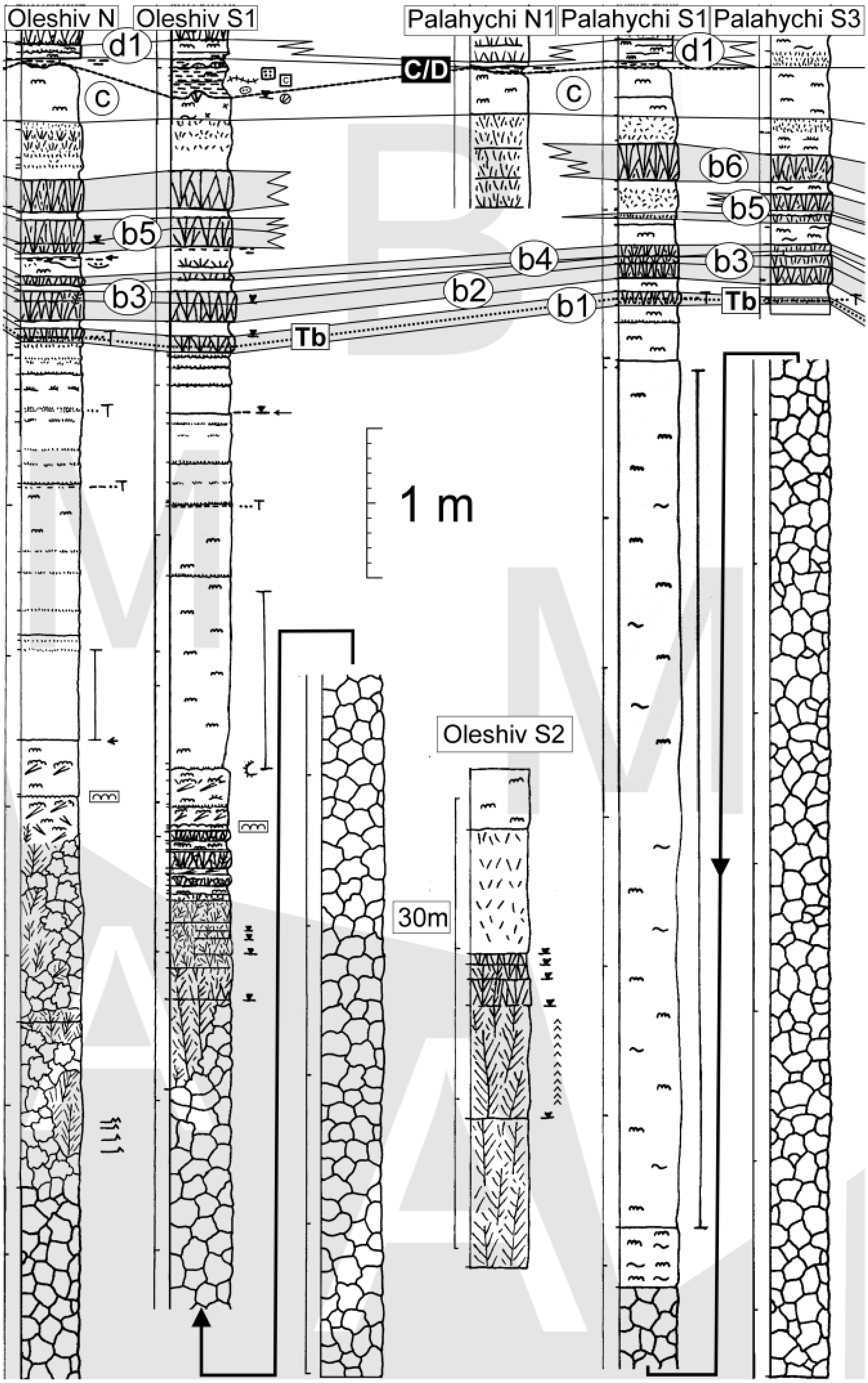

FIGURE 8D

Fig. 8A-E. Continued

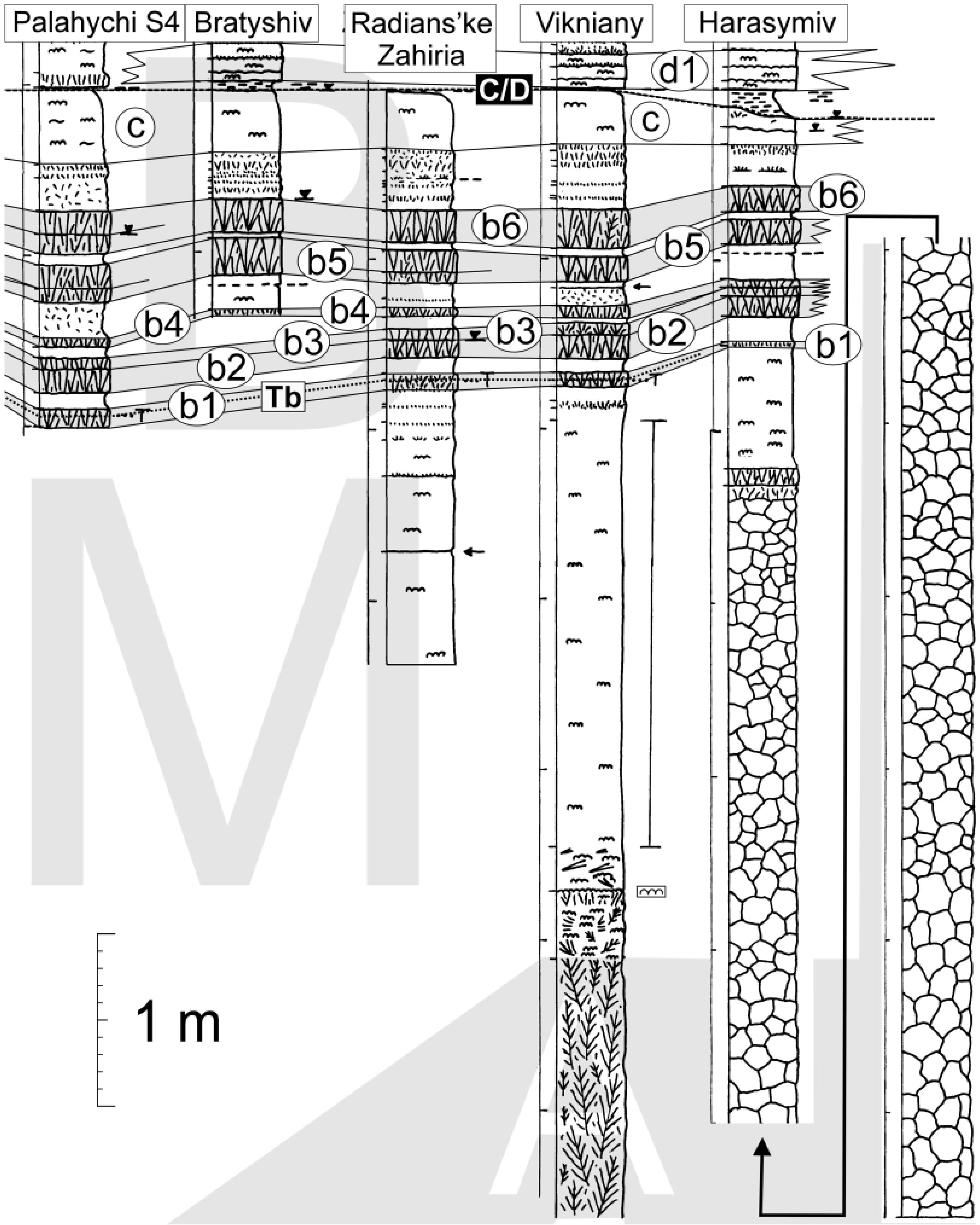

FIGURE 8E

Fig. 8A-E. Continued

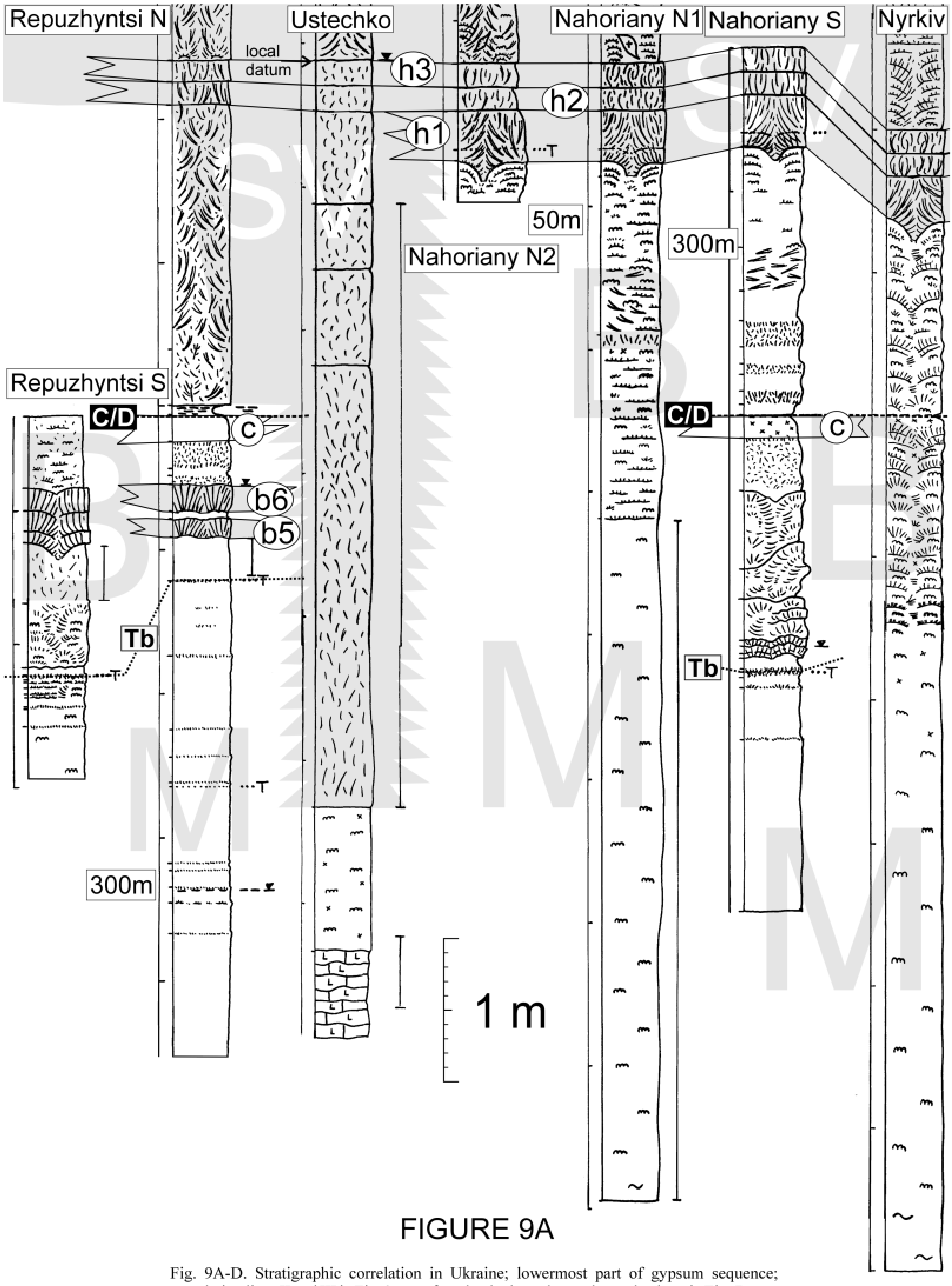

FIGURE 9A

Fig. 9A-D. Stratigraphic correlation in Ukraine; lowermost part of gypsum sequence; correlation lines II and III in Fig. 2; top of marker bed c as datum; key to hachure in Fig. 7

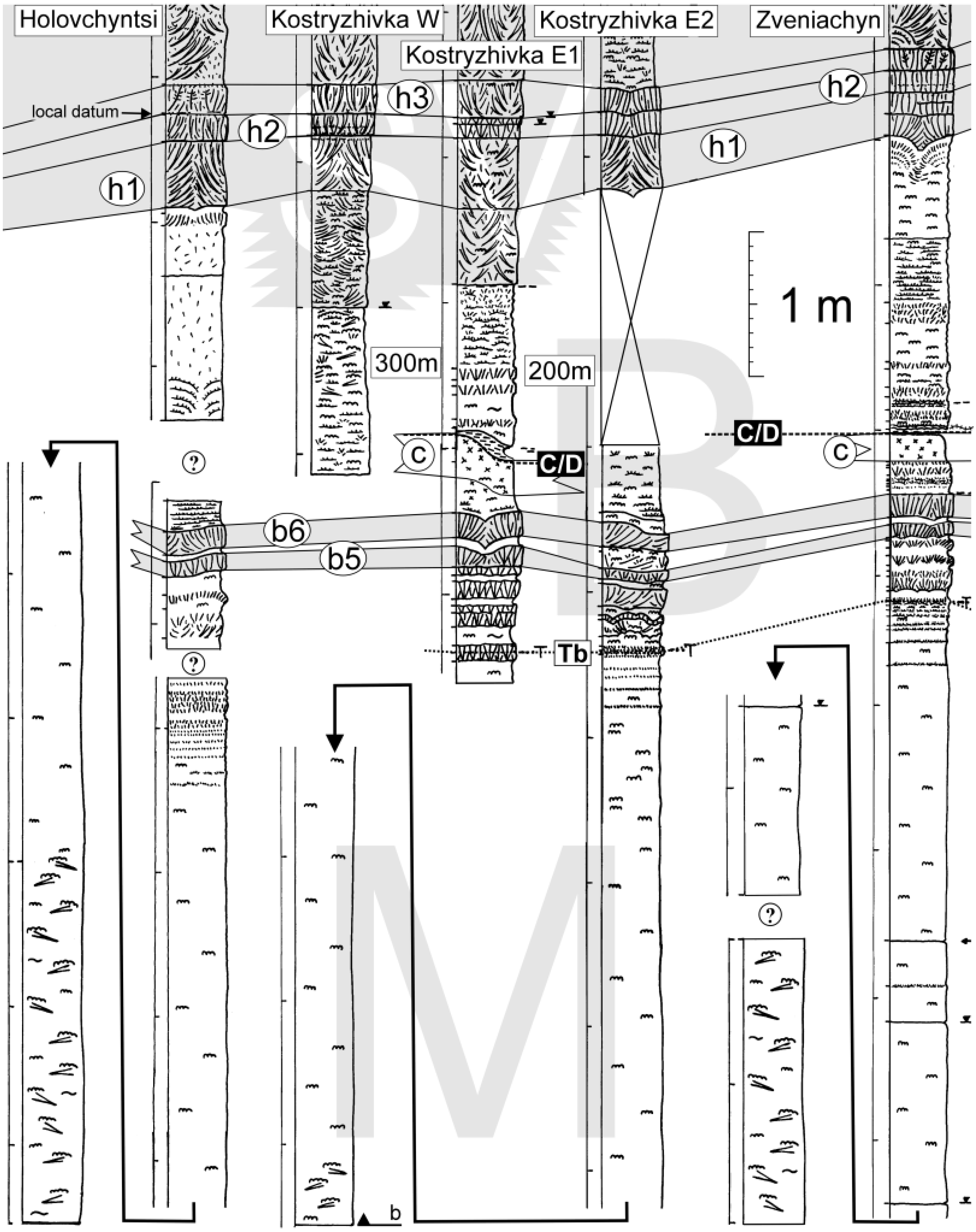

FIGURE 9B

Fig. 9A-D. Continued

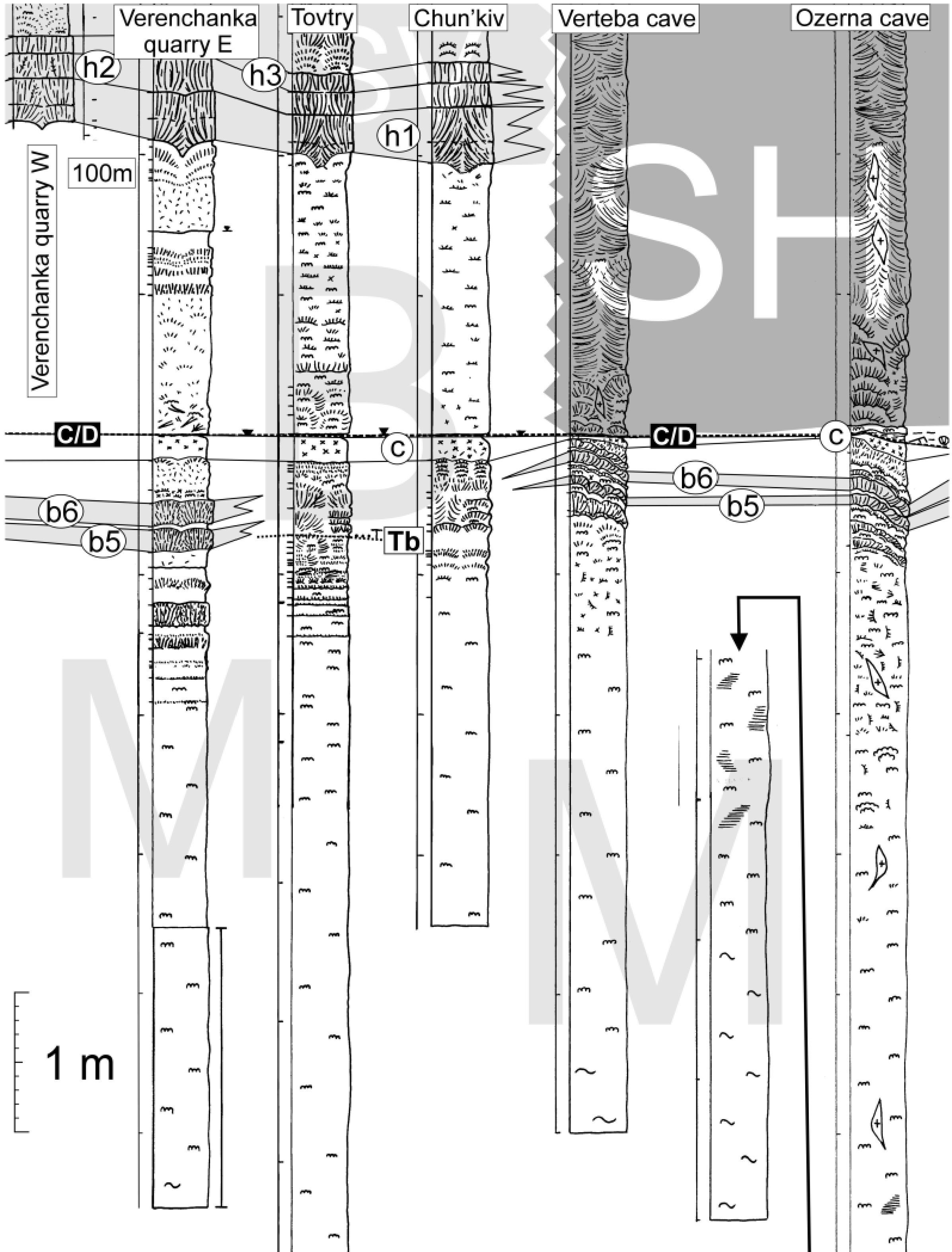

FIGURE 9C

Fig. 9A-D. Continued

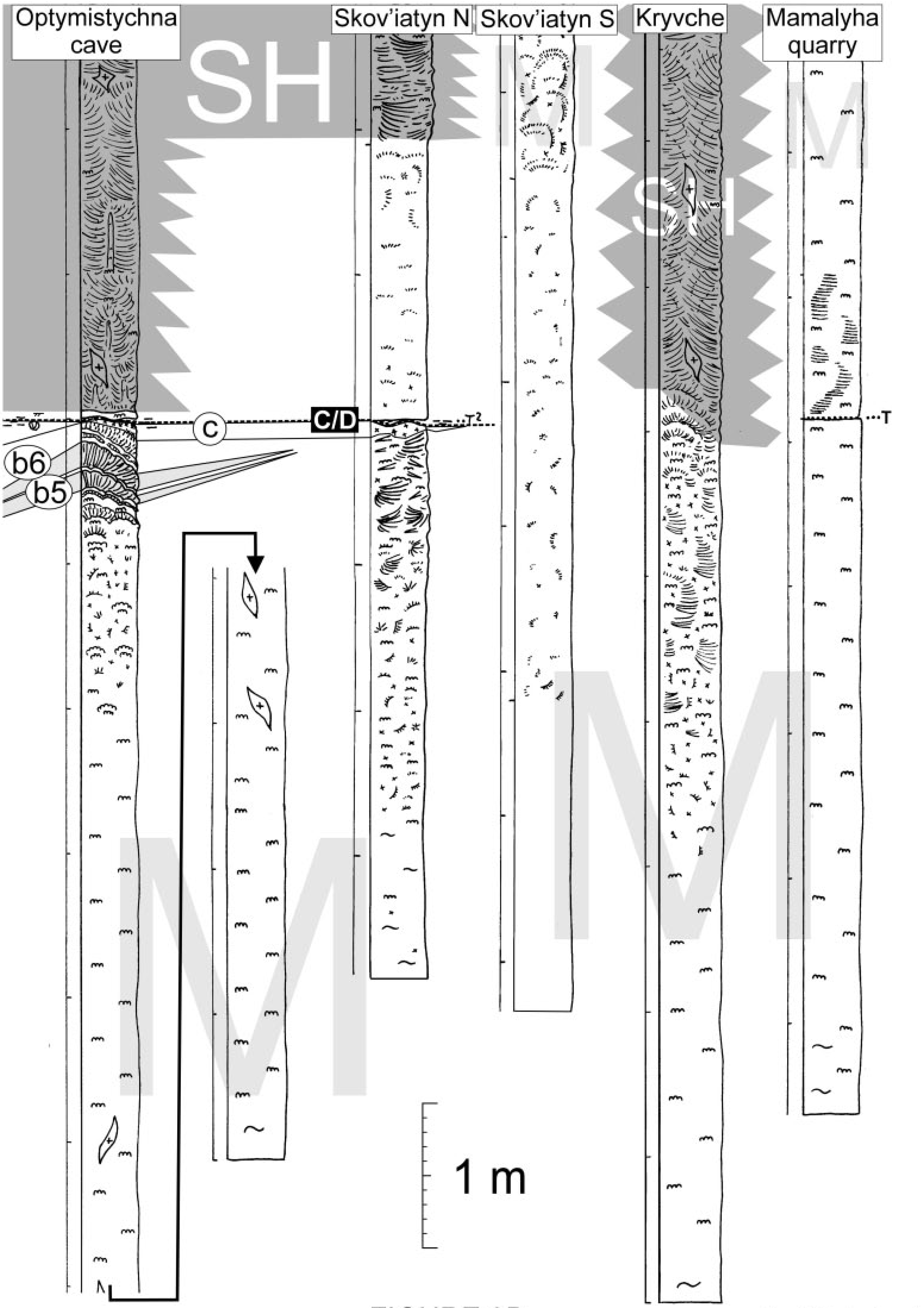

FIGURE 9D

Fig. 9A-D. Continued

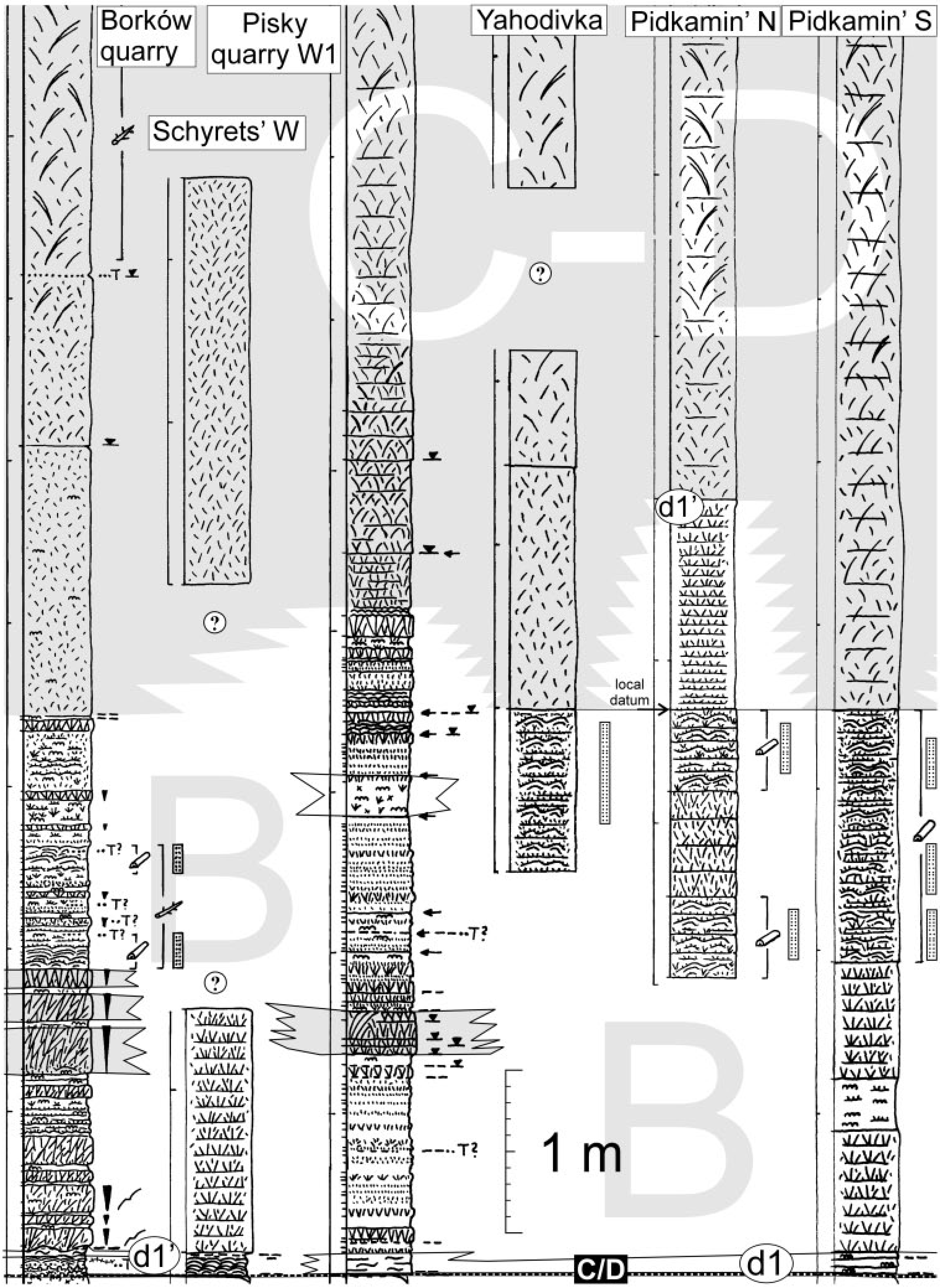

FIGURE 10A

Fig. 10A-E. Stratigraphic correlation in Ukraine; gypsum sequence between marker beds c and h; correlation line I in Fig. 2; top of bed c as datum; key to hachure in Fig. 7

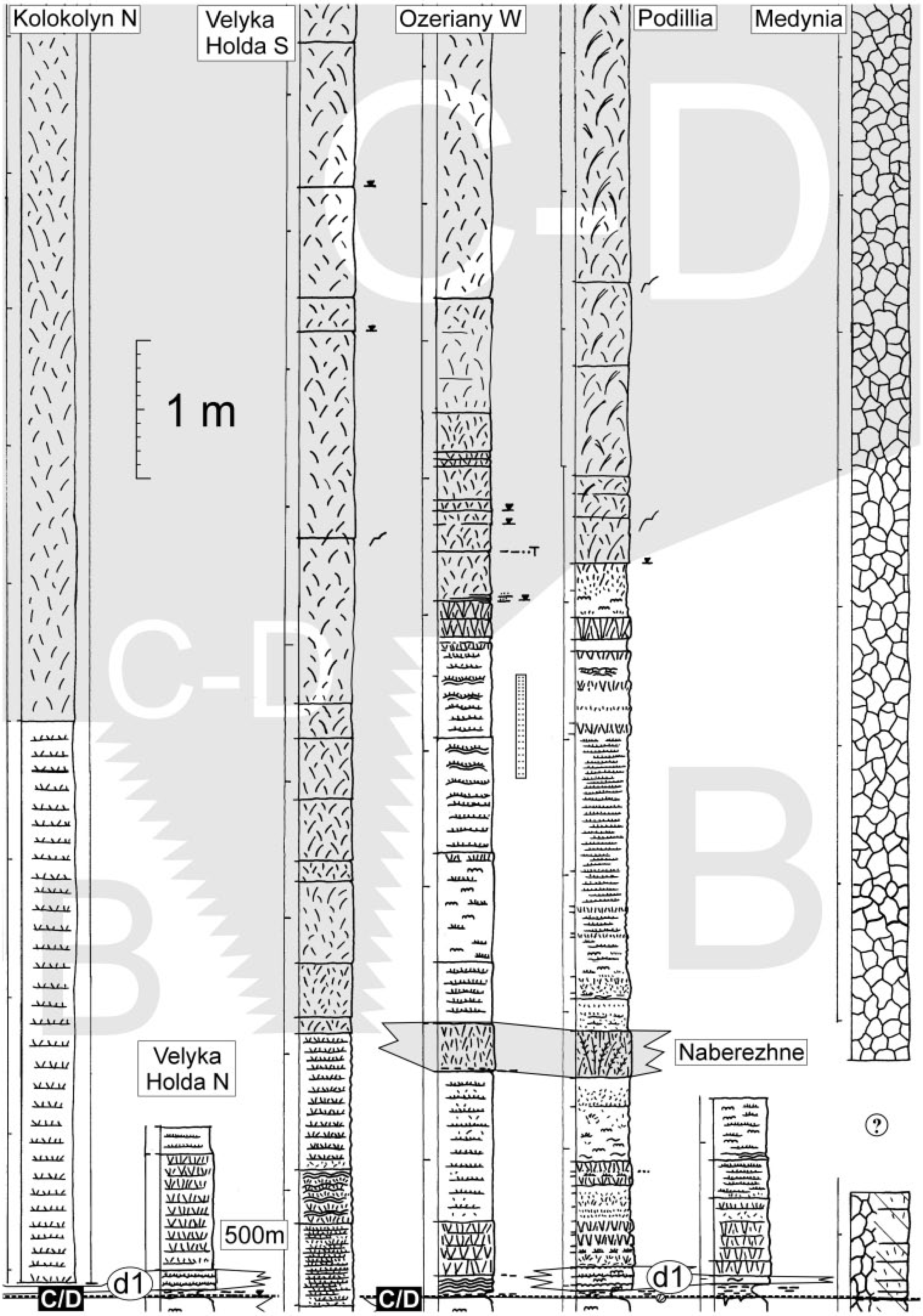

FIGURE 10B

Fig. 10A-E. Continued

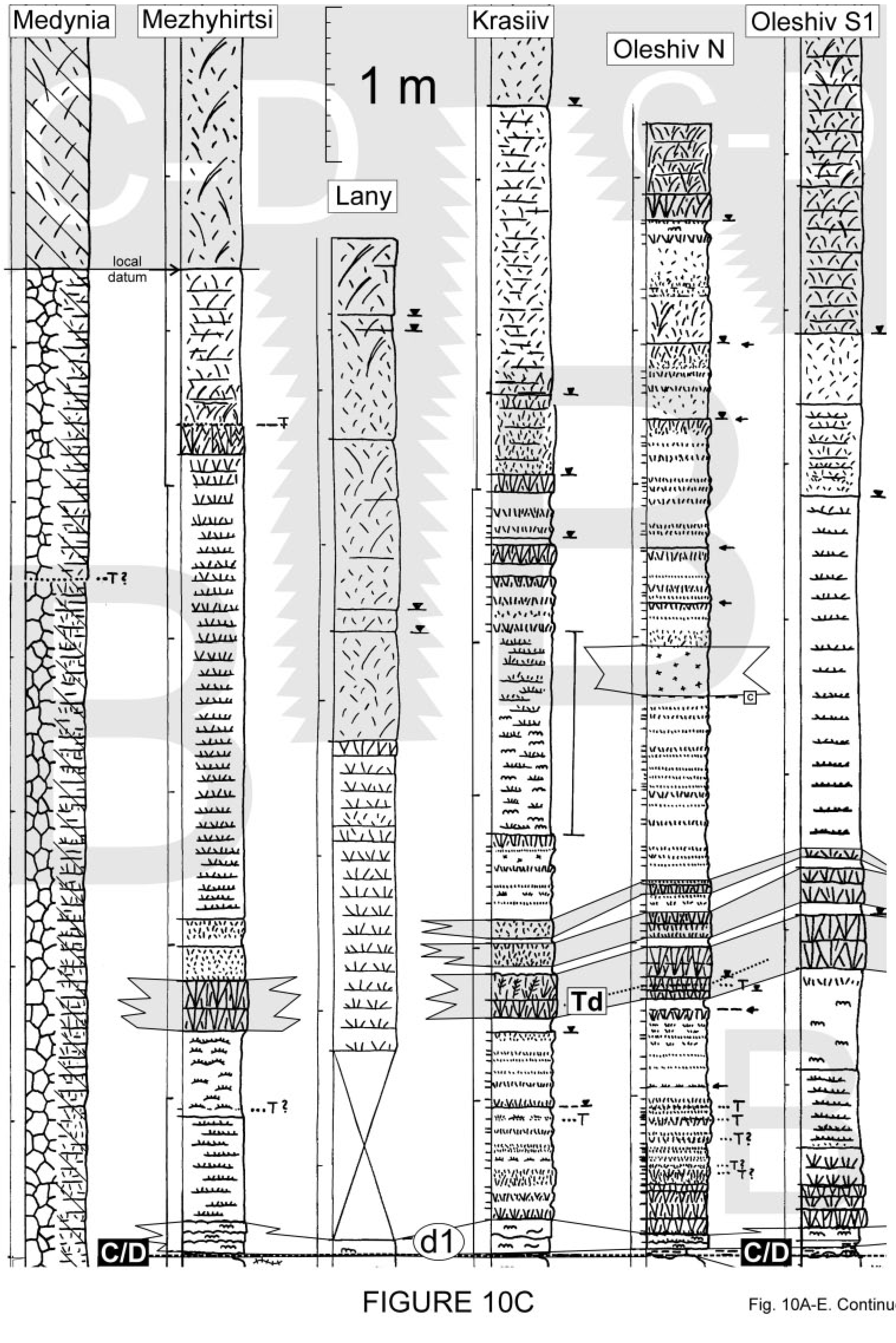

FIGURE 10C

Fig. 10A-E. Continued

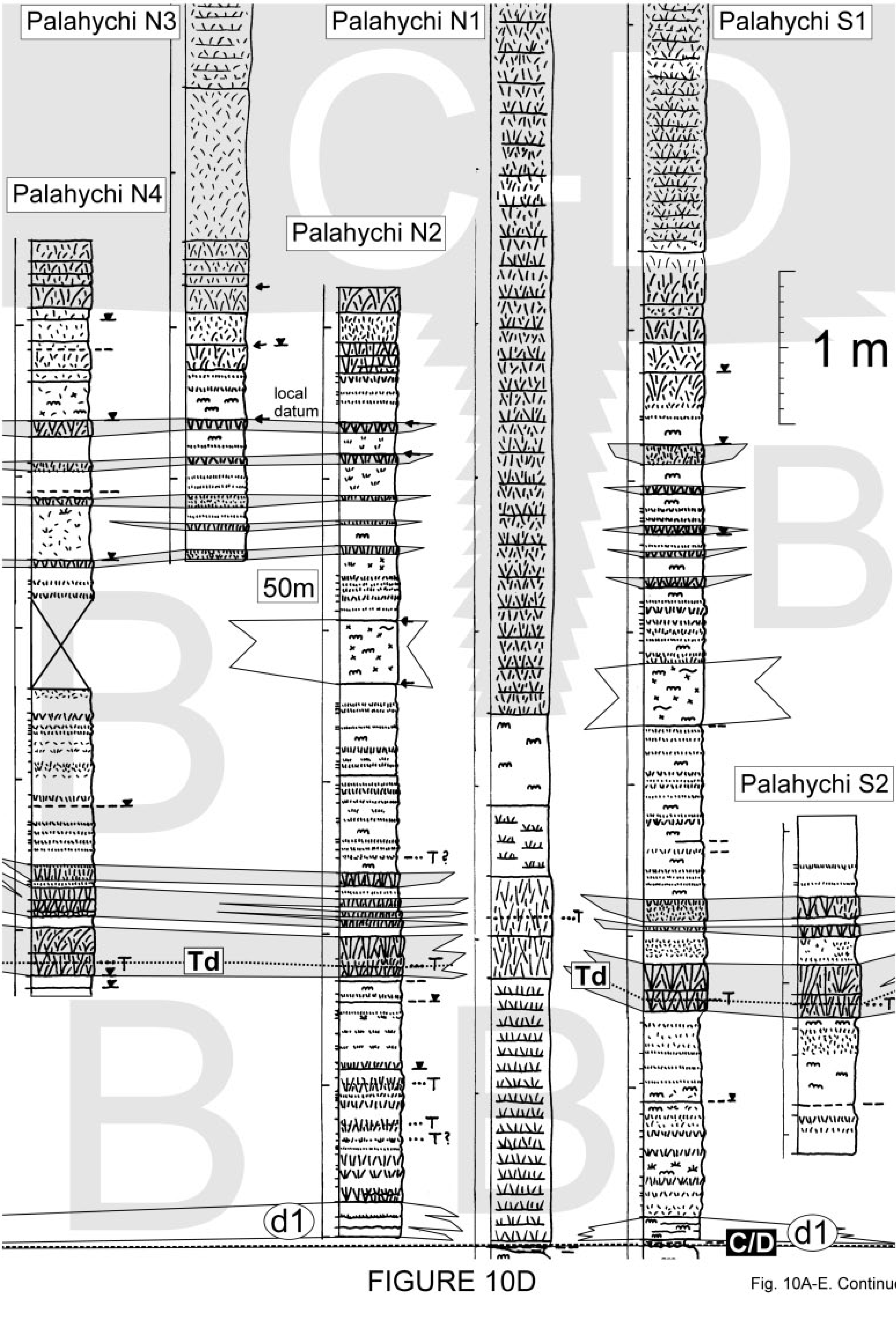

FIGURE 10D

Fig. 10A-E. Continued

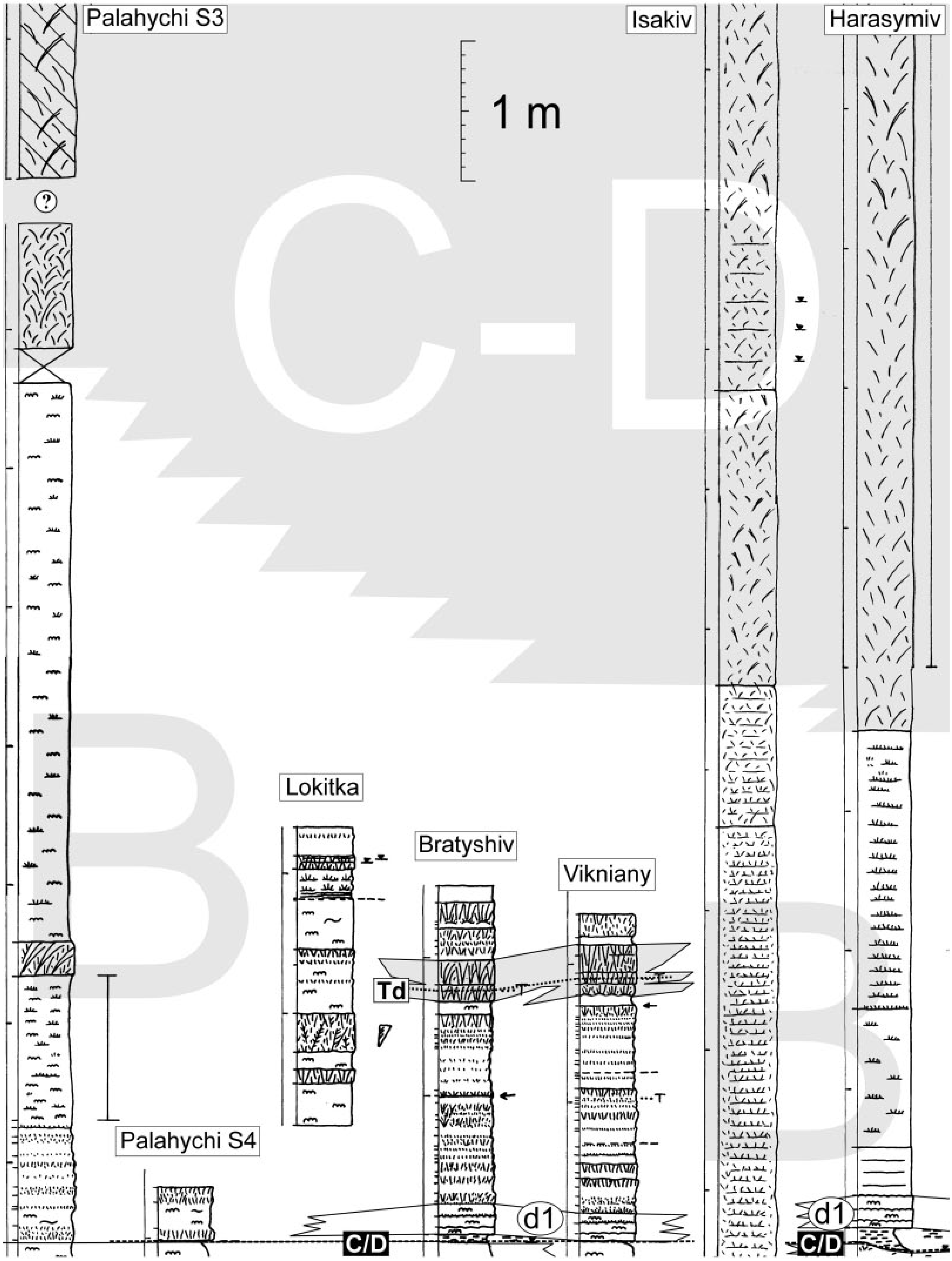

FIGURE 10E

Fig. 10A-E. Continued

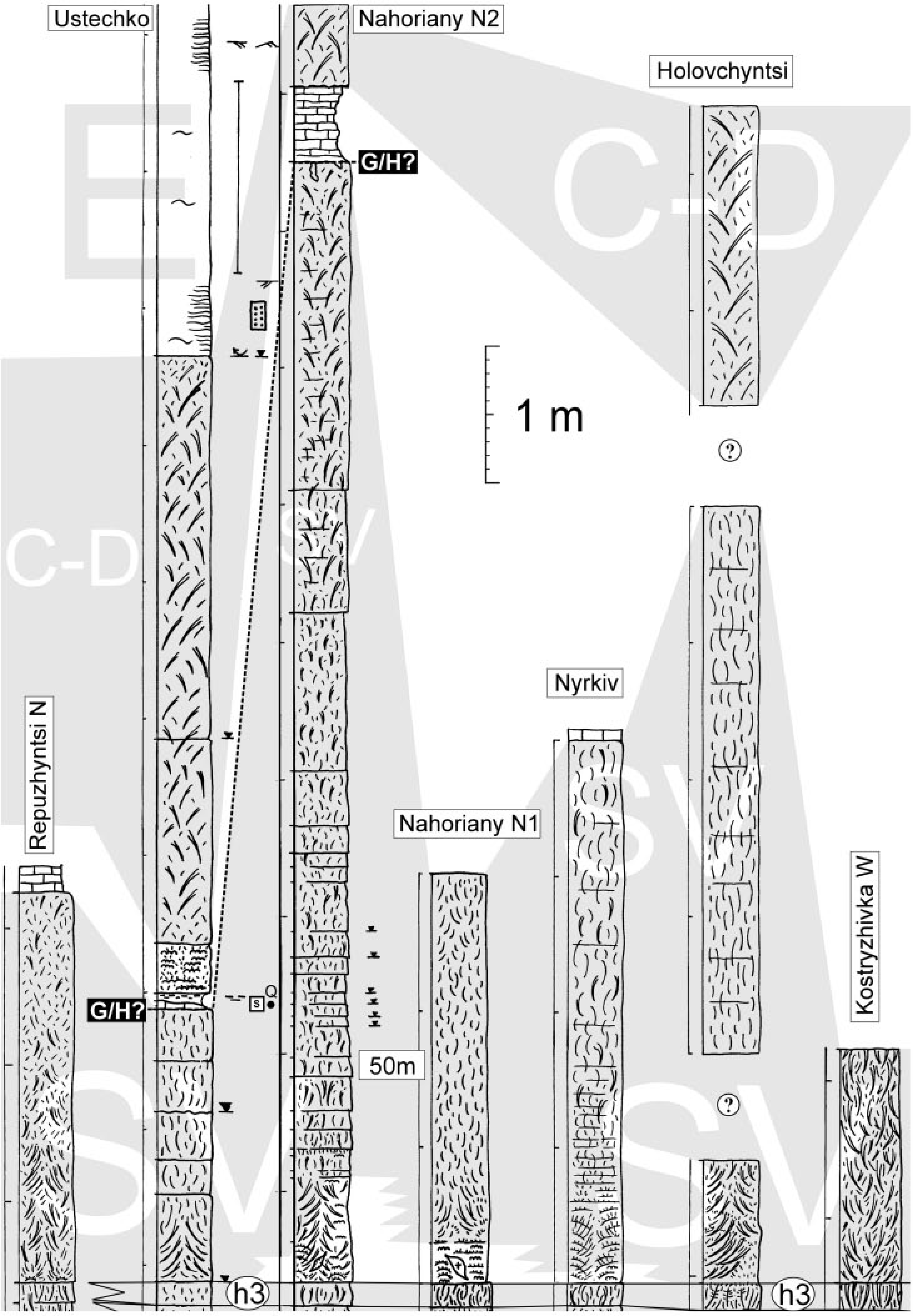

FIGURE 11A

Fig. 11A-C. Stratigraphic correlation in Ukraine; gypsum sequence above marker bed h3; correlation line I in Fig. 2; top of marker bed h3 (Figs 11A-B) and marker bed c (Fig. 11C) as datum; key to hachure in Fig. 7

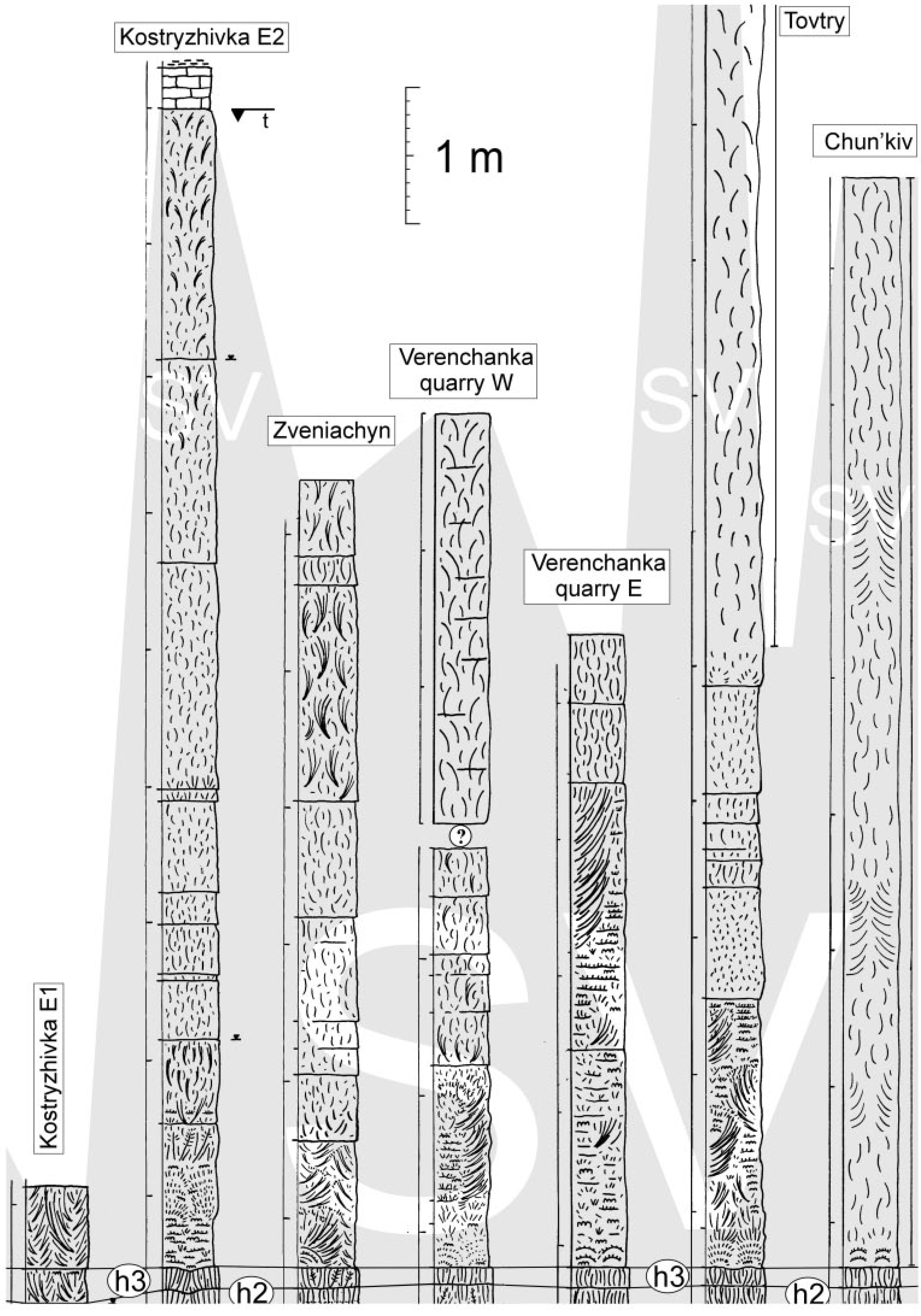

FIGURE 11B

Fig. 11A-C. Continued

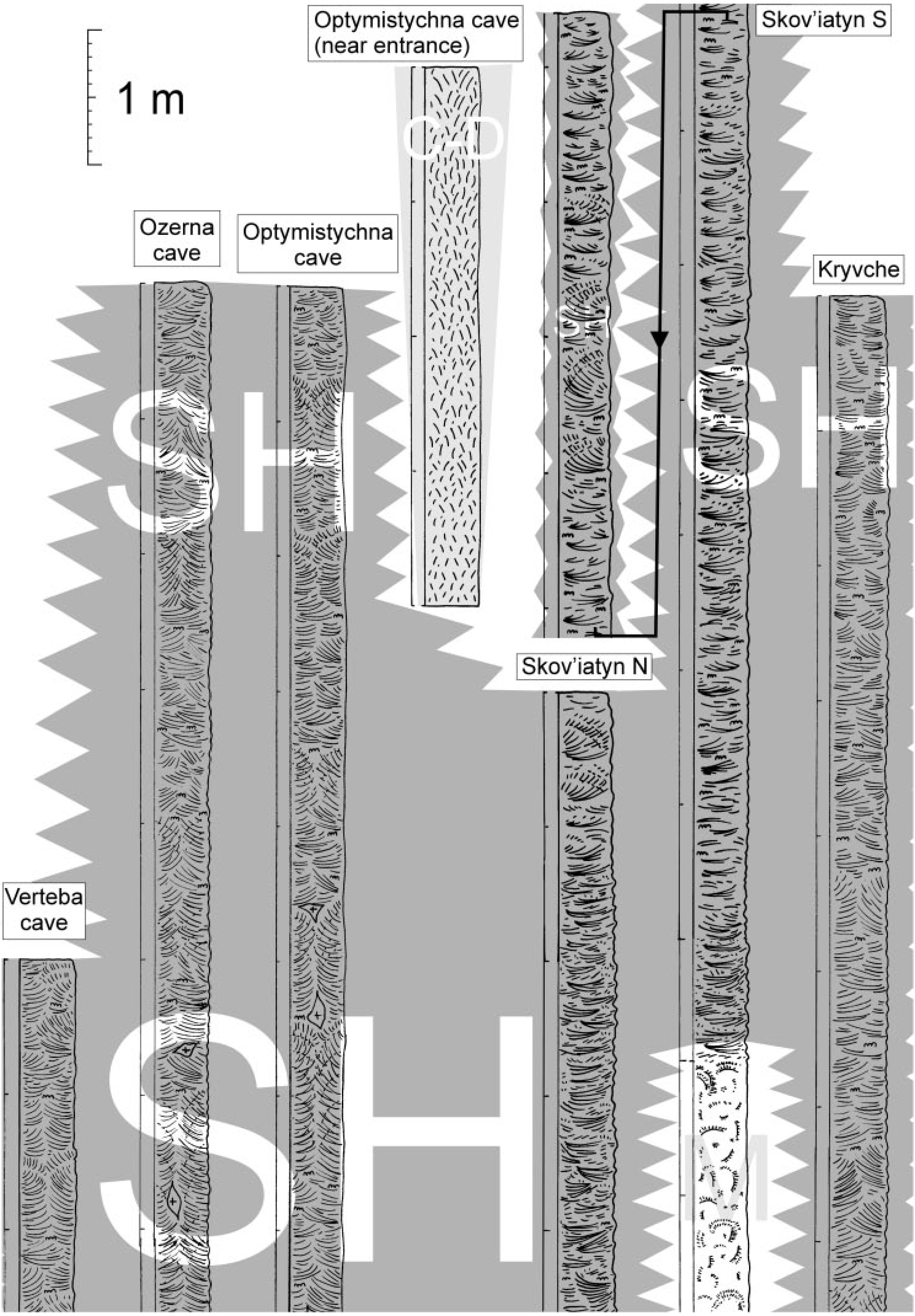

FIGURE 11C

Fig. 11A-C. Continued

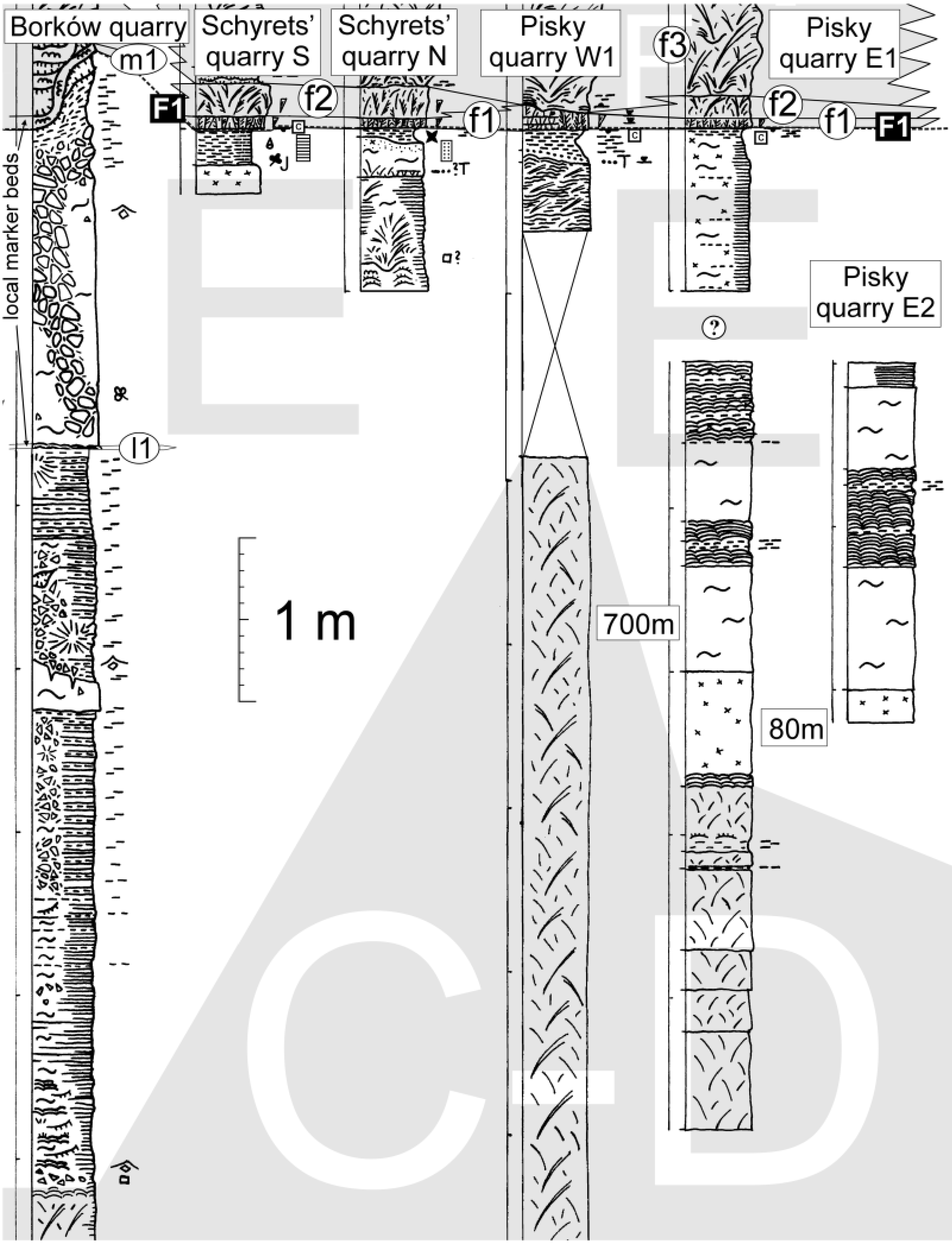

FIGURE 12A

Fig. 12A-C. Stratigraphic correlation in Ukraine; middle part of gypsum sequence below the "upper selenites" or marker bed f1; correlation line I in Fig. 2; base of bed f1 or base of the "upper selnites" as datum; key to hachure in Fig. 7

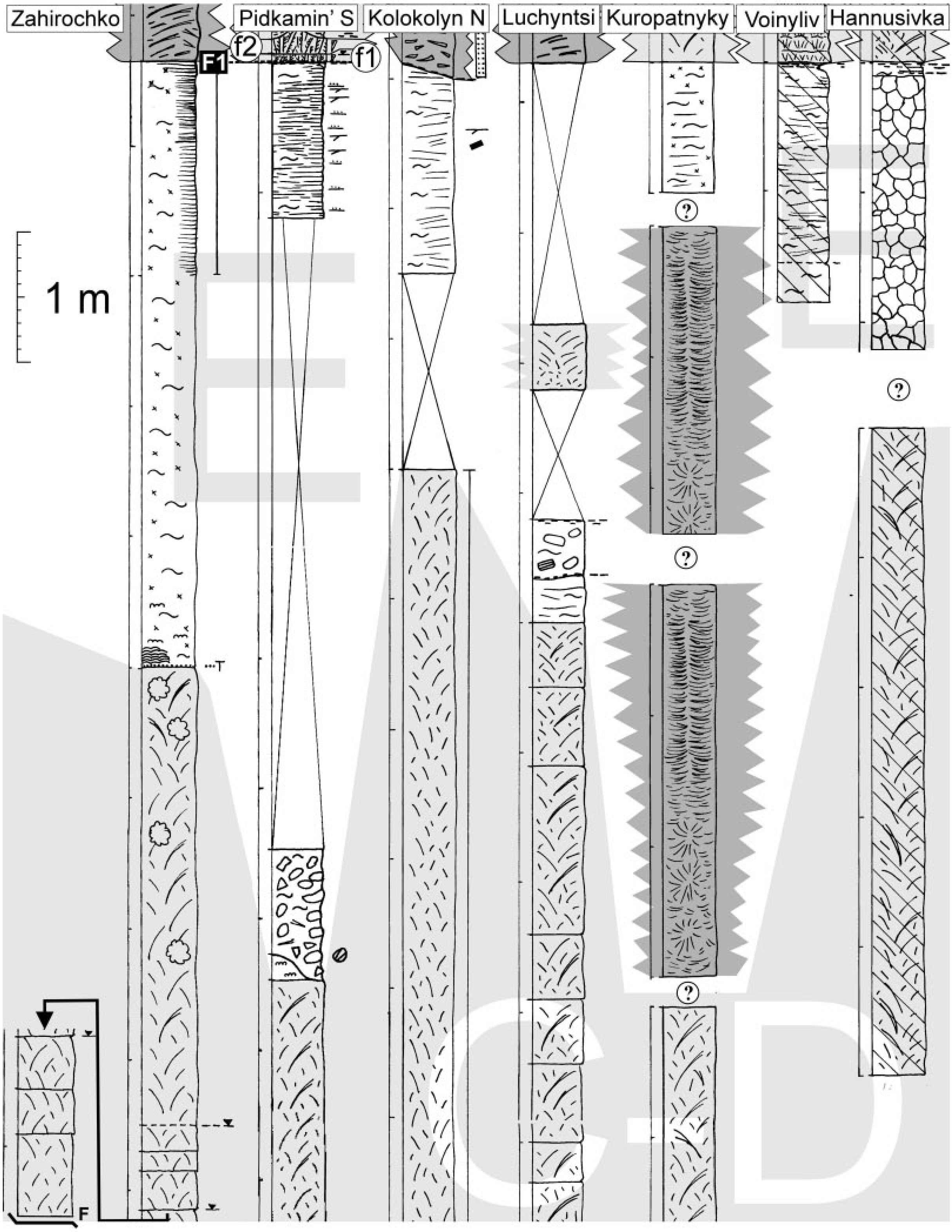

FIGURE 12B

Fig. 11A-C. Continued

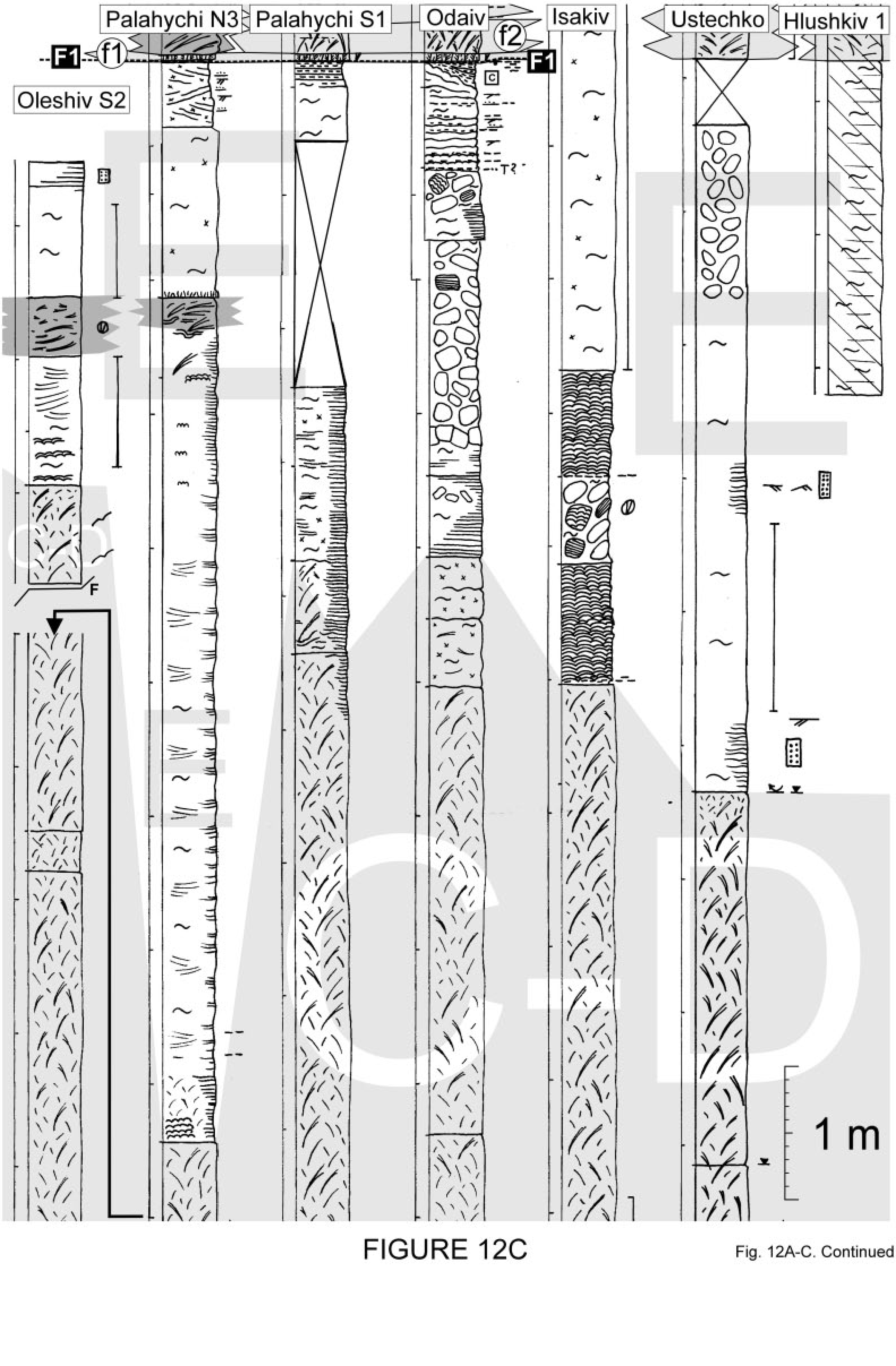

FIGURE 12C

Fig. 12A-C. Continued

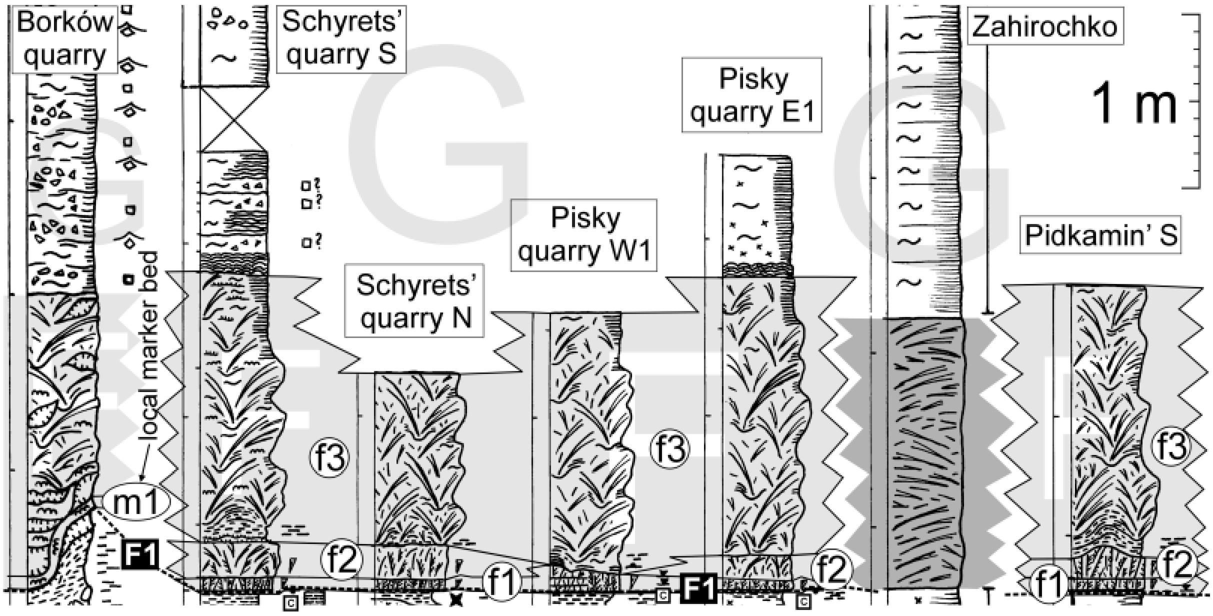

FIGURE 13A

Fig. 13A-C. Stratigraphic correlation in Ukraine; upper part of gypsum sequence containing "upper selenites", above marker bed f1; correlation line I in Fig. 2; base of bed f1 or base of "upper selnites" as datum; key to hachure in Fig. 7

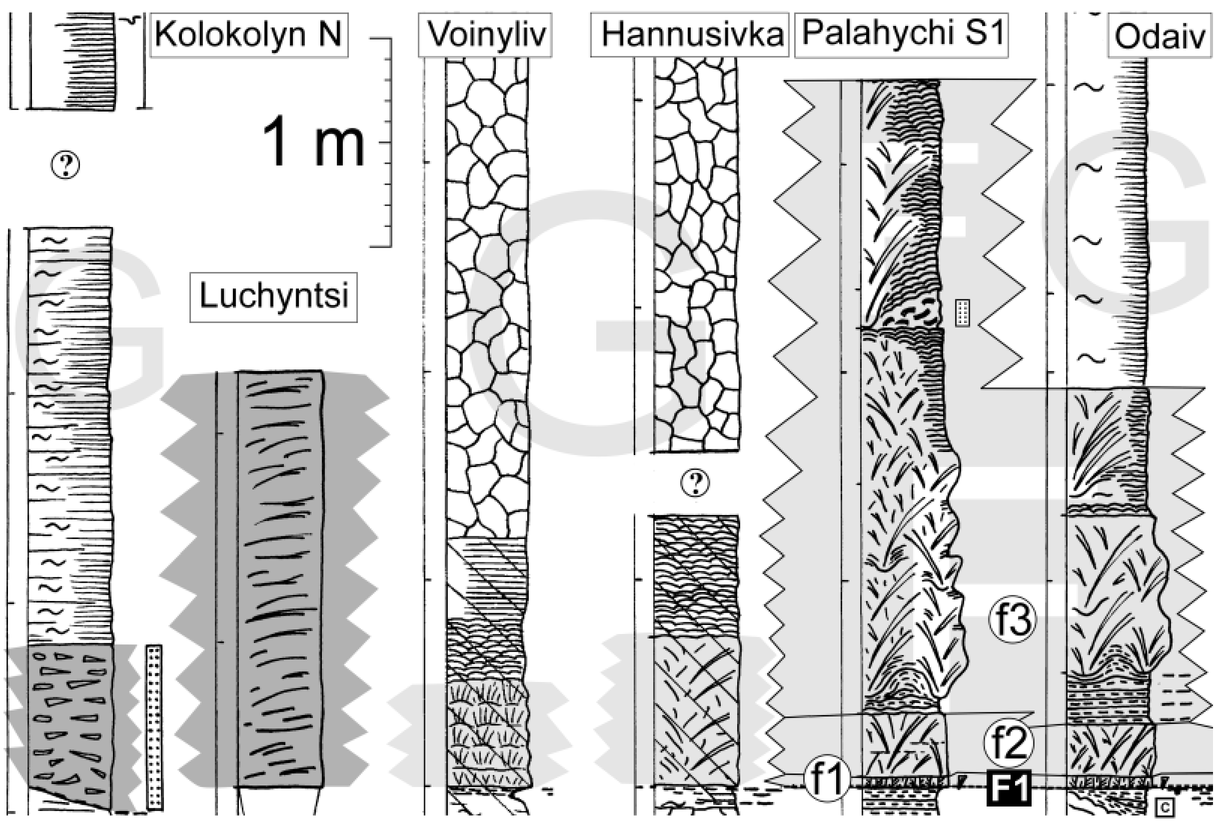

FIGURE 13B

Fig. 13A-C. Continued

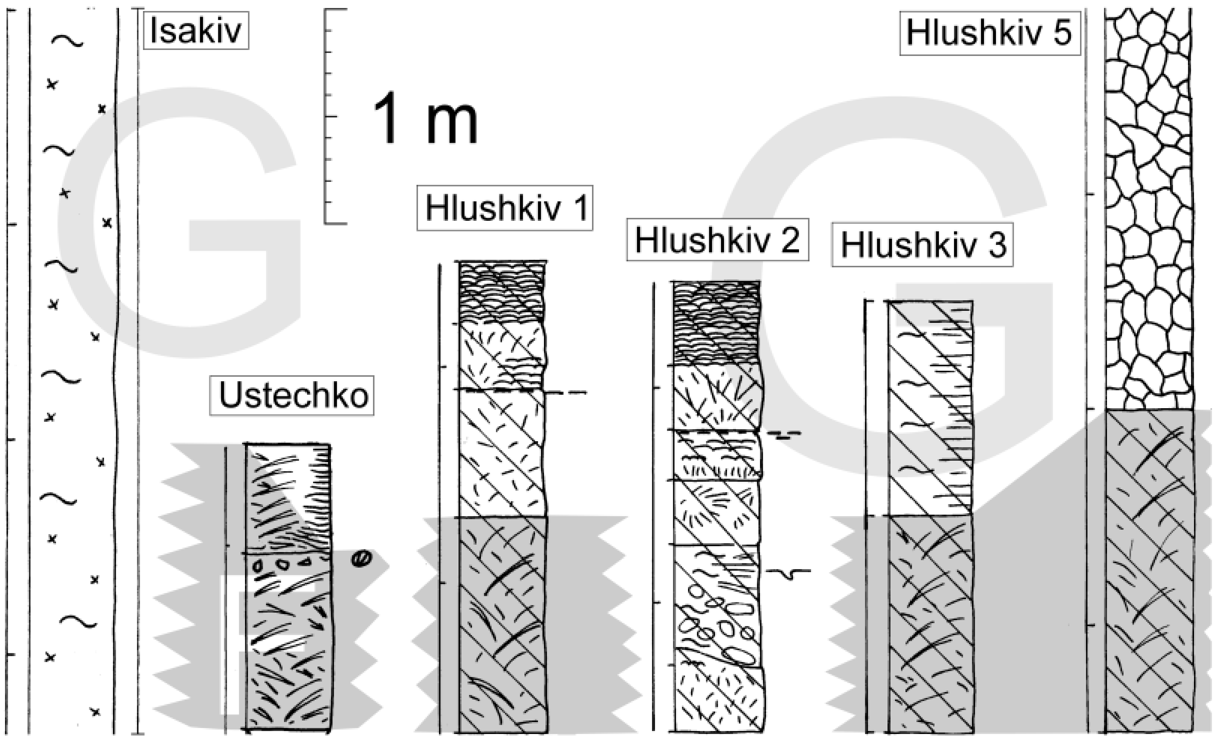

FIGURE 13C

Fig. 13A-C. Continued

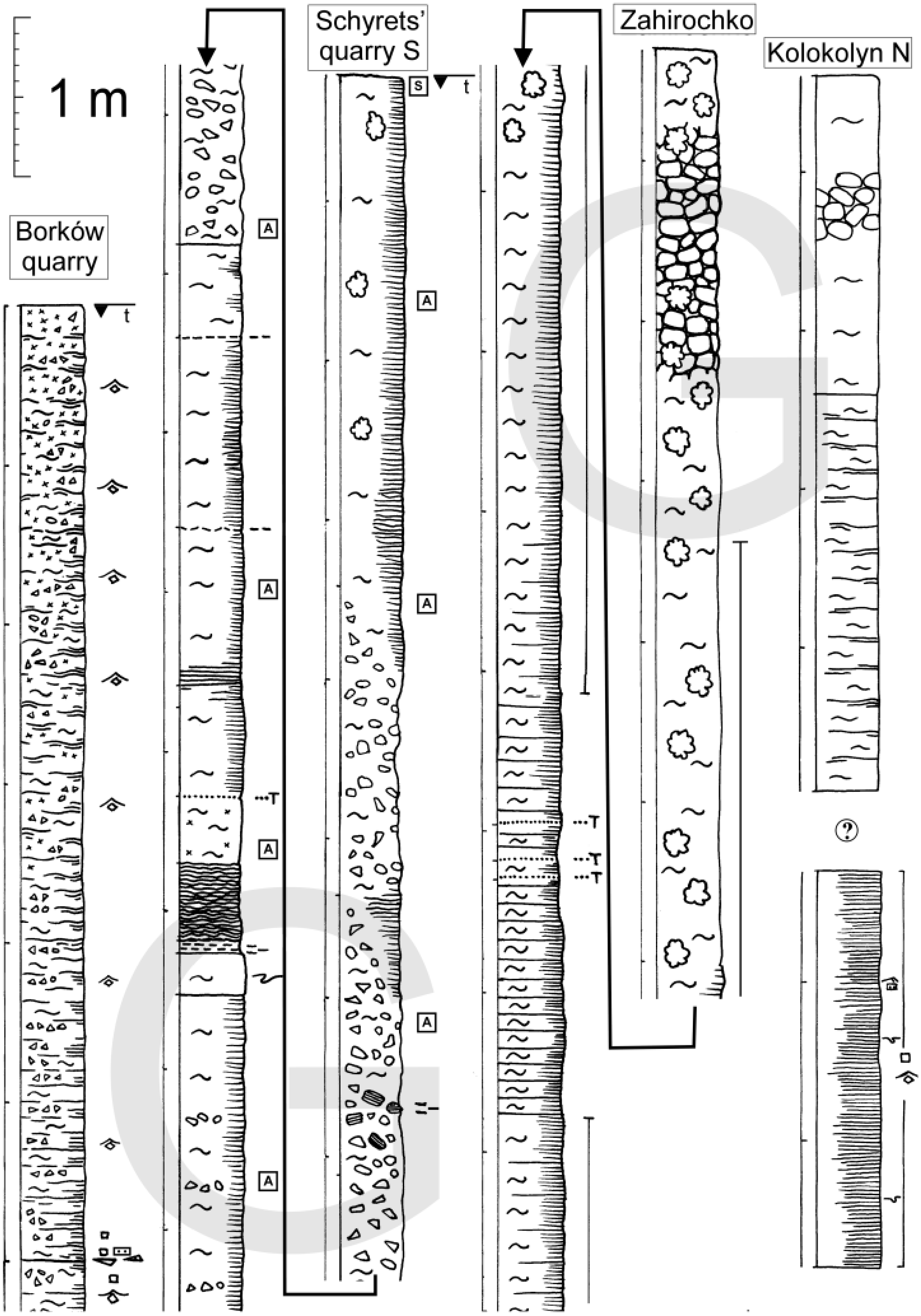

FIGURE 14A

Fig. 14A-B. Stratigraphic correlation in Ukraine; uppermost part of gypsum sequence above "upper selenites" or marker bed f3; correlation line I in Fig. 2; datum as in Fig. 13; key to hachure in Fig. 7

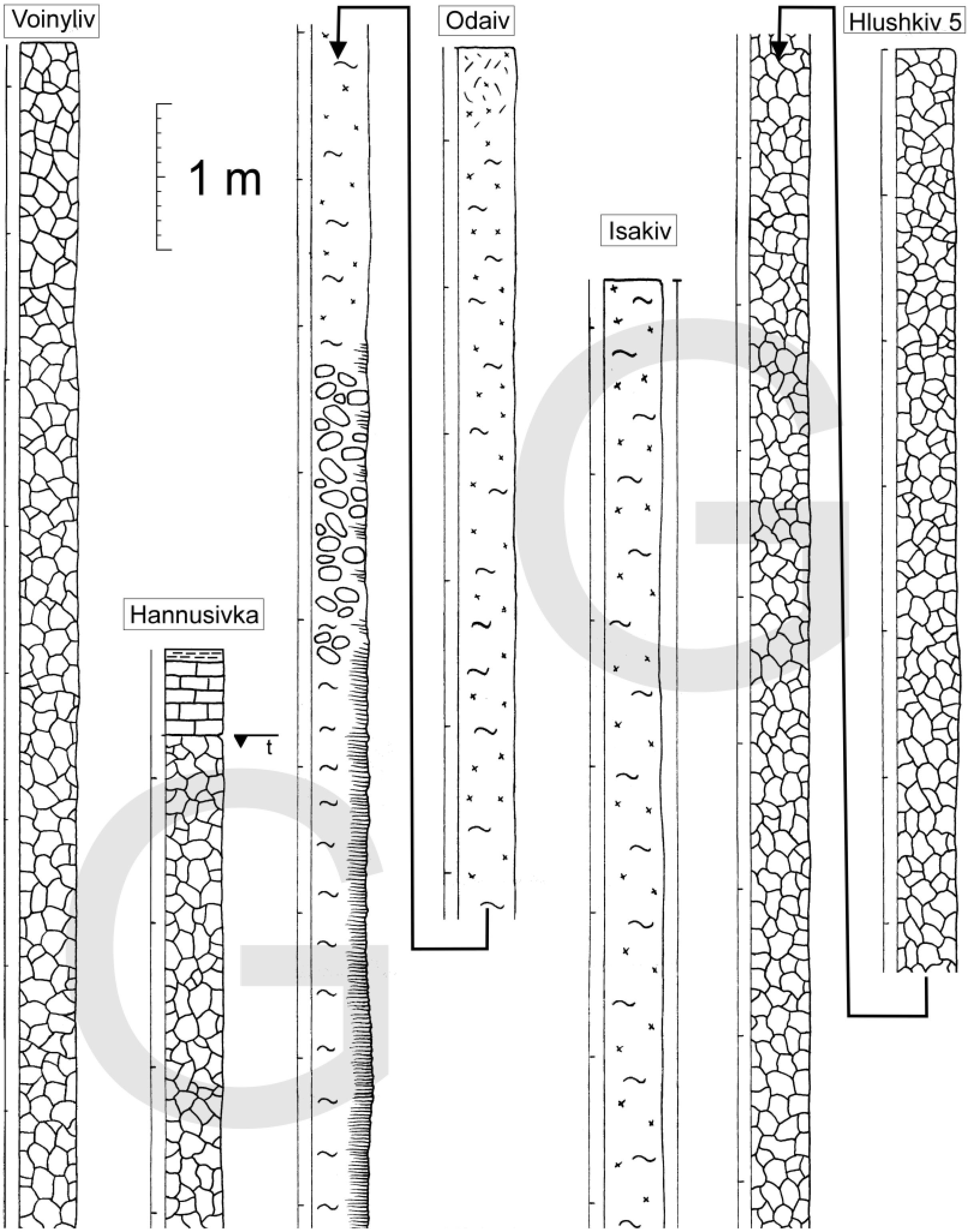

FIGURE 14B

Fig. 14A-B. Continued

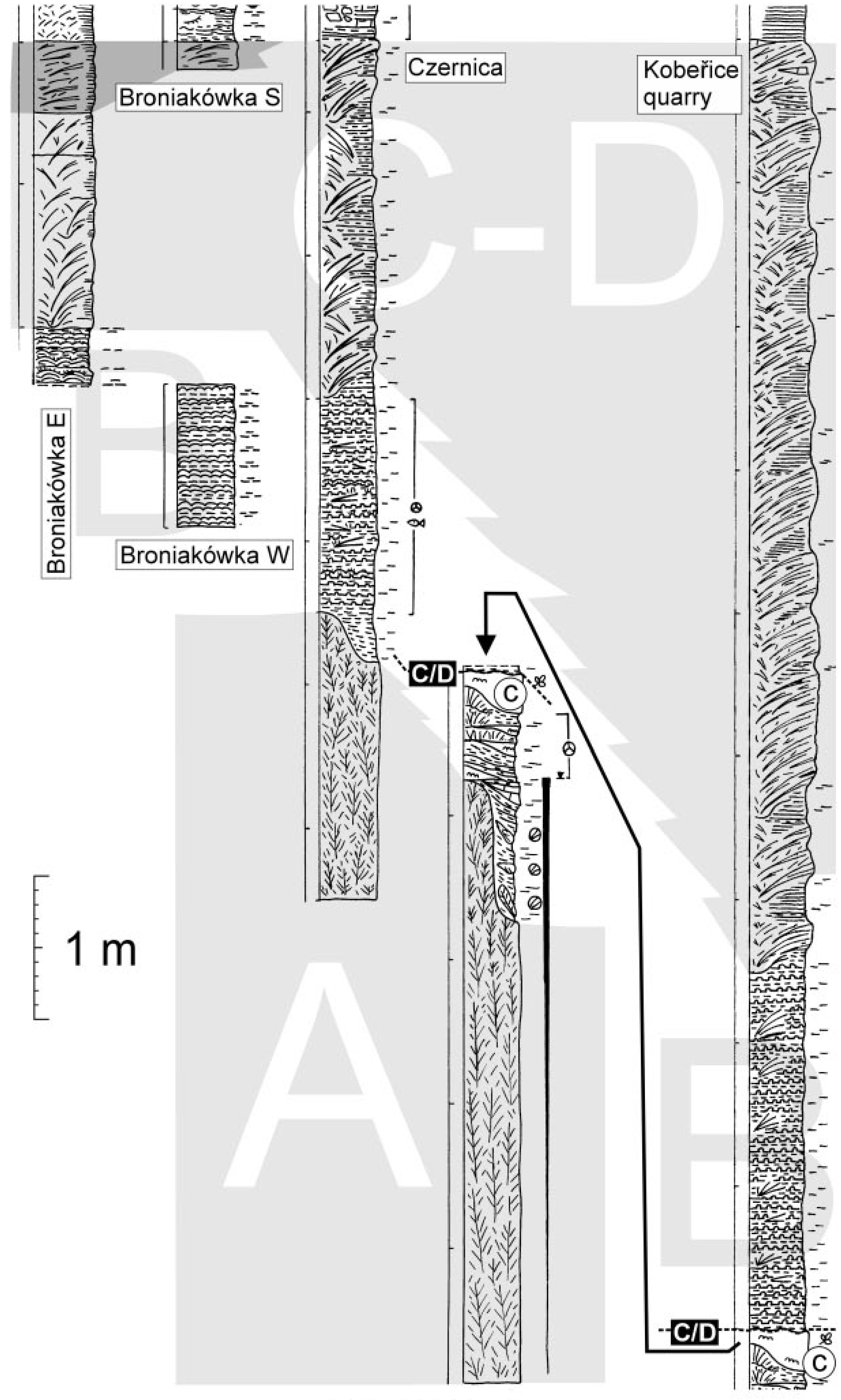

FIGURE 15A

Fig. 15A-B. Stratigraphic correlation between southern Poland and the Czech Republic, section at Kobeřice after PERYT & *al.* 1997a, b, and own data; Czernica after KRACH 1954, RANIECKA-BOBROWSKA 1957, SARNACKA 1968, and own data; correlation line in Fig. 1; top of sabre gypsum unit C-D as datum; key to hachure in Fig. 7; A - lower part of gypsum sequence

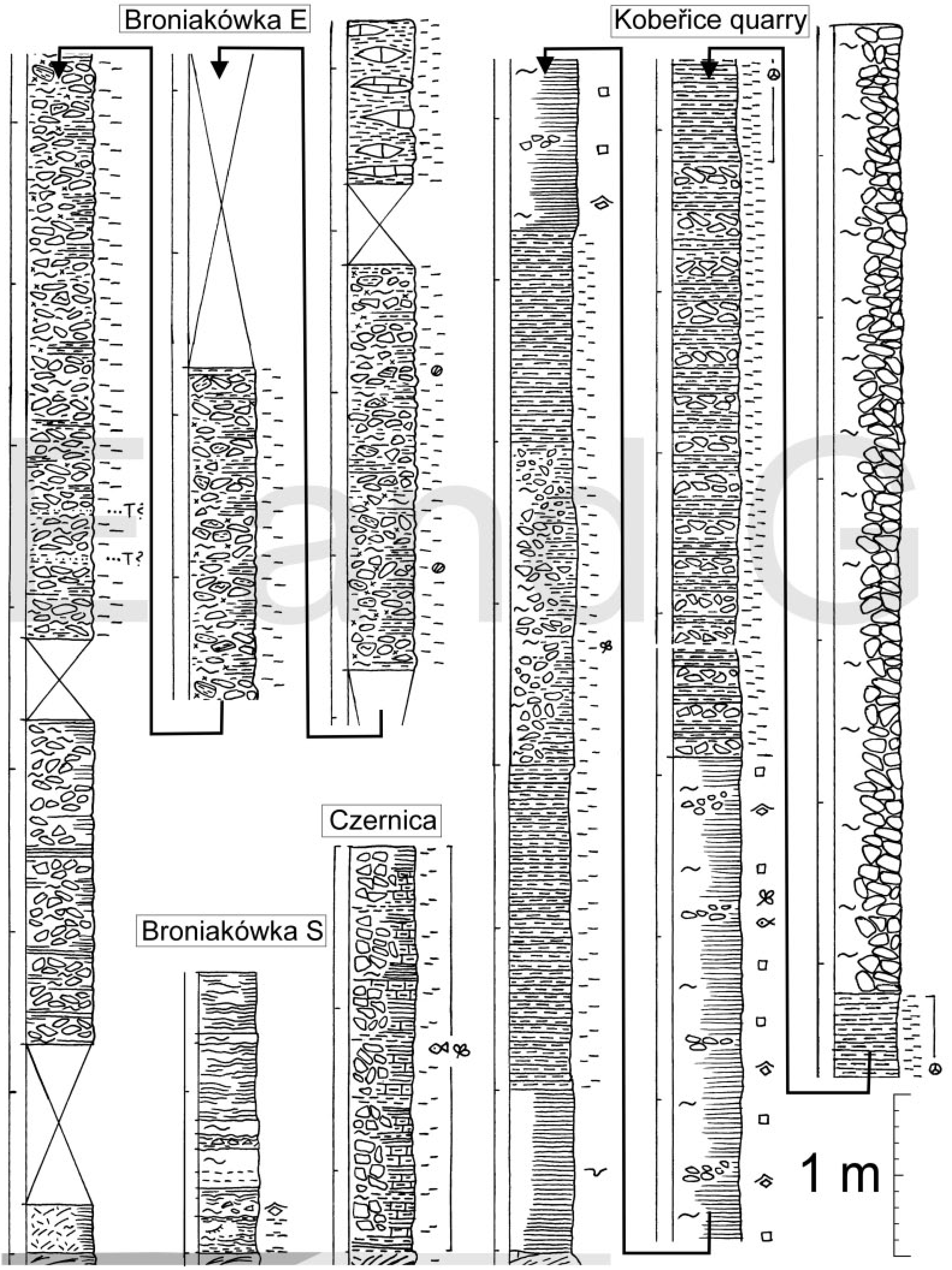

FIGURE 15B

Fig. 15A-B. Continued. B - upper part of gypsum sequence

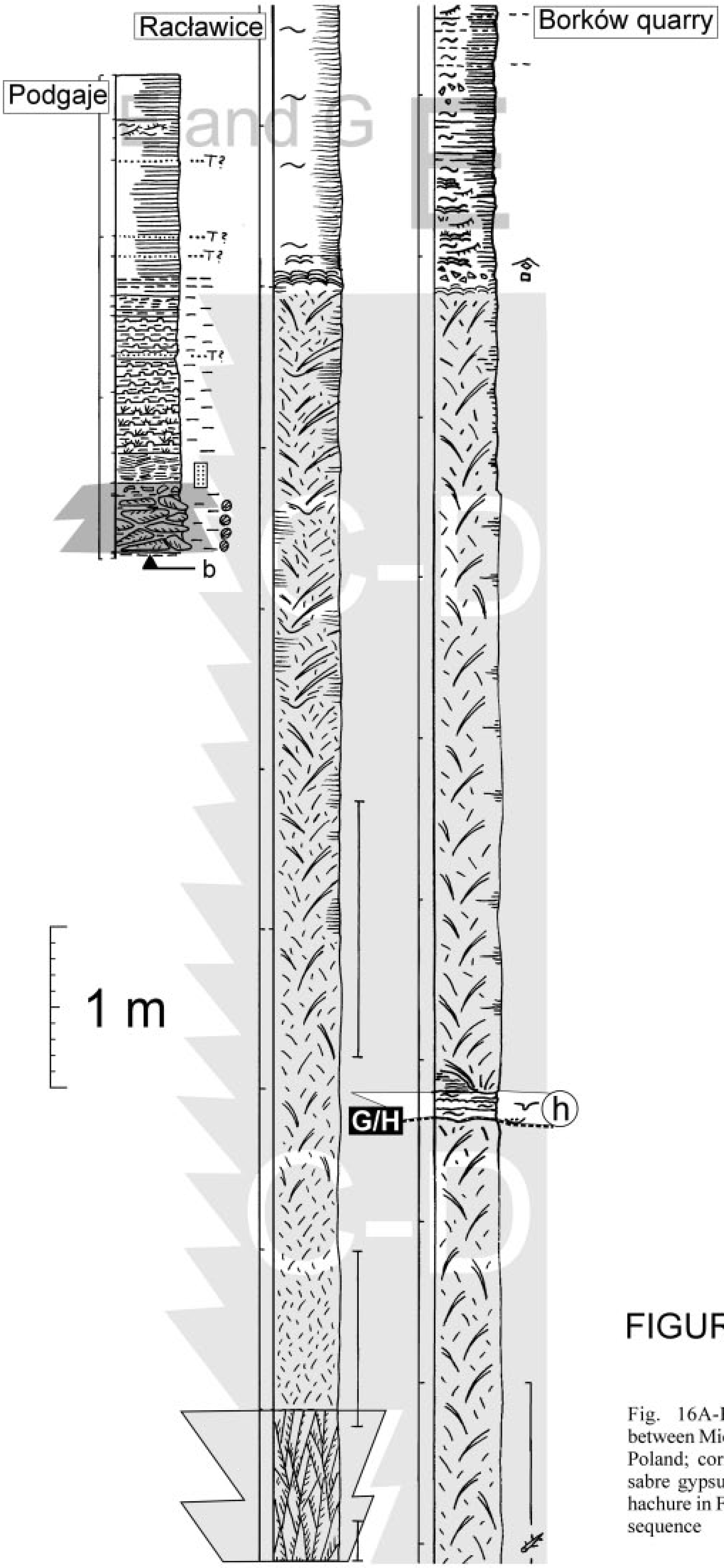

FIGURE 16A

Fig. 16A-B. Stratigraphic correlation between Miechów Upland and Nida area in Poland; correlation line in Fig. 1; top of sabre gypsum unit C-D as datum; key to hachure in Fig. 7; A - lower part of gypsum sequence

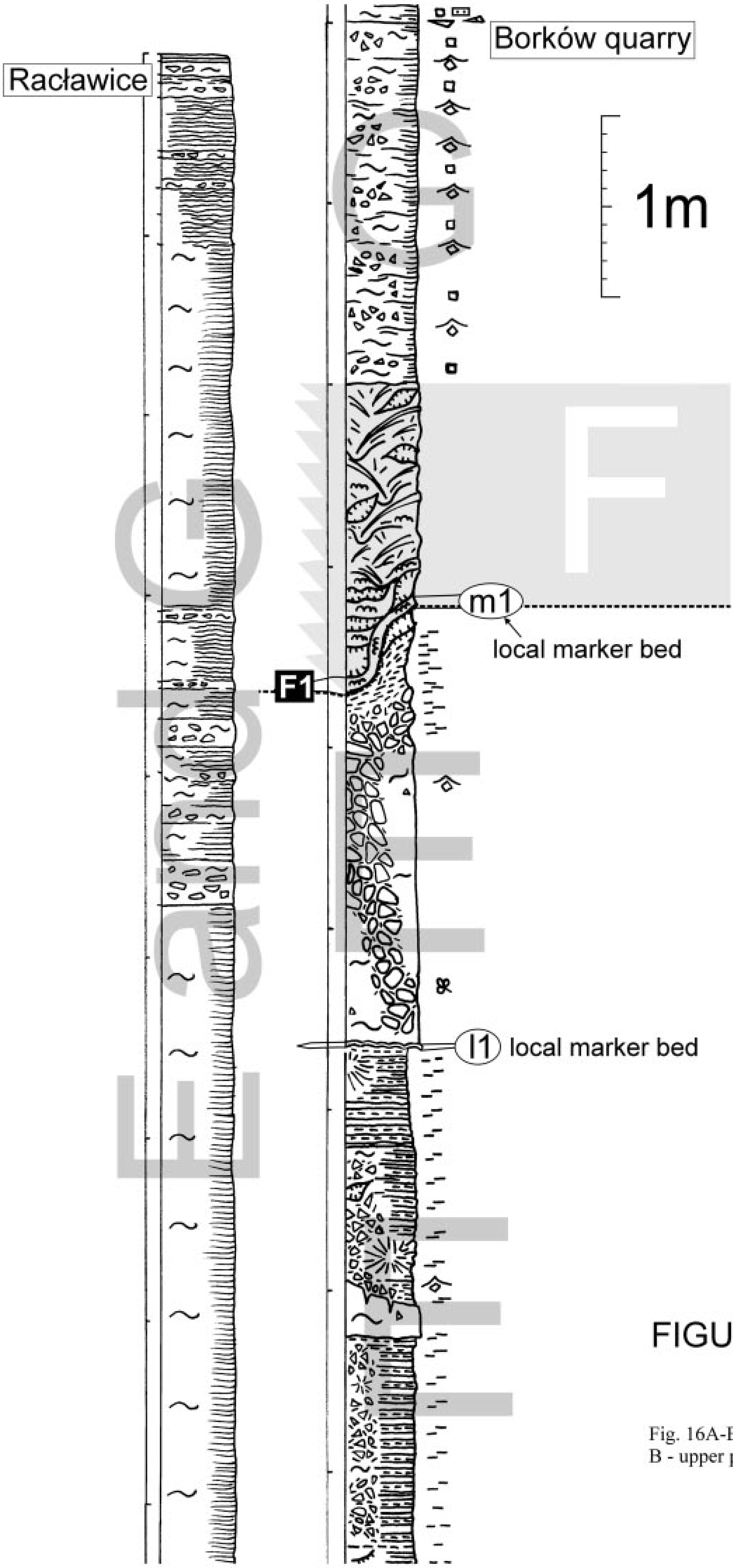

FIGURE 16B

Fig. 16A-B. Continued.
B - upper part of gypsum sequence

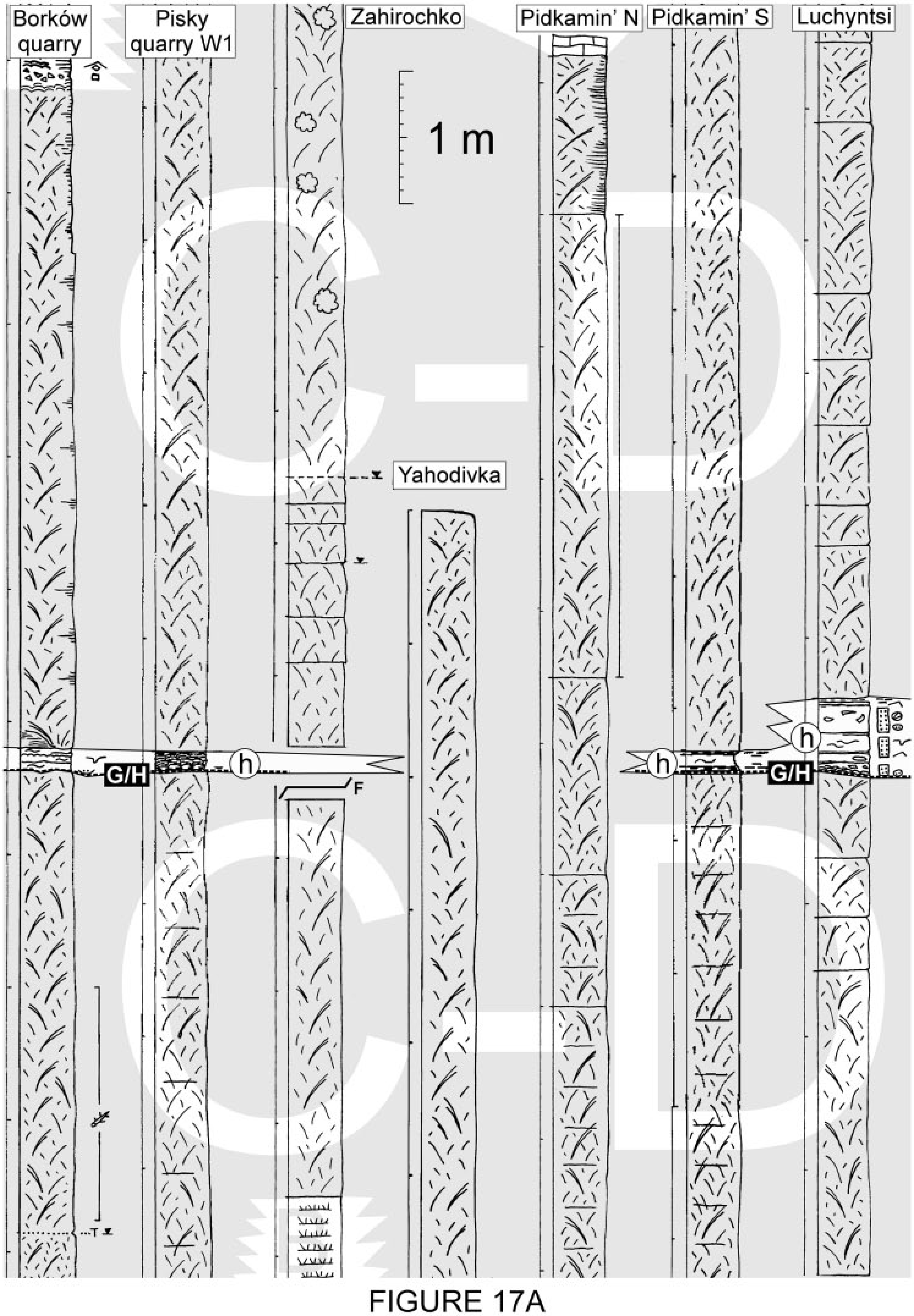

FIGURE 17A

Fig. 17A-D. Stratigraphic correlation in Ukraine; gypsum sequence around marker bed h; correlation line I in Fig. 2; base of bed h as datum; key to hachure in Fig. 7

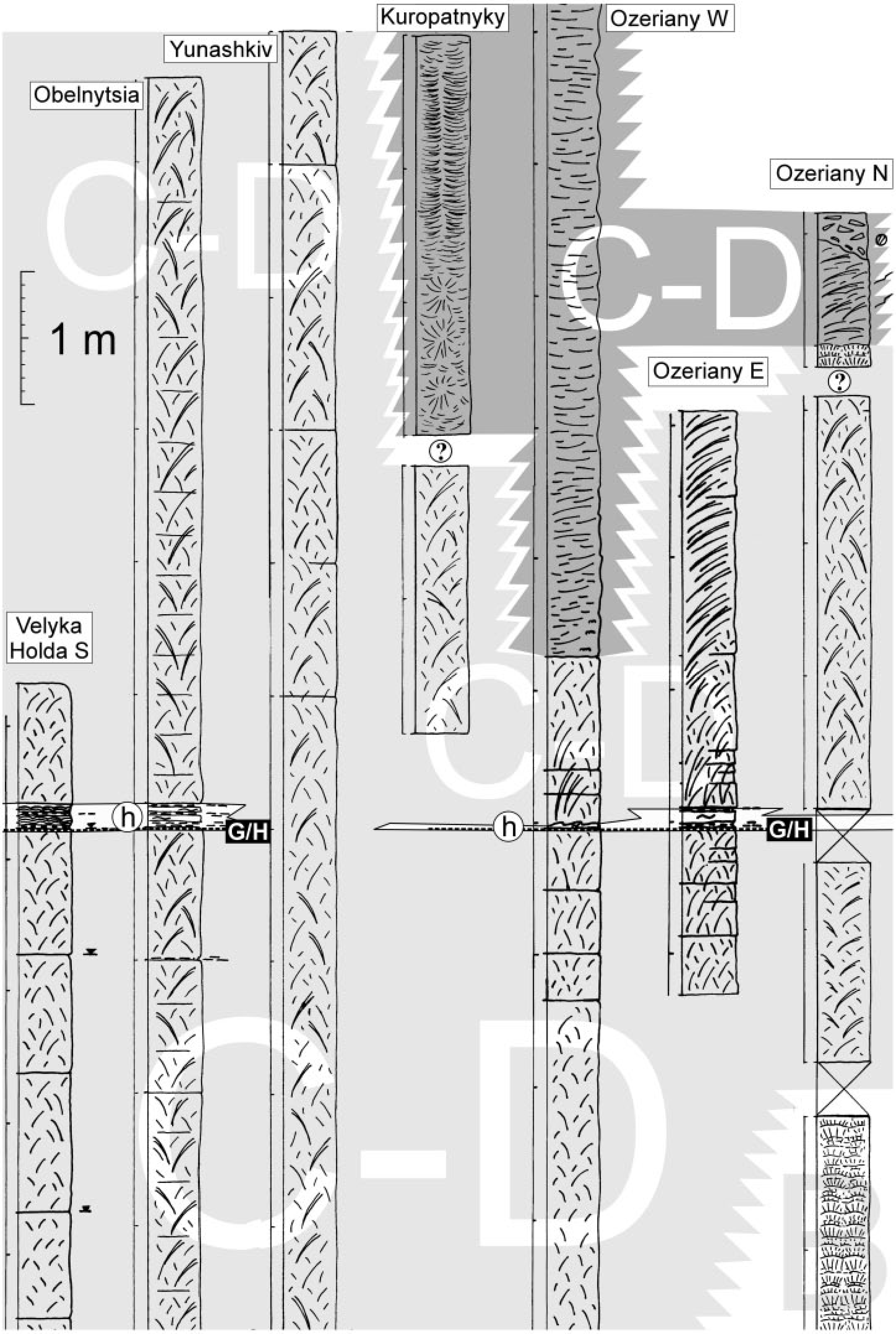

FIGURE 17B

Fig. 17A-D. Continued

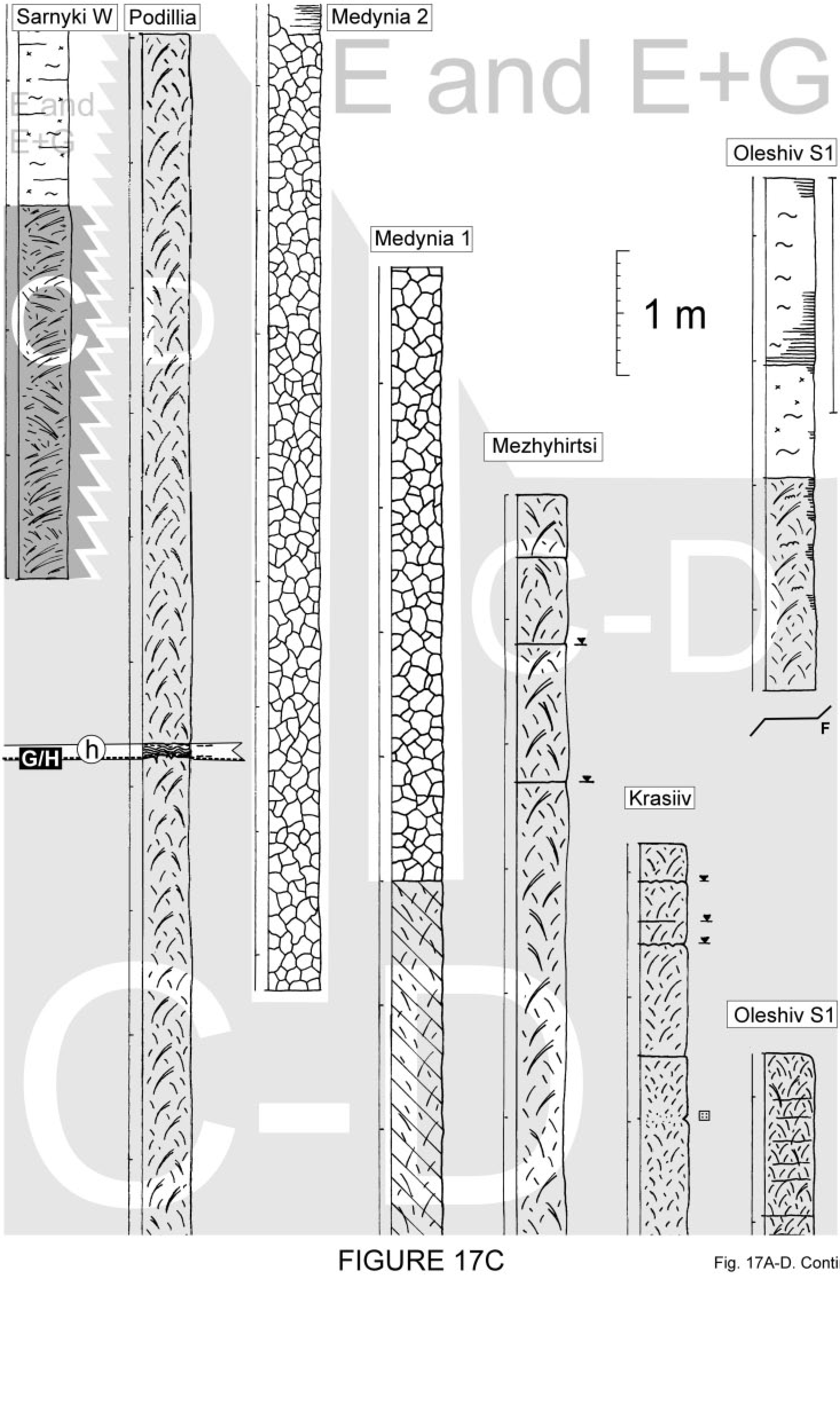

FIGURE 17C

Fig. 17A-D. Continued

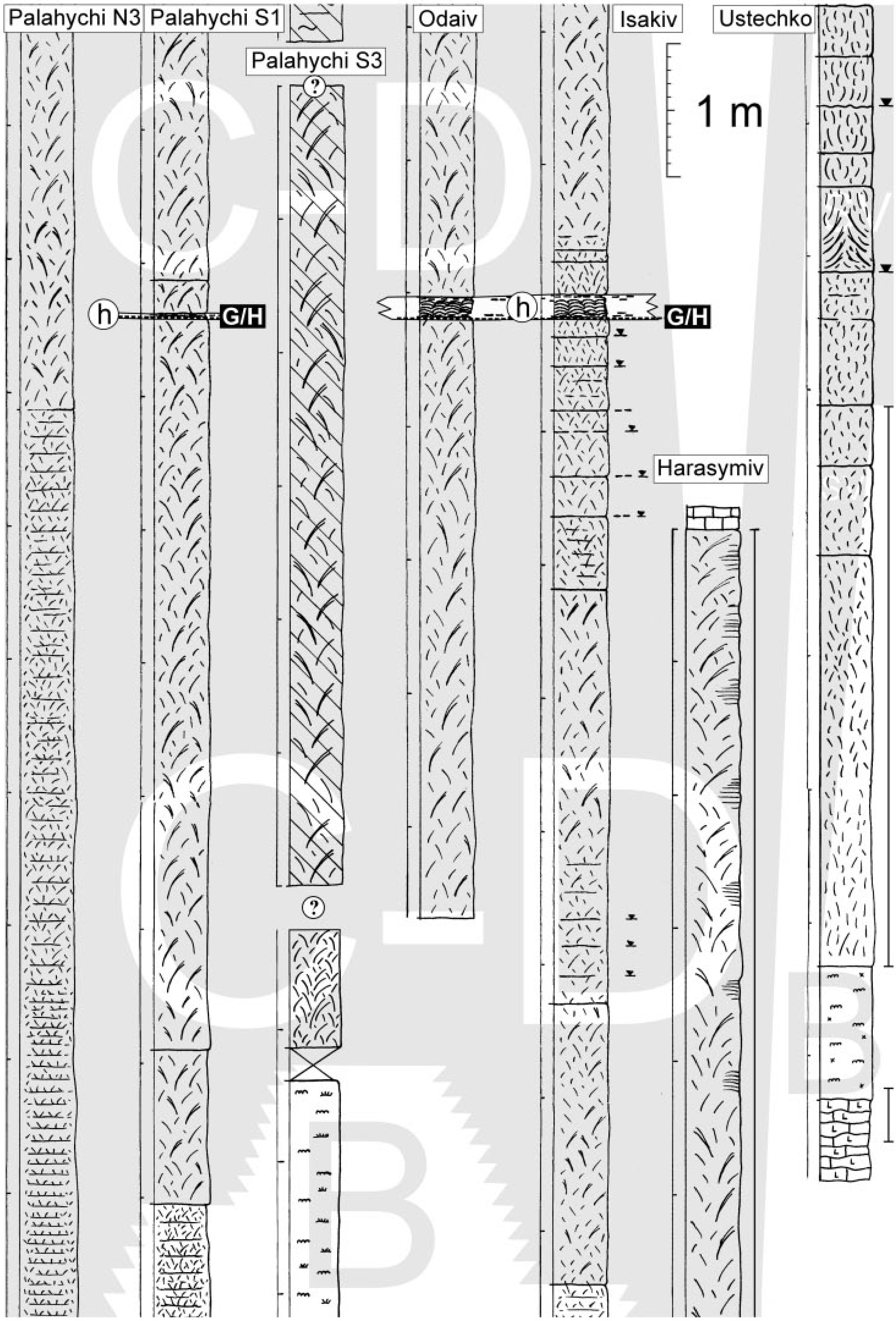

FIGURE 17D

Fig. 17A-D. Continued

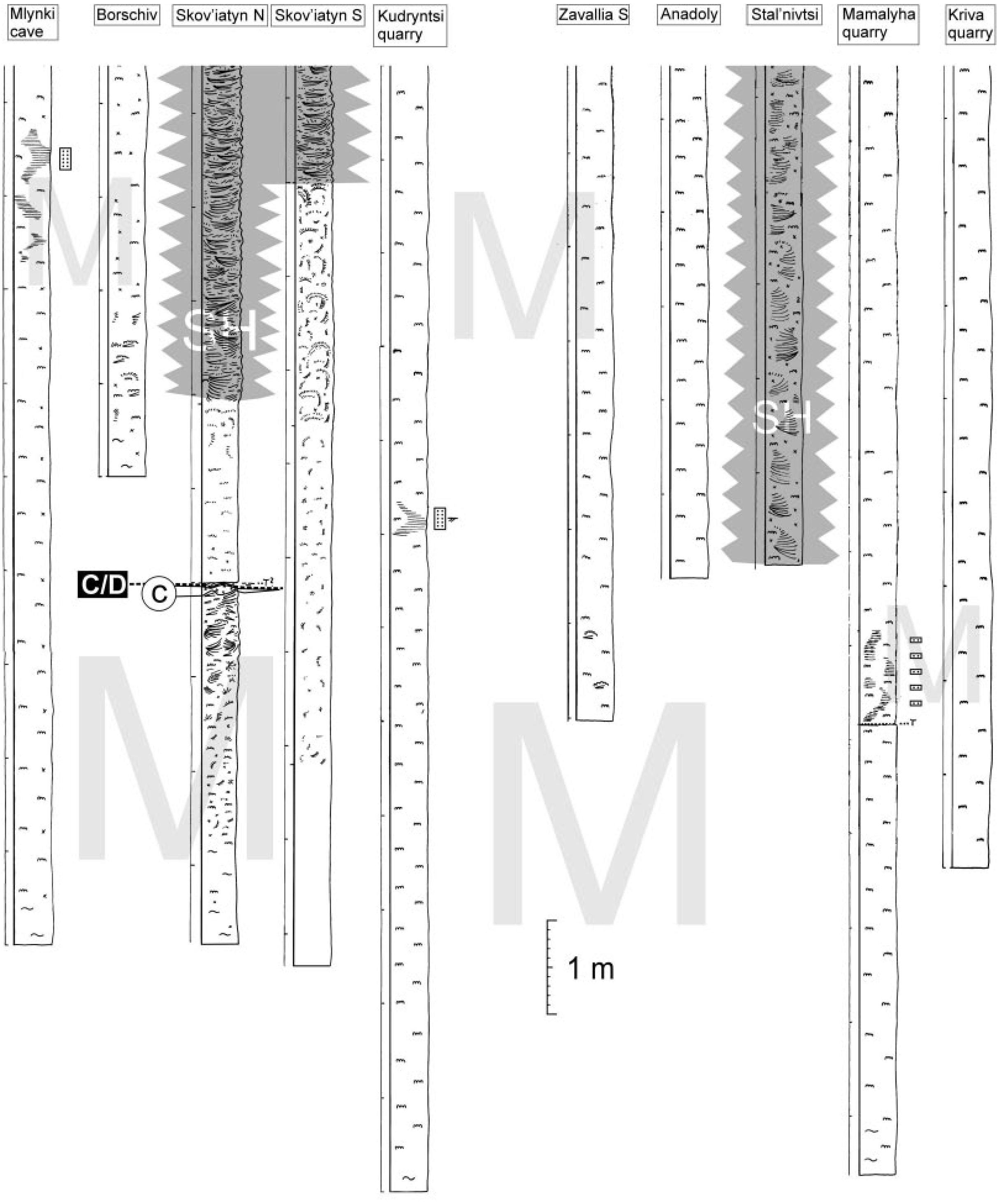

FIGURE 18A

Fig. 18A-B. Stratigraphic correlation in Ukraine and Moldova, section at Kriva in Moldova after PERYT & *al*. 1995; correlation line III in Fig. 2; without datum; key to hachure in Fig. 7; A - lower part of gypsum sequence

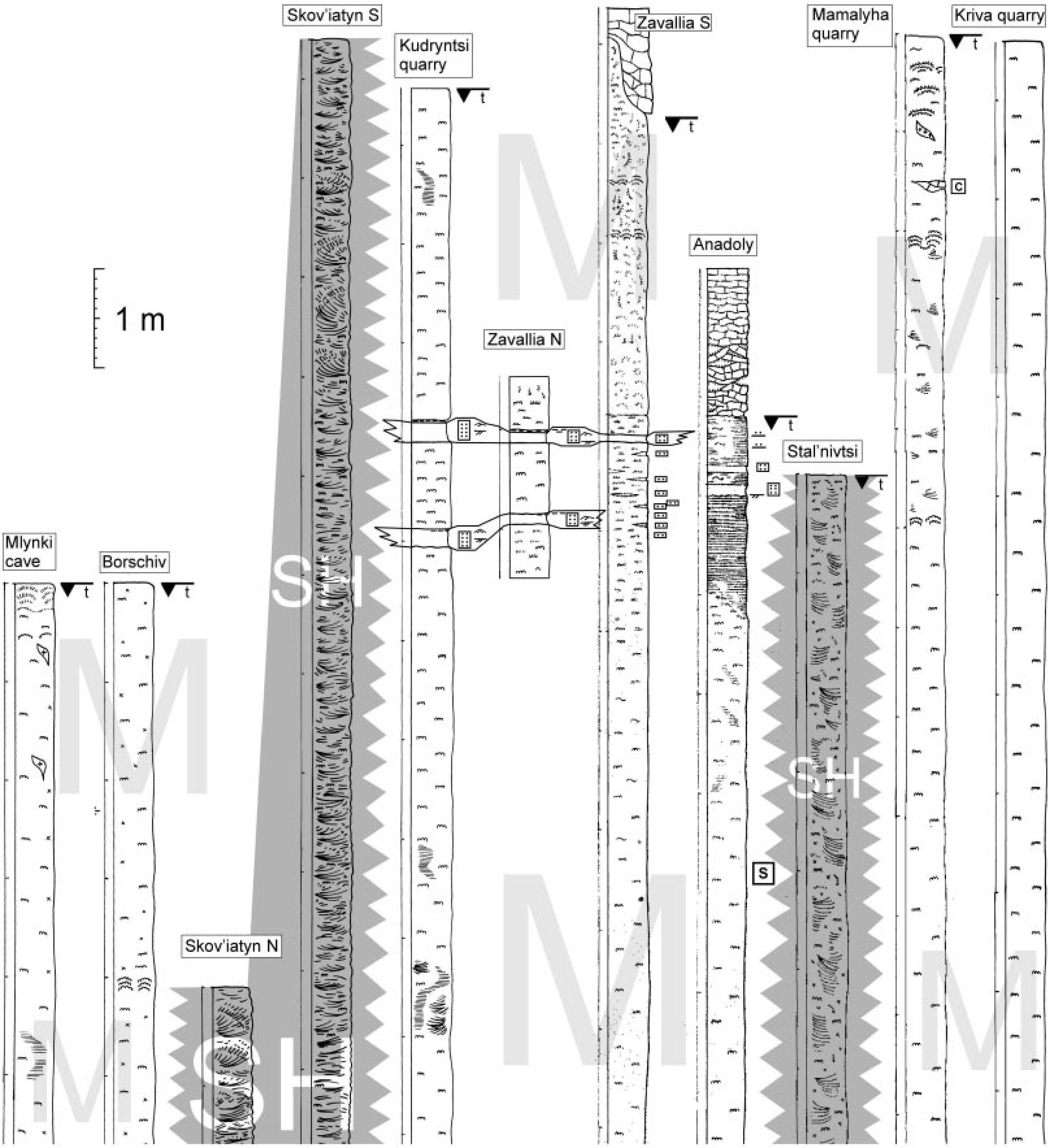

FIGURE 18B

Fig. 18A-B. Continued.
B - upper part of gypsum sequence

Table 1. List of studied localities

Localities in Ukraine

In English	*In Ukrainian*	*In Russian*	*In Polish* [*In Romanian*]	
Anadoly	Анадолы	Анадолы	[Anadol]	Fig. 1, map 26; Figs 2, 18A-B
Borschiv	Борщів	Борщев	Borszczów	Fig. 1, map 24; Figs 2, 18A-B
Bratyshiv	Братишів	Братышев	Bratyszów	Fig. 1, map 16; Figs 2, 8E, 10E
Chortova Hora	Чортова Гора	Чертова Гора	Czortowa Góra	Fig. 1, map 10; Figs 2, 8B
Chun'kiv	Чуньків	Чуньков	Czinkeu [Cinčau]	Fig. 1, map 23; Figs 2, 9C, 11B
Hannusivka	Ганнусівка	Ганнусовка	Hanusowce	Fig. 1, map 15; Figs 2, 12B, 13B, 14B
Harasymiv	Гарасимів	Герасимов	Harasimów	Fig. 1, map 18; Figs 2, 8E, 10E, 17D
Hlushkiv	Глушків	Глушков	Głuszków	Fig. 1, map 20; Figs 2, 12C, 13C, 14B
Holovchyntsi	Головчинці	Головчинцы	Hołowczyńce	Fig. 1, map 21; Figs 2, 9B, 11A
Isakiv	Ісаків	Ісаков	Isaków	Fig. 1, map 17; Figs 2, 10E, 12C, 13C, 14B, 17D
Kasova Hora	Касова Гора	Касова Гора	---	Fig. 1, map 10, Figs 2, 5, 8C
Kolokolyn	Колоколин	Колоколин	Kołokolin	Fig. 1, map 9; Figs 2, 5, 10B, 12B, 13B, 14A
Kostryzhivka	Костриживка	Кострижевка	Kostryżówka	Fig. 1, map 23; Figs 9B, 11A
Krasiiv	Красіїв	Красиев	Krasiejów	Fig. 1, map 14; Figs 2, 8C, 10C, 17C
Kryvche	Кривче	Кривче	Krzywcze	Fig. 1,map 24; Figs 2, 9D, 11C
Kudryntsi	Кудринці	Кудринцы	Kudryńce	Fig. 1, map 25; Figs 2, 18A-B
Kuropatnyky	Куропатники	Куропатники	Kuropatniki	Fig. 1, map 10; Figs 12B, 17B
Lany	Лани	Ланы	Łany	Fig. 1, map 13, Figs 2, 8C, 10C
Lokitka	Локітка	Локотка	Łokutki	Fig. 1, map 16; Figs 2, 10E
Luchyntsi	Лучинці	Лучинцы	Łuczyńce	Fig. 1, map 10; Figs 2, 12B, 13B, 17A
Mamalyha	Мамалига	Мамалыга	Mamałyga [Mamaliga]	Fig. 1, map 27; Figs 2, 9D, 18A-B
Medynia	Мединя	Мединя	Medynia	Fig. 1, map 12; Figs 2, 8C, 10B-C, 17C
Mezhyhirtsi	Межигірці	Межигорцы	Międzyhorce	Fig. 1, map 13; Figs 2, 8C, 10C, 17C
Mlynky, cave	Млинки, печера	Млынки, пещера	---	Fig. 1, map 22; Figs 2, 18A-B
Naberezhne	Набережне	Набережное	---	Fig. 1, map 10; Figs 2, 8C, 10B
Nahoriany	Нагоряни	Нагоряны	Nagórzany	Fig. 1, map 19; Figs 2, 9A, 11A
Nyrkiv	Нирків	Нирков	Nyrków	Fig. 1, map 19; Figs 2, 9A, 11A
Obelnytsia	Обельниця	Обельница	Obelnica	Fig. 1, map 10; Fig. 17B
Odaiv	Одаїв	Одаев	Odaje	Fig. 1, map 16; Figs 2, 12C, 13B, 14B, 17D
Oleshiv	Олешів	Олешев	Oleszów	Fig. 1, map 16; Figs 2, 5, 8D, 10C, 12C, 17C
Optymistychna, cave	Оптимістична, печера	Оптимистическая, пещера	---	Fig. 1, map 24; Figs 2, 9D, 11C
Ozeriany	Озеряни	Озеряни	Jezierzany	Fig. 1, map 10; Figs 2, 8B, 10B, 17B
Ozerna, cave	Озерна, печера	Озерная, пещера	---	Fig. 1, map 24; Figs 2, 9C, 11C
Palahychi	Палагичі	Палагичи	Pałahicze	Fig. 1, map 16; Figs 2, 8D, 10D-E, 12C, 13B, 17D
Pidkamin'	Підкамінь	Подкамень	Podkamień	Fig. 1, map 8; Figs 2, 8B, 10A, 12B, 13A
Pisky	Піски	Пески	Piaski	Fig. 1, map 6; Figs 2, 8A, 10A, 12A, 13A, 17A
Podillia	Поділля	Подолье	Podole	Fig. 1, map 10; Figs 2, 5, 8B, 10B, 17C
Pryozerne	Приозерне	Приозерное	Psary	Fig. 1, map 8; Figs 2, 5
Radians'ke Zahiria	Радянське Загір'я	Радянськое Загорье	---	Fig. 1, map16; Fig. 8E
Repuzhyntsi	Репужинці	Репужинцы	Repużyńce	Fig. 1, map 19; Figs 2, 9A, 11A
Rohatyn	Рогатин	Рогатин	Rohatyn	Fig. 1, map 10; Figs 2, 5, 8B
Sarnyky	Сарники	Сарники	Sarnki	Fig. 1, map 10; Fig. 17C
Skov'iatyn	Сков'ятин	Сковятин	Skowiatyn	Fig. 1, map 24; Figs 2, 9D, 11C, 18A-B
Schyrets'	Щирець	Щирец	Szczerzec, Szczyrec	Fig. 1, map 6; Figs 2, 5, 8A, 10A, 12A, 13A, 14A
Stal'nivtsi	Стальнівці	Стальновцы	[Stalinesti]	Fig. 1, map 27; Figs 2, 18A-B
Tovtry	Товтри	Товтры	Toutry [Tauteni]	Fig. 1, map 23; Figs 2, 9C, 11B
Ustechko	Устечко	Устечко	Uścieczko	Fig. 1, map 19; Figs 2, 9A, 11A, 12C, 13C, 17D
Velyka Holda	Велика Холда	---	Góra Korosty	Fig. 1, map 10; Figs 2, 8B, 10B, 17B
Verenchanka	Веренчанка	Веренчанка	Werenczanka [Vranceni]	Fig. 1, map 23; Figs 2, 9C, 11B
Verteba, cave	Вертеба, печера	Вертеба, пещера	Werteba, jaskinia	Fig. 1, map 24; Figs 2, 9C, 11C
Vikniany (Bilohirka)	Вікняни (Білогірка)	Викняни (Белогорка)	Okniany	Fig. 1, map 16; Figs 2, 8E, 10E
Voinyliv	Войнилів	Войнилов	Wojniłów	Fig. 1, map 11; Figs 2, 12B, 13B, 14B
Yahodivka	Ягодівка	Фрага	Fraga	Fig. 1, map 8; Figs 2, 10A, 17A
Yunashkiv	Юнашків	Юнашков	Junaszków	Fig. 1, map 10; Figs 2, 17B
Zahirochko	Загірочко	Загорочко	Zagóreczko	Fig. 1, map 7; Figs 2, 12B, 13A, 14A, 17A
Zavallia	Завалля	Завалье	Zawale	Fig. 1, map 25; Figs 2, 18A-B
Zhalybory	Жалибори	Жалиборы	Żelibory	Fig. 1, map 10; Figs 2, 8C
Zveniachyn	Звенячин	Звенячин	Zwiniacze	Fig. 1, map 23; Figs 2, 9B, 11B

Localities in Poland

Bilczów	Fig. 1, map 5; Fig. 4B
Biniatki	Fig. 1, map 5; Fig. 4A
Bogucice-Skałki	Fig. 1, map 5; Fig. 4B
Borków	Fig. 1, map 5; Figs 6A-B, 8A, 10A, 12A, 13A, 14A, 16A-B, 17A
Broniakówka	Fig. 1, map 3; Figs 15A-B
Bronina	Fig. 1, map 5; Fig. 4A
Chotel Czerwony	Fig. 1, map 5; Fig. 4C
Chotel Czerwony-Zagórze	Fig. 1, map 5; Fig. 4B
Chotelek Zielony	Fig. 1, map 5; Fig. 4A
Chwałowice	Fig. 1, map 5; Figs 4A, 6A-B
Czernica [Czernitz *in German*]	Fig. 1, map 2; Figs 15A-B
Gacki	Fig. 1, map 5; Fig. 4B
Galów	Fig. 1, map 5; Fig. 4A
Gartatowice	Fig. 1, map 5; Figs 6A-B
Gorysławice	Fig. 1, map 5; Fig. 4C
Góry Wschodnie	Fig. 1, map 5; Fig. 4C
Leszcze	Fig. 1, map 5; Fig. 4B
Łagiewniki	Fig. 1, map 5; Fig. 4A
Łatanice	Fig. 1, map 5; Fig. 4B
Marzęcin	Fig. 1, map 5; Fig. 4B
Owczary	Fig. 1, map 5; Fig. 4A
Podgaje	Fig. 1, map 4; Fig. 16A
Przęślin	Fig. 1, map 5; Fig. 4C
Racławice	Fig. 1, map 4; Figs 16A-B
Sielec Rządowy	Fig. 1, map 5; Fig. 4C
Skorocice	Fig. 1, map 5; Fig. 4B
Stawiany	Fig. 1, map 5; Figs 6A-B
Wola Zagojska	Fig. 1, map 5; Fig. 4B

Localities in Czech Republic and Moldova

Kobeřice, Czech Republic	Fig. 1, map 1; Figs 15A-B
Kriva, Criva; Moldova	Fig. 1, map 27; Figs 18AB

References:

ALTH, A. 1885a. Jagielnica - Czernelica, 1:75000. Atlas Geologiczny Galicyi. Zakład wojskowy geograficzny w Wiedniu.

- 1885b. Zaleszczyki, 1:75000. Atlas Geologiczny Galicyi. Zakład wojskowy geograficzny w Wiedniu.

ATLAS GEOLOGICZNY GALICYI, 1885-1914. Zeszyty 1-21, 23, 25-27. 99 arkuszy map 1:75000. *Wydawnictwo Komisyi Fizyograficznej Akademii Umiejętności*; Kraków.

BĄBEL, M. 1996. Wykształcenie facjalne, stratygrafia oraz sedymentacja badeńskich gipsów Ponidzia. *In*: P.H. KARNKOWSKI (*Ed*.), Analiza basenów sedymentacyjnych a nowoczesna sedymentologia. Materiały **5** Krajowego Spotkania Sedymentologów, pp. B1-B26. Warszawa.

- 1999. Facies and depositional environments of the Nida Gypsum deposits (Middle Miocene, Carpathian Foredeep, southern Poland). *Geological Quarterly*, **43**, 405-428.

- 2002. Brine palaeocurrent analysis based on oriented selenite crystals in the Nida Gypsum deposits (Badenian, southern Poland). *Geological Quarterly*, **46**, 49-62.

- 2004. Badenian evaporite basin of the northern Carpathian Foredeep as a drawdown salina basin. *Acta Geologica Polonica*, **54**, 313-337.

BIENIASZ, F. 1885a. Monasterzyska, 1:75000. Atlas Geologiczny Galicyi. Zakład wojskowy geograficzny w Wiedniu.

- 1885b. Tyśmienica - Tłumacz, 1:75000. Atlas Geologiczny Galicyi. Zakład wojskowy geograficzny w Wiedniu.

- 1898a. Borszczów, 1:75000. Atlas Geologiczny Galicyi. Zakład wojskowy geograficzny w Wiedniu.

- 1898b. Brzeżany, 1:75000. Atlas Geologiczny Galicyi. Zakład wojskowy geograficzny w Wiedniu.

- 1898c. Mielnica - Okopy, 1:75000. Atlas Geologiczny Galicyi. Zakład wojskowy geograficzny w Wiedniu.

DRONKERT, H. 1985. Evaporite models and sedimentology of Messinian and Recent evaporites. *GUA Papers of Geology*, Ser. **1**, No. **24**, pp. 1-283. Utrecht.

KASPRZYK, A. 1993. Lithofacies and sedimentation of the Badenian (Middle Miocene) gypsum in the northern part of the Carpathian Foredeep, southern Poland. *Annales Societatis Geologorum Poloniae*, **63**, 33-84.

KRACH, W. 1954. Materials to the stratigraphy of the Upper Silesia Miocene. *Biuletyn Instytutu Geologicznego*, **71**, 153-180. [*In Polish with English summary*]

KUBICA, B. 1992. Lithofacial development of the Badenian chemical sediments in the northern part of the Carpathian Foredeep. *Prace Państwowego Instytutu Geologicznego*, **133**, 1-64. [*In Polish with English summary*]

KUCIŃSKI, T. & NOWAK, W. 1967. Arkusz Strzyżów. *In*: Szczegółowa mapa geologiczna Polski, 1:50000, wydanie tymczasowe. Region Karpat i Przedgórza, zeszyt **4**. *Wydawnictwa Geologiczne*; Warszawa.

KWIATKOWSKI, S. 1972. Sedimentation of gypsum in the Miocene of southern Poland. *Prace Muzeum Ziemi*, **19**, 3-94. Warszawa. [*In Polish with English summary*]

ŁOMNICKI, J. 1905a. Kołomyja, 1:75000. Atlas Geologiczny Galicyi. Zakład wojskowy geograficzny w Wiedniu.

- 1905b. Stanisławów, 1:75000. Atlas Geologiczny Galicyi. Zakład wojskowy geograficzny w Wiedniu.

MACOVEI, G. & ATANASIU, I. 1931. Geologische Beobachtungen über das Miozän zwischen dem Siret und dem Nistrau in der Bucowina und im nördlischen Bessarabien. *Anuarul Institutul Geologic al României*, **14**, 169-200. Bucareşti.

OLSZEWSKI, S. 1911. Mapa górniczo przemysłowa Galicyi według stanu w roku 1910 z objaśnieniami, pp. 1-76, I-LIII. *Nakładem Autora*, *Drukarnia Polska*; Lwów.

PANOW, G.M. & PŁOTNIKOW, A.M. 1996. Badenian evaporites of the Ukrainian part of Carpathian Foredeep: lithofacies and thickness. *Przegląd Geologiczny*, **44**, 1024-1028. [*In Polish*]

PERYT, T.M., HAŁAS, S., KAROLI, S. & PERYT, D. 1997a. Isotopic record of environmental changes during deposition of Badenian (Middle Miocene) gypsum at Kobeřice near Opava (Czech Republic). *Przegląd Geologiczny*, **45**, 807-810. [*In Polish with English summary*]

PERYT, T.M., KAROLI, S., PERYT, D., PETRICHENKO, O.I., GEDL, P., NARKIEWICZ, W., ĎURKOVIČOVÁ, J. & DOBIESZYŃSKA, Z. 1997b. Westernmost occurrence of the Middle Miocene Badenian gypsum in central Paratethys (Kobeřice, Moravia, Czech Republic). *Slovak Geological Magazine*, **3**, 105-120.

PERYT, T.M., POBEREZHSKY, A.V. & YASINOVSKY, M. 1995. Facies of Badenian gypsum of the Dnister river region. *Geologiia i Geochimiia Goryuchikh Kopalyn*, No. 1-2/90-91, 16-27. Lviv. [*In Ukrainian with English summary*]

RANIECKA-BOBROWSKA, J. 1957. A few plant remnants from the Tortonian of Upper Silesia. *Kwartalnik Geologiczny*, **1**, 275-398. [*In Polish with English summary*]

ROMAN, A. 1998. Wykształcenie i sedymentacja badeńskich gipsów okolic Racławic na Wyżynie Miechowskiej, pp. 1-69. *MSc Thesis*; University of Warsaw.

SARNACKA, Z. 1956. Arkusz Rydułtowy. Szczegółowa mapa geologiczna Polski, 1:50000. *Wydawnictwa Geologiczne*; Warszawa 1960.

- 1968. Objaśnienia do szczegółowej mapy geologicznej Polski. Arkusz Rydułtowy, 1:50 000, pp. 1-37. *Wydawnictwa Geologiczne*; Warszawa.

TEISSEYRE, W. 1892-1893. Rohatyn, 1:75000. Atlas Geologiczny Galicyi. Zakład wojskowy geograficzny w Wiedniu. [Kraków 1912]

- 1894-1895. Mikołajów i Bóbrka, 1:75000. Atlas Geologiczny Galicyi. Zakład wojskowy geograficzny w Wiedniu. [Kraków 1912]

- 1895. Żydaczów i Stryj, 1:75000. Atlas Geologiczny Galicyi. Zakład wojskowy geograficzny w Wiedniu. [Kraków 1912]

- 1896. Kałusz i Halicz, 1:75000. Atlas Geologiczny Galicyi. Zakład wojskowy geograficzny w Wiedniu. [Kraków 1912]

TURCZYNOW, I.I. & ANDRIJCZUK, W.M. 1995. Dome-like structures in the Middle Miocene Badenian gypsum of the Dnister River region (West Ukraine). *Przegląd Geologiczny*, **43**, 403-405. [*In Polish with English summary*]

WALCZOWSKI, A. 1984. Arkusz Kazimierza Wielka. Szczegółowa mapa geologiczna Polski, 1:50000. *Wydawnictwa Geologiczne*; Warszawa.

WOIŃSKI, J. 1989. Arkusz Działoszyce. Szczegółowa mapa geologiczna Polski, 1:50000. *Wydawnictwa Geologiczne*; Warszawa.